Dissertation zur Erlangung des Doktorgrades
der Fakultät für Chemie und Pharmazie
der Ludwig-Maximilians-Universität München

# Cryo-EM structures of eukaryotic translation termination and ribosome recycling complexes containing eRF1, eRF3 and ABCE1

Anne Preis
aus
Tallinn, Estland

2020

Erklärung

Diese Dissertation wurde im Sinne von § 7 der Promotionsordnung vom 28. November 2011 von Herrn Prof. Dr. Roland Beckmann betreut.

Eidesstattliche Versicherung

Diese Dissertation wurde eigenständig und ohne unerlaubte Hilfe erarbeitet.

München, 21.01.2020

Anne Preis

Dissertation eingereicht am: 21.01.2020

1. Gutachter: Prof. Dr. Roland Beckmann

2. Gutachter: Prof. Dr. Alexej Kedrov

Mündliche Prüfung am: 15.05.2020

# Abstract

Translation of an mRNA template into a polypeptide chain is terminated on a stop codon. The stop is recognized in the ribosomal A site by release factors, that subsequently release the polypeptide. This event is followed by ribosome recycling leading to a dissociation of the ribosome into subunits. In contrast to bacterial termination factors RF1 and RF2 with overlapping stop codon specificities, eukaryotic translation termination factor eRF1 recognizes all three stop codons and is unrelated to RF1 or RF2 in sequence and structure. eRF1 is delivered to the ribosomal A site in a ternary complex with GTP-bound eRF3, with the catalytically relevant central domain of eRF1 packed tightly against eRF3. For peptide release, eRF1 must undergo dramatic conformational changes, which were first modeled on the basis of structural rearrangements of the homologous no-go mRNA decay factor Pelota. In complex with its respective GTPase partner Hbs1, Pelota binds the ribosome in a packed state. Available cryo-EM structural evidence additionally showed that, during ribosome recycling, ABCE1, a highly conserved ATPase across multiple kingdoms of life and the main factor driving ribosome recycling in eukaryotes, binds Pelota and stabilizes its extended conformation in the intersubunit space.

The first goal of this work was to study the structural rearrangements of eRF1, eRF3 and ABCE1 on the ribosome during translation termination and ribosome recycling. Two cryo-EM structures were obtained at sub-nanometer resolution: the pre-termination complex containing eRF1 and eRF3, and a termination/pre-recycling complex containing eRF1 and ABCE1. The pre-termination stage showed eRF1 packed against eRF3, unable to catalyze peptide release. In the termination/pre-recycling complex, eRF1 assumed an extended conformation which is further stabilized by ABCE1, with the central domain of eRF1 swung out toward the CCA end of the P-site tRNA. The conformational changes observed for eRF1 were very similar to those of Pelota during ribosome rescue during translational stalling. ABCE1 adopted a half-closed conformation of its two nucleotide-binding domains in the termination/pre-recycling complex, which is identical to the ribosome- and Pelota-bound conformation observed previously.

According to a model based of these results, splitting the ribosome would require the closing of the two nucleotide-binding domains and a rotation of the iron-sulfur cluster domain of ABCE1, which would in turn push eRF1 into the intersubunit space. Supporting this idea, ABCE1 was shown to remain bound to the small ribosomal subunit after in vitro splitting. 40S-bound ABCE1 adopted a fully closed conformation and in which re-association of the large ribosomal subunit is prevented.

As a second goal of this work, native *S. cerevisiae* ABCE1-bound small ribosomal subunits were purified to complement the in vitro studies and explore the supposed involvement of ABCE1 in translation initiation. Cryo-EM of native 40S-ABCE1 complexes indeed confirmed the closed conformation of ABCE1. Moreover, these complexes were associated with initiator tRNA and eIF1A, an initiation factor which binds the ribosomal A site and is involved in multiple processes in initiation including subunit joining. Mass spectrometry analysis also identified all subunits of eIF2 and eIF3 in these native pull-downs, both of which are multimeric factors involved in the formation of the 43S pre-initiation complex. These results are clearly hinting at an active role of ABCE1 during translation initiation. Yet, the exact role of ABCE1 will be subject of further studies.

# CONTENTS

# 1 INTRODUCTION

## 1.1 THE FLOW OF GENETIC INFORMATION

All kingdoms of life depend on the replication and expression of their specific genetic information stored in the form of deoxyribonucleic acid (DNA). DNA exists in the cell as a complementary double-stranded helix, which ensures its ability to be replicated by DNA-dependent DNA polymerases. The universal genetic code is defined by sequential triplets of DNA building blocks called nucleotides (nt). Three nucleotides comprise one codon, and sequential codons constitute genes. Broadly defined, a gene is a DNA sequence which codes for a molecule of protein or ribonucleic acid (RNA). Messenger RNA (mRNA) molecules serve as readable forms of the respective protein-encoding genes. They are copied off the DNA sequence by DNA-dependent RNA polymerases in a process called transcription, and this process is tightly controlled by numerous activators and repressors.

An mRNA molecule defines the amino acid sequence of a protein. Protein building blocks, *i.e.* amino acids, are chemically different from DNA or RNA, thus a decoding system must be ensured to translate codons into amino acids. All cells accomplish translation of genetic code into an amino acid sequence by additionally employing a set of transfer RNA (tRNA) molecules, translation factors, and a platform for the organization of this process, the ribosome.

Proteins function in all processes within a cell. Retention of cellular structures, transport of metabolites and communication with other cells and/or the environment, cell division and cell death are all possible thanks to various proteins. Thus, they vary greatly in function, structure, and lifetime and are subject to various forms of regulation and modification. Ultimately, proteins are broken down and the amino acids can be recycled for synthesizing new proteins.

## 1.2 RIBOSOME COMPOSITION ACROSS KINGDOMS OF LIFE

The ribosome is a large macromolecular complex comprised of ribosomal RNA (rRNA) and ribosomal proteins (r-proteins). Ribosomes are conserved in their overall architecture and function throughout all kingdoms of life (Figure 1). A functioning prokaryotic ribosome, termed 70S in accordance with its sedimentation coefficient in Svedberg units, is comprised of a small and a large subunit (30S and 50S). Bacterial 30S consists of 16S rRNA and 21 r-proteins, whereas 50S has 23S rRNA, 5S rRNA and 33 r-proteins. Eukaryotic 80S ribosomes are generally larger and more complex, with the exact size and composition varying among different species (reviewed by Klinge et al., 2012; Melnikov et al., 2012). *Saccharomyces cerevisiae* (*S.cerevisiae*; baker's yeast) 40S consists of 18S rRNA and 33 r-proteins, and 60S has 25S rRNA, 5.8S rRNA, 5S rRNA and 46 proteins. Additionally, eukaryotes have gained expansion segments in their rRNA, which are important for ribosome biogenesis and maturation of rRNA (Ramesh and Woolford, 2016), translation initiation (Hashem et al., 2013) and coordination of nascent polypeptide chain (NC)-interacting factors (Knorr et al., 2019; Leidig et al., 2013). Multiple interaction points between the subunits that keep the ribosome intact are termed inter-subunit bridges. These are formed predominantly by RNA-RNA interactions (Morgan et al., 2000).

The small subunit (SSU) serves as a platform for placement of the translated mRNA, containing the mRNA channel and the decoding center (DC), where aminoacyl-tRNA molecules recognize codons on the mRNA with their anticodon loops (Berg and Offengand, 1958; Ogle et al., 2001). There are three distinct tRNA binding sites on the small subunit: the aminoacyl site (A-site), where an aminoacyl-tRNA is initially accommodated; the peptidyl site (P-site), where the peptidyl-tRNA is formed; and the exit site (E-site), from which an uncharged tRNA leaves the ribosome (Agrawal et al., 2000). The peptidyl transferase center (PTC), where peptide bond formation is catalyzed, is located on the large subunit (LSU). The conserved PTC was shown to consist entirely of rRNA, making the ribosome a true ribozyme, with r-proteins rather possessing regulatory, scaffold- and stabilizing functions (Cech, 2000; Nissen et al., 2000). The NC is threaded

through the ribosomal exit tunnel, which extends from the PTC to the back of the LSU (Frank et al., 1995). Another conserved ribosomal site is the L12 (bacterial) or P (eukaryotic and archaeal) stalk of the LSU, which confers interactions between the ribosome and translation factors. The structural organization of this stalk is similar in all domains of life, although its r-protein components in bacteria show low homology to the respective r-proteins in archaea and eukaryotes (reviewed by Mitroshin et al., 2016). The conserved sarcin-ricin loop (SRL) and GTPase-associated center (GAC) of the bacterial 23S rRNA (or 25S rRNA in *S. cerevisiae*) in the LSU is essential for translation and interacts with translational guanosine triphosphatases (GTPases) (Sergiev et al., 2005). Also, the L1 stalk, which is located near the E-site on the LSU, is a conserved entity that coordinates translocation and release of tRNA molecules (Trabuco et al., 2010).

Structural studies of ribosomes have been conducted using X-ray crystallography and cryo-electron microscopy (cryo-EM). Crystal structures of bacterial and archaeal ribosomal subunits were resolved in the early 2000's (Ban et al., 2000; Schluenzen et al., 2000; Wimberly et al., 2000) and the first bacterial 70S crystal structure was published in 2006 (Selmer et al., 2006). The structural information has aided vastly in our understanding of the translation process, identifying the conserved ribosomal core and therefore the conservation of ribosomal catalytic processes. In the years starting from 2010, X-ray and cryo-EM marked a breakthrough in structural understanding of the eukaryotic ribosome (Anger et al., 2013; Ben-Shem et al., 2010, 2011; Khatter et al., 2015).

Cryo-EM is an advantageous choice for solving structures of ribosomal complexes in comparison to nuclear magnetic resonance (NMR) or X-ray crystallography. Firstly, the required amount of sample is a lot lower, especially considering that crystal formation requires high purity and stability of the complex. Secondly, the rapid vitrification process of samples allows retention of the solubilized conformations in buffer, whereas heterogeneity of the sample can be tackled with computational sorting. During the course of this thesis work, cryo-EM underwent a "resolution revolution" allowing to obtain near-atomic maps of a variety of marcomolecules (reviewed by Bai et al., 2015).

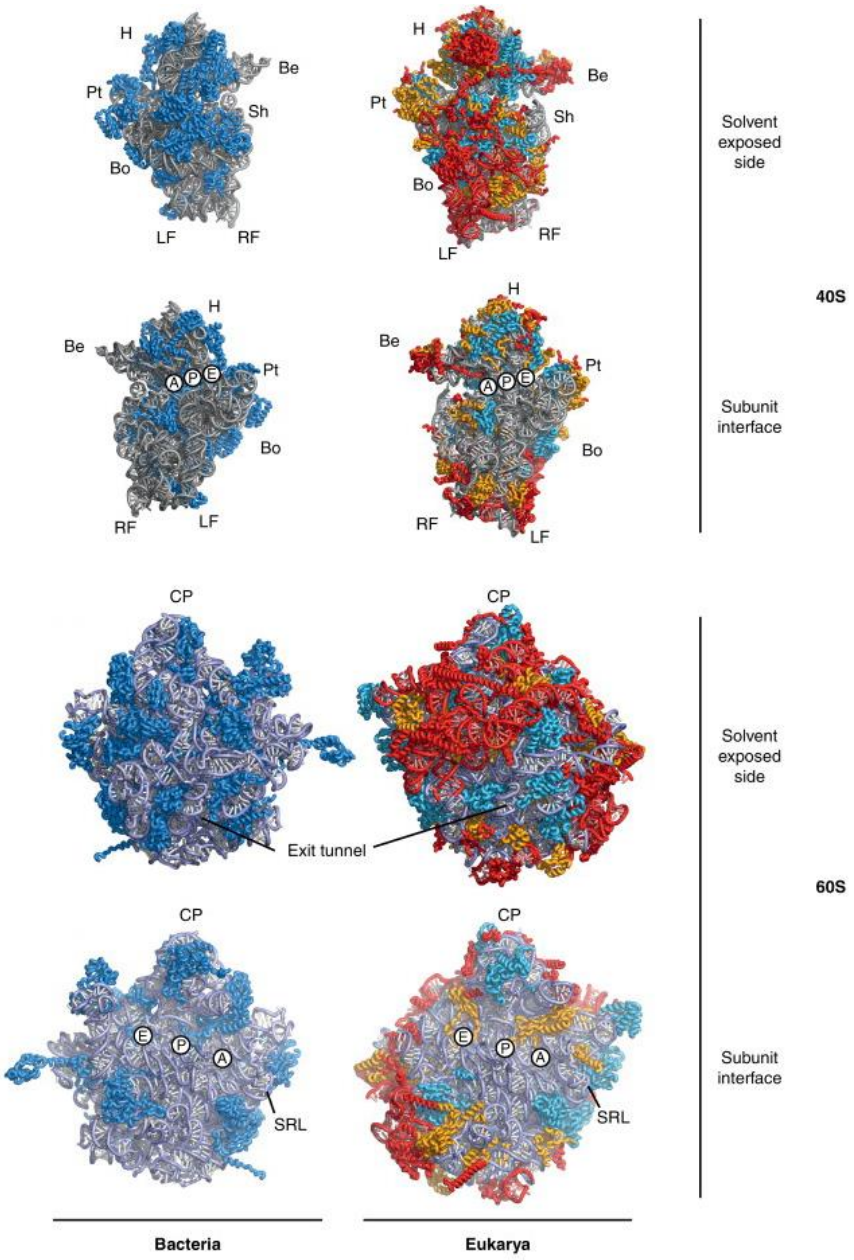


Figure 1. **Comparison of bacterial and eukaryotic ribosomal subunits.** *Thermus thermophilus* 30S (PDB code 2j00) and 50S (PDB code 2j01) vs *Tetrahymena thermophila* 40S (PDB code 2xzm) and 60S (PDB codes 4A17 and 4A19). Universally conserved proteins are shown in light blue; proteins present in archaea and eukarya in gold; and protein and RNA elements exclusively present in eukarya in red. Hallmarks of the SSU: head (H), beak (Be), platform (Pt), shoulder (Sh), body (Bo), left foot (LF), right foot (RF). On the LSU: central protuberance (CP), SRL, protein exit tunnel; A-, P- and E-site are marked with circles. From Klinge et al., 2012.

## 1.3 THE TRANSLATION CYCLE – AN OVERVIEW

Translation of an mRNA into a polypeptide sequence by ribosomes can be divided into four functional steps: initiation, elongation, termination and recycling (Figure 2).

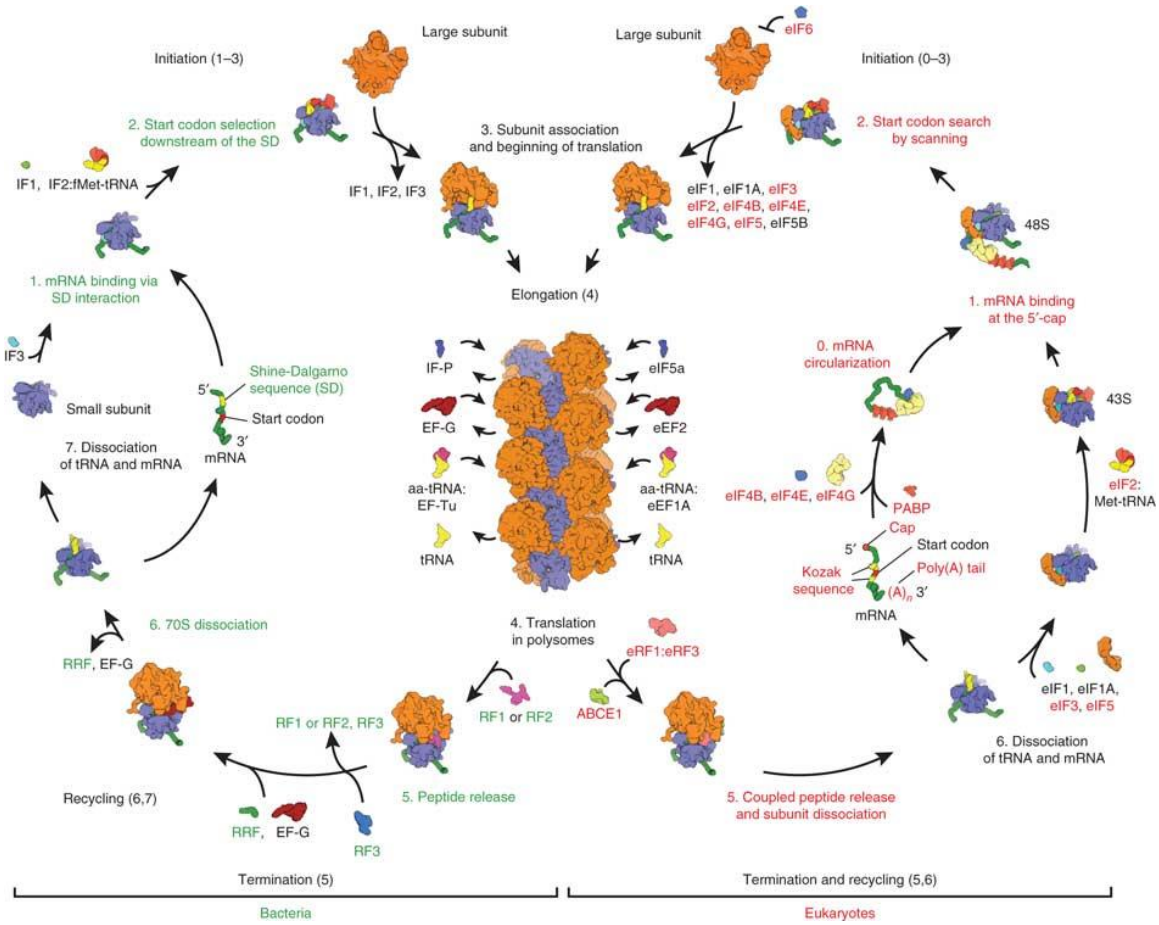


Figure 2. **Translation is a four-stage process consisting of initiation, elongation of the polypeptide chain, termination and recycling of the ribosomes.** Initiation factors (IFs in bacteria or eIFs in eukaryotes), elongation factors (EFs or eEFs), release factors (RFs or eRFs) and recycling factors are indicated. Homologous factors and common steps of translation are labeled black. During elongation, ribosomes assemble in polysomes. The other steps of the translation cycle have diverged and include several stages (indicated by numbers) that differ between bacteria (green) and eukaryotes (red). From Melnikov et al., 2012.

## 1.4 INITIATION OF TRANSLATION

Initiation is the rate-determining step in the translational cycle (Laursen et al., 2005). It ensures the proper selection of a start codon (AUG), its positioning into the ribosomal P-site and its pairing with initiator tRNA. Eukaryotes possess a multitude of regulatory factors compared to bacteria.

### 1.4.1 Initiation of translation in bacteria

In bacterial initiation of translation, the Shine-Dalgarno sequence of an mRNA, located 7-10 nt upstream of the start codon (Shine and Dalgarno, 1974), pairs directly with the anti-Shine-Dalgarno sequence in the 16S rRNA of the SSU, directing correct positioning of the start codon in the P-site (Kaminishi et al., 2007; Korostelev et al., 2007). Formation of a 30S initiation complex is facilitated by three initiation factors (IFs): IF1 associates with 30S in the A-site thus blocking it from aminoacyl-tRNA entry and stimulates binding of IF2; IF2 in its GTP-bound form recruits initiator tRNA (fMet-tRNA$^{fMet}$) to the P-site, and IF3 promotes binding of 30S to the initiation site on the mRNA. Joining of the 50S is monitored by IF2 and IF3, and the IFs ultimately dissociate to yield a 70S initiation complex, where a ribosome is positioned on a start codon of the mRNA with initiator tRNA in the P-site (reviewed by Melnikov et al., 2012).

### 1.4.2 Initiation of translation in eukaryotes

Initiation of translation in eukaryotes is a process that is more extensively regulated in comparison to that of bacteria. In addition to canonical initiation factors, the process employs additional RNA helicases, anti-association factors and likely poly-A-binding protein (PABP) (Jackson et al., 2010). The largest initiation factor, eIF3, is a complex of core and peripheral subunits and its composition varies between different species. Mammals have 13 subunits (eIF3a-eIF3m) weighing ~ 800 kDa, whereas *S. cerevisiae* and most fungi encode for two core (eIF3a, eIF3c) and four peripheral subunits (eIF3b, eIF3i, eIF3g, eIF3j) weighing ~ 395 kDa. Similar to bacterial IF2, GTP-bound eIF2 (itself consisting of α, β and γ subunits) forms a ternary complex with the initiator tRNA (Met-tRNA$_i$ and binds the small ribosomal subunit in the P-site.

As a first step of eukaryotic initiation, a 43S preinitiation complex forms, where the 40S subunit is bound by the eIF2-GTP-Met-tRNA$_i$ ternary complex and initiation factors eIF3, eIF1, eIF1A and likely eIF5. For mRNA binding, the complex interacts with eIF4A, eIF4B and eIF4F. The latter are bound to the 5' end m7GpppG cap structure of the mRNA and unwind the secondary structure of the 5' proximal mRNA, facilitating attachment of the 43S complex. Next, scanning for an initiation codon (AUG) in 5' to 3' direction can take place. After recognition of AUG, established codon-anticodon interactions and thus 48S preinitiation complex formation, eIF5 and eIF5B stimulate GTP hydrolysis by eIF2 and promote joining of 60S. Together with eIF1A, eIF1 plays a key role in maintaining the fidelity of initiation, discriminating against codon-anticodon mismatches and preventing premature eIF5-induced hydrolysis of eIF2-bound GTP and $P_i$ release (reviewed by Jackson et al., 2010 and Hinnebusch and Lorsch, 2012).

Structural and cross-linking data indicate the localization of the multimeric, five-lobed eIF3 exclusively at the solvent side of 40S (Siridechadilok et al., 2005). Along with crystal structures of parts of eIF3 (ElAntak et al., 2007; Khoshnevis et al., 2010; Wei et al., 2004), cryo-EM structures were solved for a mammalian 43S preinitiation complex containing DHX29 (an mRNA DExH-box helicase that binds directly to the 40S subunit, Figure 3) (Hashem et al., 2013), 40S-eIF1-eIF1A-eIF3 (Aylett et al., 2015), and for "open" and "closed" states of the scanning 48S complex (Llácer et al., 2015a). eIF2 binds to 40S via its α subunit and stabilizes the initiator tRNA. eIF1A and eIF1 serve as anti-association factors at the subunit interface, binding (cooperatively) to the A-site and near the P-site, respectively (Jackson et al., 2010). Overall, determining structures of initiation complexes by cryo-EM has remained a challenge due to spontaneous dissociation of factors on the cryo grid during vitrification.

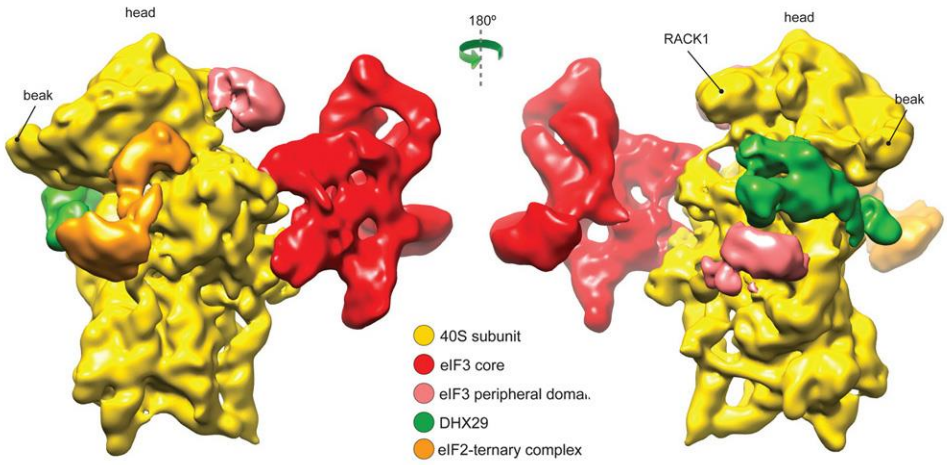


Figure 3. **Localization of translation initiation factors in a 43S rabbit preinitiation complex containing helicase DHX29.** The five-lobed eIF3 core is located at the solvent side of 40S. eIF2-ternary complex is bound in the P-site. RACK1 (receptor for activated C-kinase), the head and beak of 40S are marked. From Hashem et al., 2013.

## 1.5 ELONGATION OF POLYPEPTIDE CHAIN

Between bacteria and eukaryotes, the elongation step of translation is the most conserved and the most processive (Melnikov et al., 2012). The general mechanism can be subdivided into three steps: delivery of the cognate tRNA, peptide bond formation in the PTC and translocation of the ribosome on the mRNA.

When a codon is exposed in the ribosomal A-site, a cognate tRNA is delivered by translational GTPase EF-Tu (bacterial)/eEF1α (eukaryotic) in a ternary complex with GTP (Agirrezabala and Frank, 2009; Dever and Green, 2012). Bases A1492 and A1493 in 16S rRNA read out the geometry of the Watson-Crick A-helix formed by the codon and the anticodon with a cognate aminoacyl tRNA by forming A-minor interactions (Ogle and Ramakrishnan, 2005). In case of proper decoding in the A-site, EF-Tu/eEF1α hydrolyzes its bound GTP and is released from the ribosome. A peptide bond is then formed between the initiator methionyl tRNA and the delivered cognate tRNA in the ribosome's PTC, leaving the uncharged initiator tRNA in the P-site. This invokes dynamic, hybrid A/P and P/E states in the attached tRNAs, whereby the fluctuations are due to the movements of

the ribosomal subunits relative to each other (Agrawal et al., 2000). In the translocation step, EF-G/eEF2, another translational GTPase and a mimic of the EF-Tu/eEF1α-GTP-tRNA ternary complex, partially inserts into the A-site and, acting as a molecular ratchet, moves the ribosome three nucleotides downstream. EF-G/eEF2 has a high affinity to the hybrid state of the ribosome, in contrast to other translational GTPases that prefer the non-rotated state (Dever and Green, 2012). The empty tRNA is ultimately pushed into the E-site and the A-site exposes the next codon in the open reading frame (ORF). EF-Tu /eEF1α is regenerated to its GTP-bound form by the guanine nucleotide exchange factor (GEF) EF-Ts/eEF1βγ. This way, EF-Tu/eEF1α is ready to escort another tRNA and the elongation process can continue until a stop codon is reached. Beside the canonical elongation factors, some fungi possess an additional elongation factor eEF3, an ATPase which helps clear the ribosomal E-site (Andersen et al., 2006). Also, an additional elongation factor EF-P/eIF5A has evolved to facilitate translation of polyproline stretches (Gutierrez et al., 2013).

## 1.6 TERMINATION OF TRANSLATION AND RIBOSOME RECYCLING

Termination of translation occurs when a stop codon (UAA, UGA or UAG) is exposed in the ribosomal A-site. There are no tRNAs in the cell that would decode the stop codon. Translation is terminated instead by specific proteins *i.e.* termination (or release) factors. There are two kinds of termination factors: class I termination factors bind directly to the ribosomal A-site, engage with the stop codon and catalyze peptide release whereas class II termination factors confer GTP-dependency of the process.

### 1.6.1 Termination of translation in bacteria

In bacteria, class I release factor 1 (RF1) recognizes stop codons UAA and UAG, and RF2 recognizes UAA and UGA. RF1 or RF2 is composed of four domains: domain 1 binds near the ribosomal GTPase associated center (GAC) and contacts class II RF as well as the L11 stalk, domains 2 and 4 compact into a super-domain which is involved in stop codon recognition, and the long domain 3 bridges between the DC of 30S and the PTC of 50S (Korostelev, 2011).

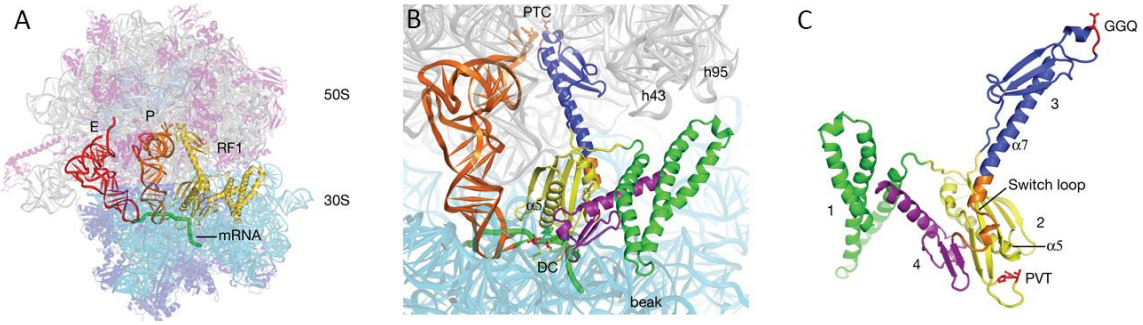


Figure 4. **Structural basis of translation termination on a bacterial ribosome.** Overall architecture of a bacterial termination complex containing RF1, with P- and E-site tRNA (**A**); Positioning of RF1 in the A-site and contacts with the ribosome (**B**); Domain organization of RF1, PVT motif (pink) in the recognition loop and GGQ loop (red) are marked (**C**). From Laurberg et al., 2008.

Biochemical studies and X-ray crystallographic structures provided complete deciphering of the stop codon decoding mechanism in bacteria (Laurberg et al., 2008; Pallesen et al., 2013; Zhou et al., 2012). RF1 or RF2 contains a reading head, which, similarly to a base-pairing cognate tRNA, forms hydrogen bonds with the mRNA in the A-site. However, the conformation of the stop codon is different to that of a sense codon: the third nucleotide is unstacked from the first two and is recognized by the release factor separately. Also, the conserved nucleotides of the ribosomal DC A1492 and A1493, which discriminate between cognate and non-cognate tRNAs in elongation, rather stabilize the active conformation of the release factor. There are specific motifs in domain 2 of RF1 or RF2 that make decoding the stop codon possible. The N-terminal tip of helix α5 recognizes the first U by forming specific H-bonds from the backbone of helix α5. The specificity for the second nucleotide is conferred by conserved amino acids in the recognition loop, namely the PxT and SPF motifs of RF1 and RF2, respectively. The third nucleotide is recognized by the N- and C-terminal ends of the recognition loop in the G530 pocket of the decoding center (Korostelev, 2011).

Recognition of the stop codon and peptidyl-tRNA hydrolysis are strongly cooperative events. Stop codon recognition causes a rearrangement in the switch loop connecting domain 3 and 4 of RF1/RF2, which allows docking of the conserved catalytic Gly-Gly-Gln (GGQ) motif of domain 3 into the PTC for peptide release. Positioning of the GGQ loop causes rearrangements of the rRNA in the PTC, exposing the ester bond of the peptidyl-tRNA and allowing entry of a water molecule for peptide hydrolysis (reviewed by Loh and Song, 2010). Therefore, fidelity of translation termination could be explained by an "induced fit" mechanism, where the active, "open" conformation of RF1 or RF2 is only attained on the ribosome upon stop codon recognition (Trappl and Joseph, 2016).

RF3, the class II termination factor in bacteria, has high affinity to GDP and is therefore found in the cell in its GDP-bound form. When a ribosome is bound by RF1 or RF2 and peptide release has taken place, this ribosome-RF1/2 complex serves as a GEF for RF3-GDP (Zavialov et al., 2001). GTP binding to RF3 causes conformational changes in RF3 itself as well as in the ribosome, resulting in a ratchet-like movement of 30S relative to 50S. This conformational change drives the class I RF to dissociate (Zavialov et al., 2001, 2002). RF3 then rapidly hydrolyzes its bound GTP and resumes the GDP-bound form, which has low affinity for the ribosome and therefore uncouples as well (Gao et al., 2007).

### 1.6.2 Ribosome recycling in bacteria

For a new round of translation, the post-termination complex containing mRNA, the deacylated tRNA in the P-site and an empty A-site must be disassembled. In bacteria, this is achieved by the essential ribosome recycling factor (RRF) in concert with EF-G (Zavialov et al., 2005). RRF is comprised of two domains connected via a flexible linker and is, in its shape, similar to a tRNA (Nakano et al., 2003). How exactly the events of tRNA and mRNA release are coordinated is still debated. RRF and EF-G have been proposed to displace the tRNA from the 70S destabilizing the post-termination complex (Hirokawa et al., 2006). However, the loss of tRNA alone does not cause spontaneous ribosome splitting, as RRF and EF-G are specifically required to split empty 70S. Ribosome splitting and mRNA release are rather dependent on GTP hydrolysis by EF-G (Hirokawa et al.,

2008). After splitting, IF3 binds to 30S subunits, thus preventing re-association with 50S and setting the scene for initiation of the next round of translation (Peske et al., 2005).

### 1.6.3 Termination of translation in eukaryotes

The eukaryotic class I release factor eRF1 (Figure 5A, left) recognizes all three stop codons, in contrast to the overlapping codon specificities of bacterial analogs RF1 and RF2 (Kisselev et al., 2003). Although functionally similar, eRF1 does not resemble RF1/RF2 in sequence or structure. It consists of three domains: the N-terminal domain (NTD) recognizes the stop codon (Bertram et al., 2000), the tip of the central domain contains the conserved GGQ loop necessary for peptidyl-tRNA hydrolysis (Frolova et al., 1999; Song et al., 2000), and the C-terminal domain (CTD) interacts with the class II release factor, eRF3 (Merkulova et al., 1999). Additionally, NMR studies have identified a mini domain in the CTD of eRF1, which was not assigned in the crystal structures (Mantsyzov et al., 2010a). The conserved NIKS and YxCxxF motifs on the tip of the NTD of eRF1 were identified to be indispensable for stop codon recognition (Chavatte et al., 2002; Cheng et al., 2009; Frolova et al., 2002). Together with additional conserved amino acids in the NTD, these motifs were supposed to form a three-dimensional interaction network with the stop codon (Bulygin et al., 2010).

Although both RF3 and eRF3 possess a G domain, eRF3 (Figure 5A, right) is different from bacterial RF3 in structure and in function (Kisselev and Buckingham, 2000). The β-barrel domains II and III of eRF3 are structurally homologous to eEF1α and EF-Tu (Kong et al., 2004), and the “prion-forming” N-terminal domain is dispensable for termination (Ter-Avanesyan et al., 1994). In contrast to the bacterial system, eRF3 does not assist in dissociation of eRF1. eRF1 alone releases peptides very inefficiently and eRF3 has been shown to strongly stimulate the process (Alkalaeva et al., 2006). This stimulation is in turn dependent on GTP hydrolysis by eRF3 (Alkalaeva et al., 2006). Thus, it has been proposed that stop codon recognition and peptidyl hydrolysis by eRF1 are coupled through the GTPase activity of eRF3 (Salas-Marco and Bedwell, 2004). eRF1 and eRF3 interact directly via their C-terminal domains and form a stable ternary complex with GTP (Merkulova et al., 1999; Figure 5B, left). This interaction is enhanced by the central

domain of eRF1 (Kononenko et al., 2007). Also, binding of this ternary complex to pre-termination complexes induces a 2-nt forward shift in their toeprint, which likely stems from conformational changes of the head relative to the body of the 40S subunit, preventing further access for the reverse transcriptase (Alkalaeva et al., 2006).

Crystallographic structures and small angle X-ray scattering (SAXS) data revealed that in solution, eRF1 alone is found in an extended conformation, which would be incompatible with its positioning in the ribosomal binding pocket (Kononenko et al.; Song et al., 2000). Crystal structures of full-length human and *Schizosaccharomyces pombe (S. pombe,* fission yeast*)* eRF1 in complex with domains II and III of eRF3 (without the G domain) indicated that eRF1 undergoes a large conformational change upon binding to eRF3, where the central domain shifts and rotates relative to the NTD (Cheng et al., 2009)
.

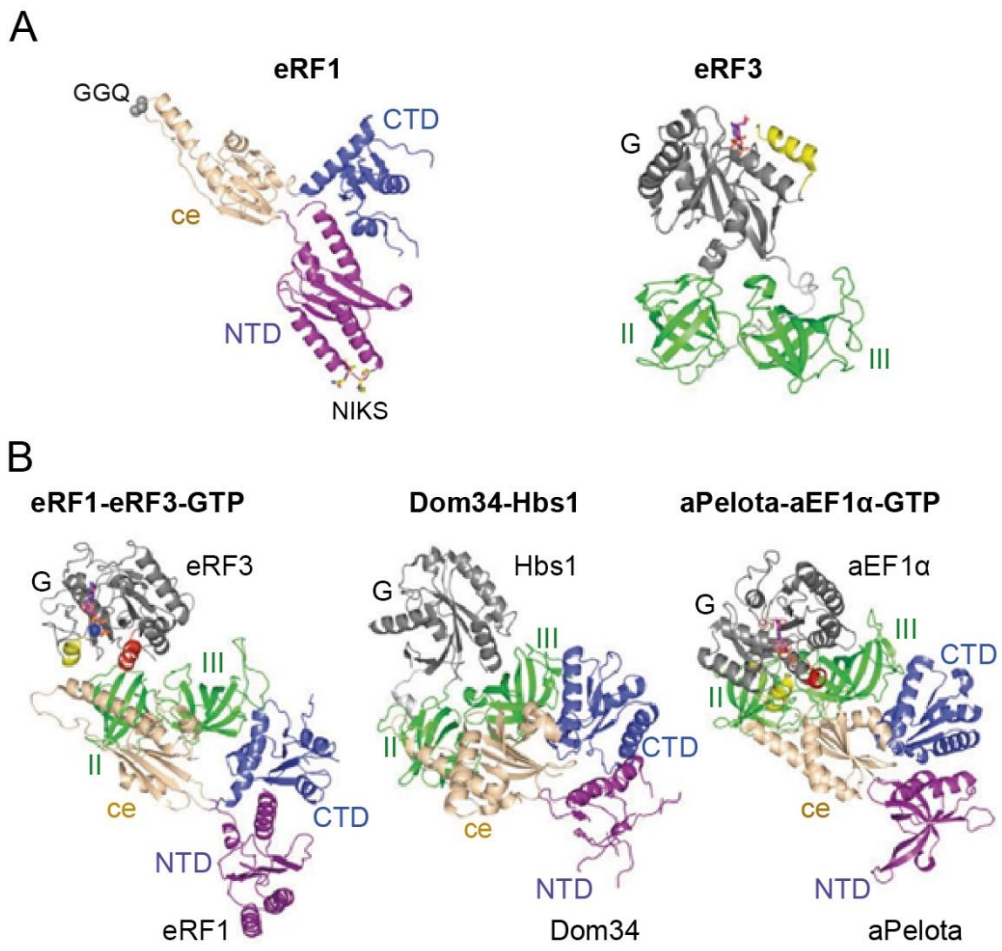


Figure 5. **Structures of individual termination factors and termination- as well as related complexes.** Individual eRF1 and eRF3 (**A**) and structures of eRF1, eRF3 and eRF1-eRF3-GTP, Dom34-Hbs1 and aPelota-aEF1α-GTP complexes (**B**). Adapted from Jackson et al., 2012.

Conclusions about the conformation of the ribosome-bound eRF1-eRF3-GTP ternary complex were first drawn from a cryo-EM reconstruction of a no-go mRNA surveillance complex (Becker et al., 2011). The no-go decay pathway of mRNA surveillance handles mRNAs that induce translational stalling due to stable secondary structure elements (pseudo-knots, stem loops) or the presence of rare codons (Shoemaker and Green, 2012). Dom34 (or Pelota in mammals and aPelota in archaea) and Hbs1 are paralogs of eRF1 and eRF3, respectively, and function in recognizing stalled ribosomes for

subsequent degradation of the aberrant mRNA (Atkinson et al., 2008; Kobayashi et al., 2010; Shoemaker et al., 2010). In archaea, the function of Hbs1 is exerted by aEF1α (Figure 5B, right) (Kobayashi et al., 2010). Dom34 consists of three domains and shares similarities in sequence and structure to the C-terminal and central domains of eRF1 (Graille et al., 2008), whereas the unrelated N-terminal domain contains an RNA-binding Sm fold (Atkinson et al., 2008; Graille et al., 2008). Although it was originally proposed that the Sm fold exhibited endonucleolytic activity on stem-loop-containing mRNAs (Lee et al., 2007), a more likely scenario is a destabilization of the mRNA in the ribosomal decoding center which renders it more accessible for subsequent degradation by auxiliary factors (Kuroha et al., 2010; Passos et al., 2009). Hbs1, like eRF3, possesses a G domain, domains II and III, and a variable N-terminal domain (Inagaki et al., 2003). Furthermore, similarly to termination factors, Dom34 and Hbs1 form a stable complex with high affinity to GTP (Carr-Schmid et al., 2002; Figure 5B, center). In crystal structures determined for both Dom34 alone (Graille et al., 2008; Lee et al., 2007) and in complex with Hbs1 (Chen et al., 2010; Kobayashi et al., 2010), the central domain of Dom34 is found in drastically different positions relative to the NTD. The cryo-EM reconstruction by Becker at el. confirmed that the conformation of Dom34-Hbs1 on the ribosome is similar to that observed in the complex crystal, and allowed modelling the active conformation of Dom34 after its delivery by Hbs1 (Becker et al., 2011). Due to these observed similarities between stalled ribosome recognition and translation termination, a homology model of eRF1-eRF3 action on the ribosome was built, where the attachment state left the central domain of eRF1 packed against eRF3, and the active terminating state would be defined as the drastic rearrangements in eRF1, allowing the GGQ loop of the central domain to move into close proximity to the CCA end of the P-site tRNA for peptidyl-tRNA hydrolysis (Becker et al., 2012).

Indeed, in a rabbit pre-termination complex visualized by cryo-EM, the central domain of eRF1 is packed tightly against eRF3 and its NTD reaches deep into the DC of the ribosome (des Georges et al., 2014; Taylor et al., 2012). Similar to the cryo-EM study with no-go decay factors (Becker et al., 2011), the complex was trapped using GDPNP, a non-

hydrolyzable analog of GTP, and therefore represents an initial stage of release factor attachment and stop codon recognition.

### 1.6.4 Ribosome recycling in eukaryotes

Contrary to the bacterial system, eukaryotes (and archaea) do not possess an RRF-like recycling factor. Instead, ABCE1, an essential adenosine triphosphatase (ATPase) is required for ribosome recycling (Pisarev et al., 2010). ABCE1 (aABCE1 in archaea, or Rli1 in humans and Rli1p in *S. cerevisiae*) was first discovered as an inhibitor of RNAse L which plays a crucial role in antiviral response in mammals (Bisbal et al., 1995). It has been suggested that in lower eukaryotes, ABCE1 inhibits RNAses involved in ribosome biogenesis (Kispal et al., 2005).

ABCE1 belongs to the highly-conserved family of ABC-cassette containing proteins. All ABC systems feature two nucleotide-binding domains (NBDs) that bind two ATP molecules. ABCE1 contains a conserved helix–loop–helix (HLH) motif, a hinge domain and an essential Iron–Sulphur (FeS) cluster domain containing two $[4Fe–4S]^{2+}$ clusters (Barthelme et al., 2007, 2011a; Karcher et al., 2005). ATP binding and hydrolysis by the NDBs likely induces a tweezer-like motion, where the protein shifts between a “closed” (ATP-bound) and an “open” conformation (upon release of ADP and inorganic phosphate) (Figure 6) (Becker et al., 2012). The two NBDs are not equal in their function or structure. The asymmetric FeS cluster domain is rather not implicated in electron transfer but plays a structural role. It extends into the cleft between the two NBDs and is presumably pushed out of this cleft when the protein adopts a “closed” conformation (Becker et al., 2012).

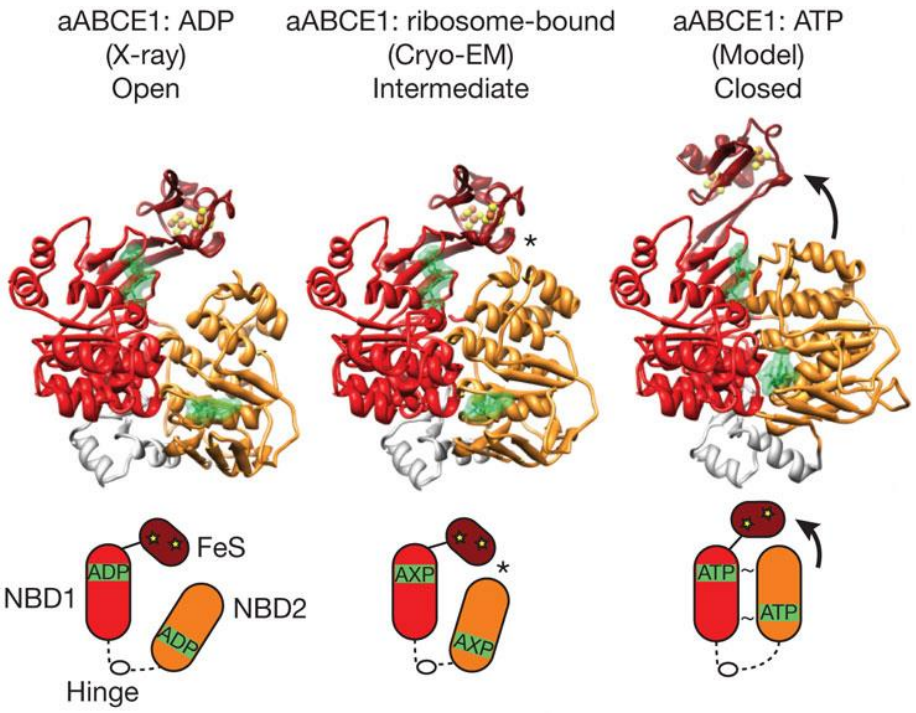


Figure 6. **Conformations of aABCE1**. FeS cluster domain marked in brown, with Fe-S clusters marked with spheres, NBD1 in red and NBD2 in orange, bound nucleotides in green. ABCE1 transitions from an "open", ADP-bound state, to a "closed", ATP-bound, conformation. An intermediate stage was observed in cryo-EM, with nucleotides not assigned. Adopting a closed conformation pushes the FeS cluster domain out from the cleft between the two NBDs. From Becker et al., 2012

Biochemical studies have indicated that ABCE1 stimulates translation termination by eRF1, independent of ATP hydrolysis and without enhancing recruitment of eRF1 to the ribosome (Shoemaker and Green, 2011). Also, peptide release is not required for ribosome splitting, as ABCE1 splits NGD substrates and vacant ribosomes in the presence of Dom34 and Hbs1, where Hbs1 has an auxiliary effect (Pisareva et al., 2011).

Important conclusions about the function of ABCE1 in translation termination and ribosome recycling were drawn from cryo-EM reconstructions of archaeal and yeast ribosome-Dom34-ABCE1 complexes (Becker et al., 2012). These structures show that ABCE1 binds the position of translational GTPases on the ribosome, therefore excluding simultaneous binding of Dom34/eRF1-Hbs1/eRF3 together with ABCE1. In these

complexes, the CTD of Dom34 contacts exclusively the FeS cluster domain of ABCE1 and its central domain is swung out toward the P-site tRNA (Figure 7A). Thus, Dom34 is fully engaged in the A-site, providing a broad interaction network in the ribosomal inter-subunit space. Importantly, ABCE1 was found in an intermediate "half-open" conformation (Figure 6), with NBD2 rotated toward NBD1 and contacting the FeS cluster domain, and the resolution of the reconstruction did not allow to identify the bound nucleotides. The conformation of the individual loops in both NBD1 and NBD2 rather resembled the ADP-bound state, possibly indicating an allosteric change in ABCE1 upon substrate binding. Assuming a "closed" conformation would require a further shift of the FeS cluster domain, which would most likely not suffice to split the ribosome. However, the shift could transmit conformational changes to Dom34 and induce ribosome splitting as a concerted action, by interrupting the inter-subunit bridges and destabilizing the P-site tRNA. Analogously, ABCE1 was predicted to stabilize the active, extended conformation of eRF1 capable of peptide release activity and facilitate ribosome splitting after canonical translation termination (Figure 7B) (Becker et al., 2012).

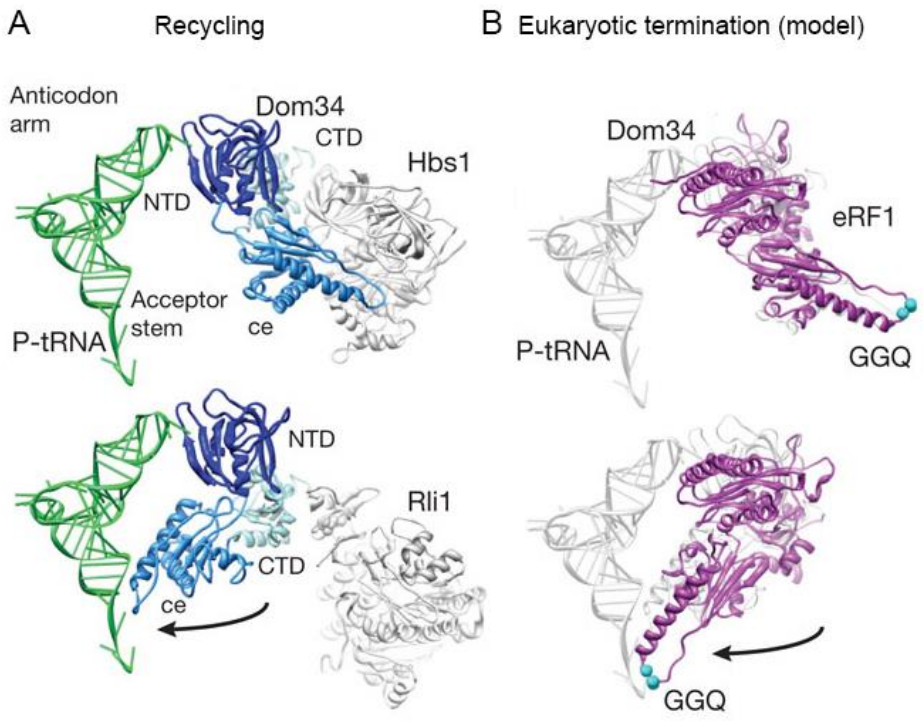


Figure 7. **ABCE1 (Rli1) stabilizes the active conformation of Dom34 or eRF1 on the ribosome.** Eukaryotic ribosome recycling in a no-go event (**A**) and model of eRF1 action on the ribosome (**B**). From Becker et al, 2012.

ABCE1 is also speculated to be involved in coupling ribosome recycling to the next round of initiation (Andersen and Leevers, 2007; Dong et al., 2004; Skabkin et al., 2013). In archaea ABCE1 was found to be bound to the small ribosomal subunit (Barthelme et al., 2011). Coimmunoprecipitation and cross-linking experiments showed that ABCE1 associates with initiation factors eIF3 (namely the non-essential eIF3j subunit), eIF2 and eIF5 in yeast, and 43S preinitiation complex formation and recruitment of eIF3 and eIF2 are strongly inhibited in ABCE1-depleted cells or with ATPase-defective ABCE1 (Dong et al., 2004). Whether ABCE1 regulates re-initiation is not clear, and there is little structural understanding of this process.

# 2 GOALS

This study had two major goals. The first goal was to obtain sub-nanometer cryo-EM structures of eukaryotic pre-termination (containing eRF1 and eRF3) and pre-recycling (containing eRF1 and ABCE1) complexes. These structures aim at getting mechanistic insights into how stop codons are recognized and how the peptide is hydrolyzed by eRF1. Furthermore, such structures challenge the model according to which conformational changes in eRF1 (Figure 7B) are similar to the observed structural rearrangements of no-go decay factor Dom34 (Becker et al., 2012).

The second goal aimed at getting structural insights into ABCE1-containing 40S complexes. This structure should clarify the conformational state of 40S-bound ABCE1 and whether 40S-ABCE1-complexes are stably associated with translation initiation factors to actively influence 43S-PIC formation.

The main obstacle for reaching the first goal was that stable termination complexes for cryo-EM have generally proven a challenge to obtain over the years, possibly due to the nature of the termination event itself and/or quick dissociation of termination factors from ribosomes during the vitrification process. Therefore, a multi-faceted approach for trapping reconstituted termination complexes had to be utilized in this work, without compromising on the overall suitability of the ribosomal substrate for a termination event. Namely, a ribosome would have to have a stop codon positioned in the A-site to be recognized by eRF1. Simultaneously, this terminating event should not have instantly proceeded to dissociation of factors and/or ribosome splitting. This challenge would be solved by saturating an *in vitro* translation extract with an mRNA coding for a stalling human cytomegalovirus (CMV) *gp48* uORF, which impairs the PTC while leaving the stop codon in the A-site (Bhushan et al., 2010). Stalling on this sequence has indeed been shown to specifically require eRF1 in human cells (Janzen et al., 2002). Then, purified termination factors would be *in vitro* reconstituted with the obtained the ribosome-nascent chain complexes (termed CMV-RNCs in this work). Reconstitution assays were to be performed with either *S. cerevisiae* or *T. aestivum* components in the

presence of non-hydrolysable GTP and ATP analogs GDPNP and ADPNP, as an additional level of arresting termination and/or recycling. The reasoning behind introducing *T. aestivum* RNCs, and therefore creating a "hybrid" system was based on previous attempts to visualize *S.cerevisiae* RNCs with *S.cerevisiae* termination factors by cryo-EM, which were not successful.

For the second goal, a native post-recycling complex was to be obtained and visualized by cryo-EM. This study complemented an *in vitro* reconstitution approach performed by colleagues in the Beckmann group and collaborators from the Tampé group at the University of Frankfurt. Native 40S-ABE1 complexes were to be obtained using affinity purification of genomically TAP-tagged ABCE1. ABCE1 was observed to associate with 40S and 80S in tandem affinity purifications (data not shown). The approach used in this work relied on separating the 40S fraction by sucrose density centrifugation and reconstructing the structures of the population of ABCE1-bound 40S using cryo-EM. Heterogeneity of the sample was then the main challenge to be expected. The purifications were thus supplemented with the non-hydrolysable analog of ATP (ADPNP): firstly, to prevent the release of ABCE1 from the small subunit; and secondly, to enable to induce conformational changes of ABCE1 required for ribosome binding.

# 3 METHODS

## 3.1 MOLECULAR BIOLOGY METHODS

### 3.1.1 Amplification of DP120 and DP120CMV DNA templates by PCR

The "CMV-stalling" construct encoded for a hexahistidine ($His_6$) tag for affinity purification of RNCs, a hemeagglutinine tag (HA-tag) for detection by Western blotting, the first 98 amino acids of a Dipeptidyl-aminopeptidase B containing a type II signal-anchor sequence and the stalling sequence of *gp48* uORF of cytomegalovirus and was prepared as described previously (Bhushan et al., 2010). The CMV DNA construct was generated by polymerase chain reaction (PCR) using a T7 standard forward primer (for subsequent *in vitro* transcription by T7 and then *in vitro* translation in wheat germ extract) with a reverse CMV (5'- TAAGGAGGAATATATTTGCAGGTCAGCAGGCTGCTCAGTTTTTTC-GCACTCAGCACCAGCGGTTCCA-TTTCAATTTTATTGTCACTAATCCATT-3') primer, using the DPAP-B120 (or "DP120") construct as a template, including the signal-anchor sequence of Dipeptidyl-aminopeptidase (Halic et al., 2004). The "DP120" construct is extensively characterized and was generated as described previously (Halic et al., 2004, 2006). Effectively, "DP120" alone yields a truncated mRNA which causes ribosome stalling, and "DP120-CMV" causes peptide-mediated stalling.

For a 200 µl PCR preparation 200 ng of template DNA fragment, 200 pmol of each forward and reverse primer, 20 µl dNPT solution (Fermentas), 20 µl of 20 x Taq- Buffer (40 mM Tris HCl (pH 8.4), 100 mM KCl) and 4 µl Taq-Polymerase (produced in house) were mixed and the volume was adjusted with water. The mixture was split into four tubes, 50 µl in each and PCR was performed as outlined in Table 1.

| Step | Temperature | Duration | Number of cycles |
|---|---|---|---|
| Initial denaturation | 98 °C | 2 min | 1 |
| Denaturation | 98 °C | 1 min | 29 |
| Annealing | 60 °C | 45 s | |
| Extension | 72 °C | 1 min | |
| Final extension | 72 °C | 2 min | 1 |

Table 1**. PCR Program for amplification of DP120 and DP120CMV DNA templates.**

The PCR-amplified fragments were purified with a QIAGEN PCR purification kit according to the manufacturers' instructions, where 50 µl water were used to elute the column-bound DNA instead of Elution buffer supplied in the kit.

### 3.1.2 *In vitro* transcription of DP120 and DP120CMV templates

mRNA transcripts were generated using T7 RNA polymerase largely according to mMessage mMachine kit (Ambion) instructions. A four-fold scale-up of the recommended single reaction volume utilized 4 µg of template DNA. No DNAse treatment was performed. The *in vitro* transcription reaction was incubated for 2 hours at 37°C and precipitated in LiCl solution. The final RNA pellet was resuspended in RNase-free water.

## 3.2 PROTEIN ANALYSIS

### 3.2.1 SDS-PAGE

Discontinuous sodium dodecylsulfate polyacrylamide gel electrophoresis (SDS-PAGE, (Laemmli, 1970) was performed on 15% polyacrylamide gels in 1xSDS running buffer (25 mM Tris, 192mM glycine, 0,1% (w/v) SDS). Before application on an SDS-gel, all samples were heated for 10 min at 65 °C. An unstained molecular weight marker from

New England Biolabs was used for molecular weight estimation. Samples in 1xSDS sample buffer (50 mM tris(hydroxymethyl)aminomethane (Tris)/HCl pH 6.8, 2% (w/v) SDS, 10% (v/v)glycerol, 0.1% (w/v) bromophenol blue, 100 mM 1,4-dithiothreitol (50 mM tris(hydroxymethyl)aminomethane (Tris) / HCl pH 6.8, 2% (w/v) SDS, 10% (v/v) glycerol, 0.1% (w/v) bromophenol blue, 100 mM 1,4-dithiothreitol) were loaded into the gel wells using a thin pipette tip and the electrophoresis was performed for 15 min at 160 V following at least 1 hour at 170 V, until the blue buffer dye was removed from the gel completely.

### 3.2.2 Simply Blue staining of SDS gels

SDS gels were carefully extracted from the glass chamber and heated in cooking water (three rounds of around 30 s in the microwave at 600 W) to remove SDS. The Simply Blue Coomassie staining solution (Novex) was then added to cover the gel, the gel was cooked for another 30 s in the solution and left for at least 10 min at ambient temperature afterwards to complete staining.

### 3.2.3 Western blotting

Proteins in SDS-page gels were transferred (Towbin et al., 1979) onto a methanol-activated polyvinylidene difluoride (PVDF) membrane (Mozdzanowski and Speicher, 1992) using the semi-dry blotting method in blotting buffer (20% (v/v) methanol, 48 mM Tris/HCl, 39 mM glycine, 0.037% (w/v) SDS) for 45 min at 1 mA/cm². Amido Black staining of the membrane allowed visualization of protein bands for assessment of blotting efficiency. Staining was performed in Amido Black solution (0.1% (w/v) naphthol blue black, 7.5% (v/v) acetic acid, 20% (v/v) ethanol) for 1 min on a laboratory shaker, then destained (40% (v/v) ethanol, 10% (v/v) acetic acid) until bands were clearly visible and the membrane background color generally reverted to white. For HA-tag detection, the membrane was first incubated in blocking solution (5% (w/v) Milk powder in 1xTBS (20 mM Tris HCl pH 7.6, 150 mM NaCl) for 30 min at ambient temperature or for 15h at 4°C to avoid unspecific antibody binding. The membrane was shortly washed in 1xTBS and then incubated in primary antibody solution (mouse α-HA diluted 1:1000 in blocking

solution) for 1 hour at ambient temperature. Next, the membrane was washed two times for 10 minutes with 1xTBS-T (1xTBS with 0,1% (v/v) Tween) and once in 1xTBS, then incubated in secondary antibody solution (Goat α-Mouse HRP conjugate, 1:5000 in blocking solution) for 1 hour at ambient temperature. Another set of three washes was performed as above and secondary antibody was detected using the Pierce ECL Western Blotting Substrate chemiluminescence detection kit (Thermo Fischer) and visualized in a Fujifilm LAS-3000 Imager.

## 3.3 PROTEIN PURIFICATION

### 3.3.1 Purification of eRFs using the IMPACT method (NEB)

eRF1 and eRF3ΔN97 were cloned into pTYB2 (part of the IMPACT system by NEB) vector between the NdeI and SmaI sites. The plasmids were kindly provided by Dan Eyler from the Rachel Green lab. The constructs were transformed into Rosetta BL21(DE3) cells according to the cell manufacturer's instructions and plated onto lysogeny broth (LB) ampicillin/canamycin (AMP100/CAM34) plates for antibiotic selection. Colonies were selected and used for propagation of 5 ml of "overnight" culture for 15 h, in LB media containing AMP100/CAM34. Cells were inoculated into 1 L of rich media (Terrific Broth) and cell growth was monitored at 37 °C. At $OD_{600}$ of around 0.6 per ml, the cultures were transferred to an ice-water bath and incubated for 20 min. IPTG was added to induce target protein expression to a final concentration of 0.1 mM. The cultures were then incubated for 15 h at 16 °C in a shaking incubator. The cells were harvested by centrifugation at 3500x g for 10 min and washed with cold 1% KCl. Cell pellets were resuspended in 40 ml lysis buffer eRF1 (20 mM HEPES pH 7.5, 500 mM NaCl, 1 mM EDTA) or lysis buffer eRF3 (20 mM HEPES pH 7.4, 500 mM NaCl, 0.1 mM GTP) and lysed using a French Press. The lysate was clarified by centrifugation at 20xk *g* for 30 min in a Type 45 Ti rotor (Beckmann Coulter) and loaded on Chitin beads (NEB), 2 ml bed volume per 1 L of expression culture. The column was washed with 20 CV of corresponding lysis buffer and 20 CV of wash buffer (20 mM HEPES pH 7.4, 1 M NaCl, 1 mM EDTA). The column was then flushed with 3 CV of elution buffer (20 mM HEPES pH 7.4, 500 mM KCl, 1 mM EDTA,

50 mM DTT) and incubated for 16 h at 4 °C. The column was then drained and washed with elution buffer until final eluate volume of 10 ml across all fractions.

### 3.3.2 Gel filtration of eRF1 and eRF1+eRF3ΔN97

Prior to gel filtration, the eRFs (160 µl for each factor, estimated 50 µg per preparation) were concentrated in Millipore centrifugal filter units (Invitrogen; threshold 10 kDa) in gradual 5-min steps in a table-top centrifuge (5417/R, Eppendorf) at 5000 rpm at 4°C. Every step 50 µl of gel filtration buffer (20mM HEPES pH 7.5, 200 mM KCl, 2 mM DTT, 1.5 mM $MgCl_2$, 10% Glycerol). eRF1 and eRF3 were incubated together in gel filtration buffer in the presence of 500 µM GDPNP on ice for 15 min prior to sample injection. Gel filtration was performed through a Superdex 200 10/300 GL column (volume 24 ml, injection volume maximum of 500 µl) on the ÄKTA purification system at a flow rate of 0.4 ml/min and fraction collection volume of 200 µl starting at 8 ml (after passing of the void volume). The collected fractions were analyzed by SDS-PAGE and Simply Blue staining.

### 3.3.3 Purification of ABCE1

C-terminally $His_6$-tagged ABCE1 was purified from *S. cerevisiae* by A. Heuer according to the procedure described by Shoemaker and Green, 2011. The cell line containing the pYES2 plasmid encoding for $His_6$-tagged ABCE1 was kindly provided by the Green lab. INVSc1 cells (Invitrogen) were induced at 30 °C for 16 h. Cells were resuspended in Ni-NTA lysis buffer (75 mM HEPES pH 8.0, 300 mM NaCl, 5 mM beta-mercaptoethanol, 1% Tween, 20 mM imidazole, 10% glycerol), frozen in pellets and lysed using a French Press. Lysate was clarified and purified over a HisTrap FF column (GE Healthcare) on an ÄKTA FPLC (GE Healthcare). Additional purification was conducted over an S200 size exclusion column (GE Healthcare) pre-equilibrated in Buffer SE (20 mM Tris-Cl pH 7.5, 200 mM NaCl, 5 mM beta-mercaptoethanol, 5% glycerol). A UV-visible absorbance scan of purified ABCE1 exhibits a pronounced shoulder at approximately 390 nm, characteristic of $[4Fe\text{-}4S]^{2+}$ cluster containing proteins. Successful purification was indicated by a brown/yellow color of the final preparation.

## 3.4 GENERATION OF RIBOSOME-NASCENT CHAIN COMPLEXES

### 3.4.1 Preparation of wheat germ translation extracts

Wheat germ translation extract was prepared according to Erickson and Blobel, 1983, with minor modifications. Wheat germs were floated twice in a mixture of 50-70 ml cyclohexane and 250 ml carbon tetrachloride and dried on filter paper under the fume hood. The wheat germs were then shock-frozen in liquid nitrogen and ground using the Retsch PM100 planetary bead mill for 5 cycles, 3 min each at 400 rpm. Further steps were performed at 4° C unless stated otherwise. The wheat germ powder was resuspended and thawed in 2x homogenization buffer (40 mM HEPES/KOH pH 7.6 100 mM KOAc, 5 mm $Mg(OAc)_2$, 2 mM $CaCl_2$, 4 mM DTT, 0.5% (w/v) EDTA-free complete protease inhibitor pill, 0.4 U/ml Anti-RNAse (Invitrogen) in such a proportion that the resuspended material had the consistency of thick paste (approximately 12 ml for 5 g of ground wheat germ). The lysate was centrifuged for 20 min at 20 000 rpm at 4°C in a SS34 rotor (Thermo Scientific), the cell debris were discarded. The clarified lysate was then further centrifuged in a TLA110 rotor (Beckman Coulter) for 30 min at 30 000 rpm and 4° C. The supernatant was applied onto PD10 Sephadex G25-M (GE Healthcare) columns pre-equilibrated with 1 x homogenization buffer (20 mM HEPES/KOH, pH 7.6, 50 mM KOAc, 2.5 mm $Mg(OAc)_2$, 1 mM $CaCl_2$, 2 mM DTT, 0.5% (w/v) EDTA-free complete protease inhibitor pill, 0.4 U/ml Anti-RNAse) and eluted in three steps with 1 x homogenization buffer. All fractions of the first elution step were pooled, and $A_{260}$ was measured to assess quality (an extract with a $A_{260}$ of 200 per 1 ml or higher was considered effective).

### 3.4.2 *In vitro* translation

DP120 and DP120CMV RNCs were generated in a total volume of 1200 µl translation mix containing 50% (v/v) wheat germ extract supplemented with 14 mM HEPES/KOH pH 7.6, 75 mM KOAc, 1.25 mM $Mg(OAc)_2$, 2 mM DTT, 1.25 mM ATP, 0.25 mM GTP, 16 mM Creatine Phosphatase, 0.45 µg/µl Creatine Kinase, 50 ng/µl tRNA (Roche), 0.4 mM spermidine, 0.1 mM amino acid mixture (Promega), 0.15 U/µl RNAsin (Promega) and 10 ng/µl mRNA template. The reaction mixture was split into three tubes equally and

incubated at 30 °C for 60 min in a thermomixer. The reaction was terminated by addition of 0.2 µg/µl cycloheximide.

### 3.4.3 $His_6$-tag affinity purification of RNCs

Each of the 400 µl *in vitro* translation reactions from a total of 1200 µl was applied onto a 800 µl sucrose cushion (50 mM Tris/HCl pH 7.0, 500 mM KOAc, 25 mM $Mg(OAc)_2$, 5 mM ß-mercaptoethanol, 1 M sucrose, 10 µg/ml cycloheximide, 0.1 % Nikkol, cOmplete protease inhibitor cocktail - 1 pill per 50 ml buffer) and centrifuged in TLA 110 rotor (Beckmann Coulter) for 45 min at 100 000 rpm at 4 °C to pellet all ribosomes. All further steps were performed on ice unless stated otherwise. The supernatants were removed immediately. The ribosomal pellets were resuspended in 750 µl of 250 buffer (50 mM Tris/HCl pH 7.0, 250 mM KOAc, 25 mM $Mg(OAc)_2$, 250 mM sucrose, 0.1 % Nikkol, 5mM ß-mercaptoethanol, 10 µg/ml cycloheximide, 0.5 % (w/v) EDTA-free complete protease inhibitor pill) for 45 minutes.

1 ml TALON metal affinity resin (GE Healthcare) slurry was transferred to two large Poly-Prep gravity flow columns (Bio-Rad). The resin was equilibrated with 5 ml 250/tRNA buffer (250 buffer with 10 µg/ml tRNA mix) in each column. The resuspended ribosomes were applied onto the resin in the closed column and incubated for 5 min on a turning wheel at ambient temperature. The preparations were then washed with 8 column volumes (CV) of 250 buffer and 2 CV of 500 buffer (250 buffer with 500 mM KoAc). The RNCs were incubated in 1.5 ml 250/100 buffer (250 buffer with 100 mM Imidazol, pH 7.1) for elution, for 5 min at ambient temperature and resuspended in additional 250/100 buffer (to total volume of 3 ml). The eluates were applied onto two 400 µl sucrose cushion solutions and centrifuged in TLA 110.4 (Beckmann Coulter) for 45 min at 100 000 rpm at 4°C. The supernatant was discarded immediately and the RNC pellets were carefully resuspended in 30 µl Grid buffer (20 mM Tris/HCl pH 7.0, 50 mM KOAc, 2.5 mM $Mg(OAc)_2$, 1 mM DTT, 125 mM Saccharose, 0.05% Nikkol, 100 µg/ml Cycloheximid, 0.5% (w/v) EDTA-free complete protease inhibitor pill, 0.2 U/µl RNAsin) for 1 h.

## 3.5 RECONSTITUTION OF RIBOSOMAL COMPLEXES

### 3.5.1 Peptide release assays

2 pmol DP120 or DP120CMV RNCs were incubated with a ten-fold molar excess of preformed eRF1-eRF3-GDPNP, eRF1 alone or eRF1 and ABCE1 in binding buffer (20 mM HEPES pH 7.5, 200 mM KCl, 1.5 MgCl2, 2 mM DTT, 10 µg/ml cycloheximide, supplied with 500 µM GDPNP, GTP or ADPNP, respectively). Puromycin was added to a final concentration of 0.1 mM. The assays were incubated for 1 h at 27 ºC and analyzed by Western blot for HA-tag.

### 3.5.2 Preparation of *in vitro* reconstituted samples for Cryo-EM

In a total volume of 25 µl, CMV RNCs were brought to a final concentration of 4 $A_{260}$ units/ml. RNCs were incubated with a ten-fold molar excess of preformed eRF1-eRF3 complex in gel filtration buffer or eRF1 and ABCE1 in grid buffer (20 mM HEPES pH 7.5, 200 mM KCl, 1.5 MgCl2, 2 mM DTT, 10 µg/ml cycloheximide, 0.05 % Nikkol, 0.03 % DBC, 500 µM GDPNP/ADPNP). Mammalian Sec61 was added at a five-fold molar excess to avoid orientational bias on the cryo-grids. Cryo-grids (diameter of 3 mm, around 80 meshes per cm) were ionized under vacuum (2.6 mbar) for 30-45 seconds in a plasma cleaner (ionization of the hydrophobic carbon film makes increases affinity to aqueous samples, see (Wagenknecht et al., 1988). 3,5 µl of sample were applied onto the grid and vitrified using a vitrification robot (Vitrobot) by assigned personnel.

## 3.6 GENERATION OF NATIVE 40S-ABCE1 COMPLEXES

### 3.6.1 Tandem-affinity purification of native ribosome-ABCE1 complexes from *S. cerevisiae* extract

The TAP-tagged ABCE1 *S. cerevisiae* strain was purchased from the EUROSCARF bank (SC1900, MATa leu2-3, 112 trp1-289 ade2 arg4 ura3-52 rli1::TAP-KlURA3). Cultures were grown in Yeast Extract Peptone Dextrose (YPD) media to an $OD_{600}$ of 1.5 (at least 5 L culture for one preparation of native 40S complexes). The cells were pelleted and washed with 1% KCl at 4 °C, then incubated for 15 min at 25 °C in 10 mM DTT, 100 mM

Tris pH 8.0, and finally gently mixed 1:1 w/v with lysis buffer (50 mM Tris-OAc, pH 7.5, 15 mM $Mg(OAc)_2$, 50 mM KOAc, 1 mM DTT, 300 nM ADPNP, 300 nM GDPNP, 500 nM PMSF, 0,5 % pill cOmplete EDTA-free Protease Inhibitor Cocktail). The cell suspension was processed in a French press at 1.5 MPa three times (or alternatively, by using HCl-washed glass beads with a diameter of 0.25 mm on a vortex in steps of 30 s and 1 min ice incubation, for 10 steps) and the lysate was centrifuged in a SS-34 rotor (Thermo Fisher) at 27,000 × g for 15 min to remove cell debris. The lysate was clarified in a Type 45 Ti rotor (Beckman Coulter) for 20 min at 119,000 × g. The cleared lysate was incubated with IgG Sepharose 6 FastFlow beads (GE Healthcare) applied on a gravity flow Bio-Rad column for 1 h at 4 °C. Beads were washed with TAP buffer (50 mM Tris-OAc, pH 7.5, 15 mM $Mg(OAc)_2$, 50 mM KOAc, 1 mM DTT, 500 nM PMSF, 0,5%pill cOmplete EDTA-free Protease Inhibitor Cocktail). For elution, the beads were incubated with AcTEV protease according to manufacturer's instructions (Invitrogen) in TAP buffer for 90 min at 4 °C.

### 3.6.2 Sucrose density gradient purification of 40S-ABCE1 complexes

5% and 30% v/v sucrose solutions were prepared in TAP buffer (see above) and gradients were prepared on the automatic gradient fractionator platform. The eluate from AcTEV cleavage was applied onto the gradient and centrifuged in a SW41 rotor (Beckman Coulter) for 15 h at 56,000 × *g.* The gradient was automatically fractionated and $UV_{280}$ reading curve was monitored for the characteristic peaks corresponding to 40S and 60S. 40S fractions were collected and sucrose was removed using a PD-10 buffer-exchange column (GE Healthcare). The sample was then applied directly on the cryo-grid for data collection.

## 3.7 CRYO-EM AND IMAGE PROCESSING

### 3.7.1 *In vitro* reconstituted pre-termination and termination/pre-recycling complexes

Both datasets (RNC-eRF1-eRF3 and RNC-eRF1-ABCE1) were collected at 300 keV at a magnification of 147,136 × at the plane of the CCD using a TemCam-F416 CMOS

camera (TVIPS GmbH, 4096 × 4096 pixel, 15.6 µm pixel, 1 s/full frame) resulting in an image pixel size of 1.06 Å (object scale). The particles were picked with starfish_boxing version 0.2.0, which is part of the StarFish single particle analysis program suite developed at the time by Andreas Hauser (Preis et al., 2014). Starfish_boxing detects electron-dense features by binarizing the raw micrographs into pixels, above or below an expected threshold. The binarization of the micrograph uses two arithmetic mean filtered images representing foreground and local background and are computed with either a very fast real space SSE2 implementation of with an FFT library. For a given dataset, two parameters are required: the expected radius of the particle and a threshold for the binarization. After the binarization, many connected components ("white areas") are generated, in the shape of the densities, i.e. particles, ice or similarly sized contamination. The connected components are then detected with the following algorithm. Based on the assumption that most connected components are particles, a filter based on the median box size is used to filter out non-particles and provide coordinates. The final coordinates were used for boxing out the particle images followed by import into SPIDER software (Frank et al., 1996).

The 80S-eRF1-eRF3 dataset (224,689 particles) was first sorted for presence of P-site tRNA, by introducing a programmed yeast ribosomal template at low resolution (20 Å) as reference and a non-ribosomal “edge” volume, followed by sorting for the presence of factors at the translation factor binding site, where one of the resulting densities from a previous sorting round would be filtered to around 20 Å and introduced as reference. For the final reconstruction, 39,309 particles were used. The 80S-eRF1-ABCE1 dataset (149,673 particles) was carried out in the same way with 51,049 particles used for the final reconstruction. The final datasets were also subjected to refinement using the “gold-standard” approach applied by the RELION software (Scheres, 2012) as advised by manuscript reviewers. According to this approach, the dataset is split into two data subsets that are refined independently. The resolution was read at a Fourier shell correlation (FSC) of 0.143 (in contrast to 0.5 in SPIDER).

### 3.7.2 Native 40S-ABCE1 post-splitting complex

The native 40S–ABCE1 data set was collected and processed in the same way as the reconstituted sample using MotionCor2, GCTF, Gautomatch and RELION-2 (see Heuer et al., 2017). 2D classes displaying non-ribosomal particles as well as the fatty acid synthetase (FAS) were discarded. After 3D refinement of 131,000 particles, 3D classification was performed. In the first round three classes (63.0%, 82,000 particles) showed a clear density for ABCE1 and two of them presented additional extra density emerging from the P-site. These two classes were combined (43.5%, 57,000 particles) and subjected to an additional round of classification. Here, four out of five classes only differ in the appearance of density in the P-site. One class displayed additional density in the position where eIF1A is located. This class (17.6%, 9,500 particles) was refined to a final resolution of 14 Å according to the gold standard criterion (FSC = 0.143).

## 3.8 MOLECULAR MODEL BUILDING

### 3.8.1 Pre-termination and terminaton/pre-recycling complexes

The *Triticum aestivum* 80S ribosome model was used as basis (updated model, pdb codes 3J5Z, 3J60, 3J61 and 3J62) (Armache et al., 2010a). Homology models of the central and NTD of eRF1 were built using HHPRED (Soding et al., 2005) on the basis of *Homo sapiens* and *S. pombe* crystal structures (Cheng et al., 2009; Loh and Song, 2010) (PDB accession 3E20 and 1DT9). The CTD (including the mini domain insert that is not present in the crystal structures) was modelled based on a NMR structure of the CTD of human eRF1 (PDB accession 2KTU) (Mantsyzov et al., 2010). The GGQ loop (residues 177-183 of eRF1) was modelled on the basis of the GGQ loop of bacterial RF2 (PDB accession 2XRT) (Jin et al., 2010) and RF1 (PDB accession 3MR8) (Korostelev et al., 2010). The eRF3 homology model was built on the basis of crystal structures of *S. pombe* Hbs1 (PDB accession 3MCA) (Chen et al., 2010) and eRF3 (PDB accession 1R5O) (Kong et al., 2004). Models for ABCE1 in the open ADP-bound, intermediate and closed ATP-bound state were described previously (Becker et al., 2012). Individual domains of eRF1 and eRF3 were fit as rigid bodies first and then manually adjusted using USCF Chimera (Pettersen et al.,

2004) and Coot (Emsley and Cowtan, 2004). Final models were minimized in UCSF Chimera and clashes were removed using VMD (Phillips et al., 2005) and MDFF (Trabuco et al., 2008). To validate the quality of the models, the cross-resolution between the maps and the model was calculated. Using Chimera, a map from the model-pdbs was generated and the resolution between the model maps and experimental maps was calculated. This was performed for the entire ribosome as well as for individual factors eRF1, eRF3 and ABCE1. Isolated densities for the factors were extracted using soft masks in SPIDER.

### 3.8.2 Native 40S-ABCE1 post-splitting complex

For molecular interpretation of the highly-resolved *in vitro* reconstituted post-splitting complex (Heuer et al., 2017), the crystal structure of the yeast 40S ribosomal subunit (PDB 4V88) (Ben-Shem et al., 2011) was used. Homology models of ABCE1 were generated based on the crystal structures of archaeal ABCE1 and known structures of the closed state of other ABC transporters MalK (Oldham and Chen, 2011), BtuCD (Korkhov et al., 2014), and MJ0796 (Smith et al., 2002). The obtained model of ABCE1 in the post-splitting state (Heuer et al., 2017) was fit as rigid body into the extra density on the 40S without any further adjustments. eIF1A from PDB 4UER, and $tRNA_i$ from PDB 3JAP were identified based on 43S and 48S initiation complex structures by Llácer et al., 2015 and Aylett et al., 2015. Difference maps were generated in UCSF Chimera (contoured at 3.5 σ).

# 4 RESULTS

## 4.1 GENERATION OF RIBOSOME-NASCENT CHAIN COMPLEXES, PURIFICATION OF TERMINATION AND RECYCLING FACTORS AND PEPTIDE RELEASE ASSAYS

The first aim of this work was *in vitro* reconstitution of pre-termination/pre-recycling complexes from purified components.

Stable ribosomal complexes were generated by employing a stalling polypeptide sequence from the human cytomegalovirus (CMV) *gp48* uORF. This sequence stalls translation by inhibiting eRF1-mediated peptide release, leaving a UAA stop codon in the ribosomal A-site (Bhushan et al., 2010). To generate pre-termination complexes, eRF1 and eRF3 were purified individually and added to the RNCs as a complex, which was formed on a Superdex 200 size exclusion column in the presence of GDPNP. For pre-recycling complexes, RNCs were reconstituted with purified eRF1 and ABCE1. Release assays were performed to assess the functional relevance of the reconstituted complexes.

### 4.1.1 Purification of recombinant eRF1 and eRF3

Purification of *S. cerevisiae* eRF1 and eRF3 for subsequent reconstitution experiments relied on the IMPACT system (NEB). This method is based on the inducible self-cleavage activity of protein splicing elements (termed inteins) (Anraku et al., 2005) to separate the target protein from the affinity tag. Each intein tag contains a chitin binding domain (CBD) for the affinity purification of the fusion protein on a chitin resin. Induction of on-column cleavage using dithiothreitol (DTT) releases the target protein from the intein tag.

The pTYB2 plasmid constructs of *S. cerevisiae* eRF1 and eRF3 were kindly provided by the Rachel Green group at Johns Hopkins University School of Medicine, USA. All experimental work was conducted with wild-type eRF1 and eRF3ΔN97, a truncation of eRF3 that lacked the prion-forming part of the N-domain (Ter-Avanesyan et al., 1994). Overnight expression of target proteins was carried out in *Rosetta*™ competent cells

(Novagen) in rich medium (Figure 8). This cell line facilitates expression of genes that encode rare *E. coli* codons. Yields were estimated at 3,7 mg and 1,5 mg purified protein of wild type eRF1 and eRF3ΔN97, respectively, per liter of induced culture. Some degradation could be observed in eRF3 elution fractions (Figure 8).

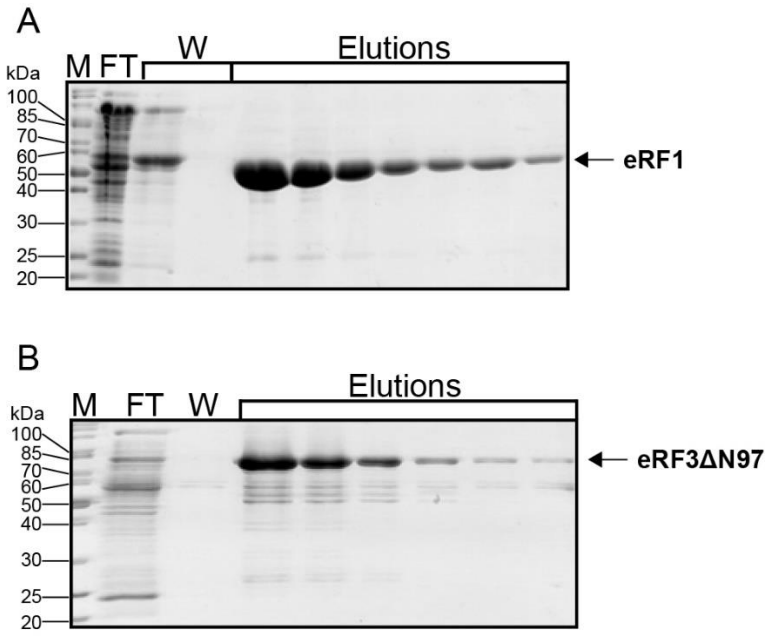


Figure 8. **Purification of recombinant eRF1 and eRF3.** SDS-PAGE analysis of purifications of wild-type eRF1 (**A**) and eRF3ΔN97 (**B**). Fractions corresponding to molecular weight marker (M), flow through (FT, 3µl), washes (W, 10 µl) and elutions (10 µl) are labelled.

### 4.1.2 Purification of ABCE1

The *S. cerevisiae* cell line containing the pYES2 plasmid encoding for $His_6$-tagged ABCE1 was kindly provided by the Rachel Green lab. C-terminally $His_6$-tagged ABCE1 was purified by Dr. André Heuer according to the procedure described by Shoemaker and Green, 2011. As a last step, size exclusion chromatography was monitored for the appearance of a pronounced shoulder at 390 nm in the purification profile. This is typical for proteins containing $[4Fe\text{-}4S]^{2+}$ clusters (Hatchikian et al., 1989). Successful purification was indicated by a brown/yellow color of the final preparation.

### 4.1.3 eRF1-eRF3:GDPNP complex formation

Similar to other translational GTPases and their A-site binding partners, eRF3 and eRF1 form a stable complex in solution (Cheng et al., 2009; Loh and Song, 2010). In this work, purified recombinant eRF1 and eRF3 were incubated together in 500 μM GDPNP and loaded onto an ÄKTA purifier equipped with a Superdex 200 10/300 GL size-exclusion column (volume 24 ml). To assess complex formation, eRF1 and eRF3 were first loaded onto the column for separate runs, to obtain their respective elution profiles indicated by $A_{280}$ absorbance (Figure 9). High-molecular weight aggregates were expected to elute early, and eRF3 had higher propensity for aggregation than eRF1. eRF3 eluted at 12,4 ml and the eRF1 elution peak was observed at 14,2 ml. When both proteins were loaded together, the new elution peak was observed at 11,8 ml, indicating the formation of a higher-molecular-weight complex. The peak fractions were collected and analyzed by SDS-PAGE (see Figure 9), and the fractions with the stoichiometric complex with minimal degradation were used for subsequent reconstitution experiments.

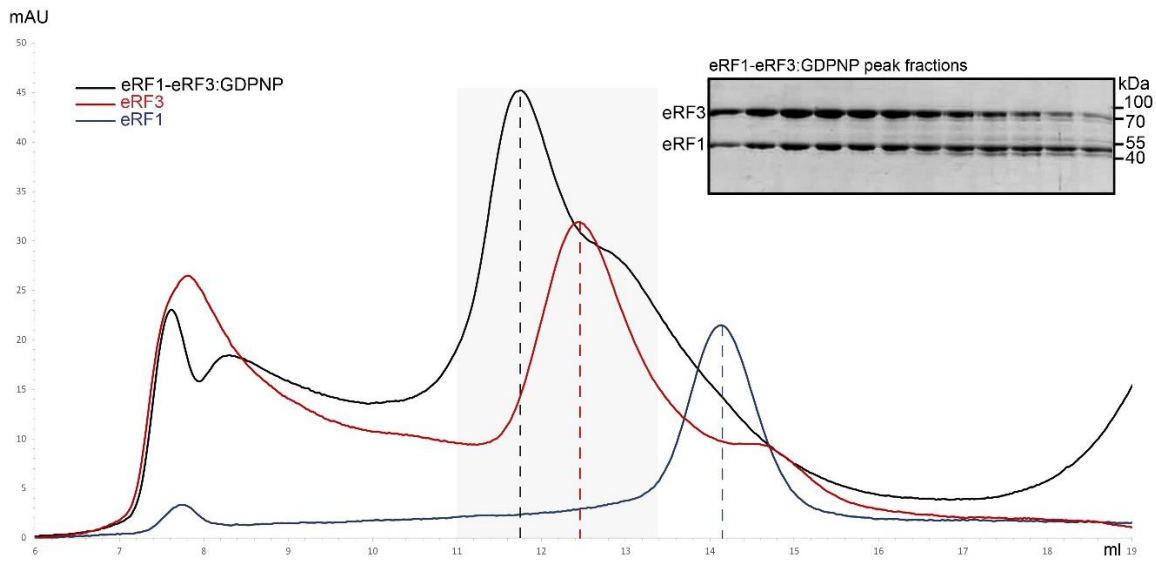


Figure 9. **Gel filtration profiles of eRF1, eRF3 and eRF1-eRF3:GDPNP complex.** Peak elutions marked with dotted lines for each profile. Peak fractions of eRF1-eRF3:GDPNP (light grey rectangle, from 11 ml to 13,4 ml mark) were analyzed by SDS-PAGE, where 10 µl of each 200 µl fraction were loaded onto the gel.

### 4.1.4 Purification of ribosome-nascent chain complexes

A self-made *T. aestivum* (wheat germ) *in vitro* translation extract was prepared according to a protocol adapted from Erickson and Blobel, 1983. The extract was programmed to generate CMV-stalled RNCs by saturating the *in vitro* translation mixture with the designed mRNA. The mRNA construct encoded for a hexahistidine ($His_6$) tag for affinity purification of RNCs, a hemeagglutinine tag (HA-tag) for detection by Western blotting, the first 98 amino acids of a Dipeptidyl-aminopeptidase B containing a type II signal-anchor sequence and the CMV stalling sequence, and transcribed *in vitro* by T7 polymerase (Bhushan et al., 2010). Additionally, a truncated mRNA (encoding the first 120 aa of Dipeptidyl-aminopeptidase B and excluding the CMV staller, (Halic et al., 2004) was used to purify RNCs for comparative functional peptide release assays (Figure 10). Translational stalling was indicated by detection of the HA-tag in the peptidyl-tRNA by Western blotting.

### 4.1.5 Peptide release assays

Peptide release assays were assembled to assess the functionality of the heterologous complexes described in this work. Release of free peptide was monitored by Western blotting and detection of the expressed HA-tag and quantified using the image analysis software ImageJ (Figure 10). Here, the relative amount of released peptide was calculated as a proportion of the intensity of chemiluminescent signal in a selected square around the free peptide band to the summed intensities of signals from the squares corresponding to both free peptide and peptidyl-tRNA. First, RNCs stalled on a truncated mRNA (TR-RNCs) and CMV-RNCs were incubated with puromycin to evaluate their overall potential to release the peptide. Puromycin is an aminonucleoside antibiotic that inhibits transfer of the peptide chain by binding the ribosomal A-site and mimicking the CCA-end of a tRNA, therefore causing premature peptide release in elongating ribosomes (Garreau de Loubresse et al., 2014). When TR-RNCs are incubated with the antibiotic, the peptide is quantitatively released (around 95% of signal can be assigned to free peptide). CMV-RNCs are less sensitive to puromycin, releasing around 75%. When incubating CMV-RNCs with eRF1 or both eRF1 and eRF3 (with either GDPNP or GTP), the relative amounts of released peptide were near negative-control levels. A spike in peptide release (up to around 70%) was observed when incubating CMV-RNCs with eRF1 and ABCE1 in the presence of ADPNP.

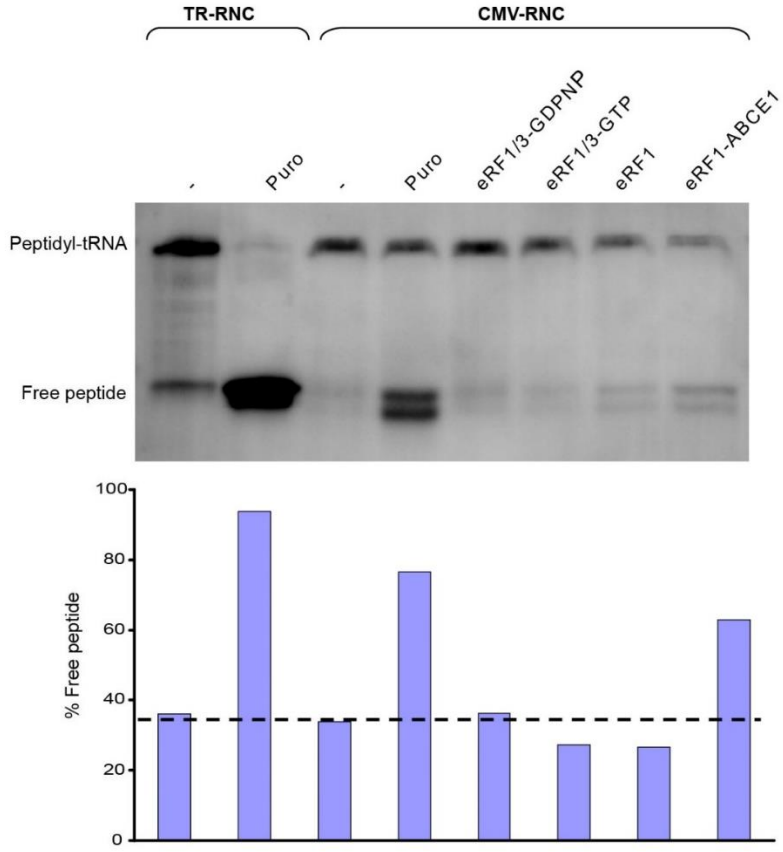


Figure 10. **Release assays of CMV-RNC with puromycin or release/recycling factors.** CMV-RNCs with a stop-codon in the A-site were either treated with puromycin or incubated with a 5-fold molar excess of release/recycling factor complexes and subjected to analysis by Western blotting where the HA-tag was detected. Bands for peptidyl-tRNA and free peptide are indicated. As a measure for release activity the relative amount of free peptide was quantified using ImageJ. Base-line release of peptide from CMV-RNCs corresponding to negative control is indicated with a dotted line. From Preis et al., 2014.

## 4.2 GENERATION OF RECONSTITUTED PRE-TERMINATION AND PRE-RECYCLING COMPLEXES FOR CRYO-EM

### 4.2.1 Sample preparation

CMV-RNCs from *T. aestivum* were incubated with a ten-fold molar excess of preformed eRF1-eRF3:GDPNP complex or with eRF1 and ABCE1 in the presence of ADPNP. Additionally, the Sec61 translocon was added in five-fold molar excess to saturate the hydrophobic signal-anchor sequence of the DPAP-B reporter emerging from the tunnel exit of the 60S. It has been observed that the hydrophobic signal-sequence tends to attach to the grid surface, resulting in a preferred orientation of the ribosomes on the cryo grid (data not shown). Sec61 is involved in the co-translational import of proteins into the endoplasmic reticulum and binds the ribosomal exit site and the signal sequence directly, therefore saturating the exposed hydrophobic sequence (Gogala et al., 2014).

The reconstituted samples were applied onto holey carbon coated Quantifoil grids and vitrified. After micrograph collection and initial pre-processing of the datasets, where micrographs containing ice contaminations or areas “burned” due to thin ice coating were removed, particles were picked, boxed out, and the images were imported into the SPIDER software package (Frank et al., 1996) for further processing.

### 4.2.2 Cryo-EM data processing and resolution determination

It was expected that not all identified particles could be ribosomal and could still include false positives such as ice contaminations. Also, heterogeneity of the sample was expected, whereby not all ribosomal particles would be factor-bound. Therefore, semi-supervised computational sorting was performed on both datasets. As a first reference volume, an 80S *S. cerevisiae* ribosome containing a P-site tRNA and filtered to 20 Å was offered, along with a non-ribosomal “edge volume” to exclude contaminations. Then, the datasets were further sorted for presence of termination or recycling factors at the translation factor binding site. Appearance of the Sec61 translocon served as an additional control for the datasets (Figure 11).

For the final 80S-eRF1-eRF3 reconstruction, 39 309 particles (17,5 %) from a total of 224 689 were used. The resolution was determined to 8.75 Å at a Fourier shell correlation (FSC) cut-off of 0.5. The final 80S-eRF1-ABCE1 reconstruction contained 51 049 particles (31 %) from the initial 149 673 and was resolved to 9.15 Å. In SPIDER, resolution is assessed by FSC curves between reconstructions from halves of the dataset, although a single model is used for the angular assignments. Therefore, this model may induce false correlations between the half-reconstructions. Furthermore, low-pass filtering to the exaggerated resolution may induce further accumulation of noise during multiple refinement iterations, ultimately leading to noise enhancement and an inflated resolution estimate. This phenomenon is termed over-refinement, or overfitting. More realistic estimates of resolution could be obtained by “gold-standard” FSCs, where two subsets of the dataset are refined independently and are therefore free of false correlations. To confirm the resolution of the final reconstructions, the “gold-standard” approach was used within the refinement framework of the RELION software (Scheres, 2016; Scheres and Chen, 2012). At the 0.143 FSC cut-off, the resolution was calculated as 8.90 Å for the 80S-eRF1-eRF3 reconstruction, and 8.56 Å for the 80S-eRF1-ABCE1 reconstruction, which was in good agreement with the estimates obtained in SPIDER (Figure 11).

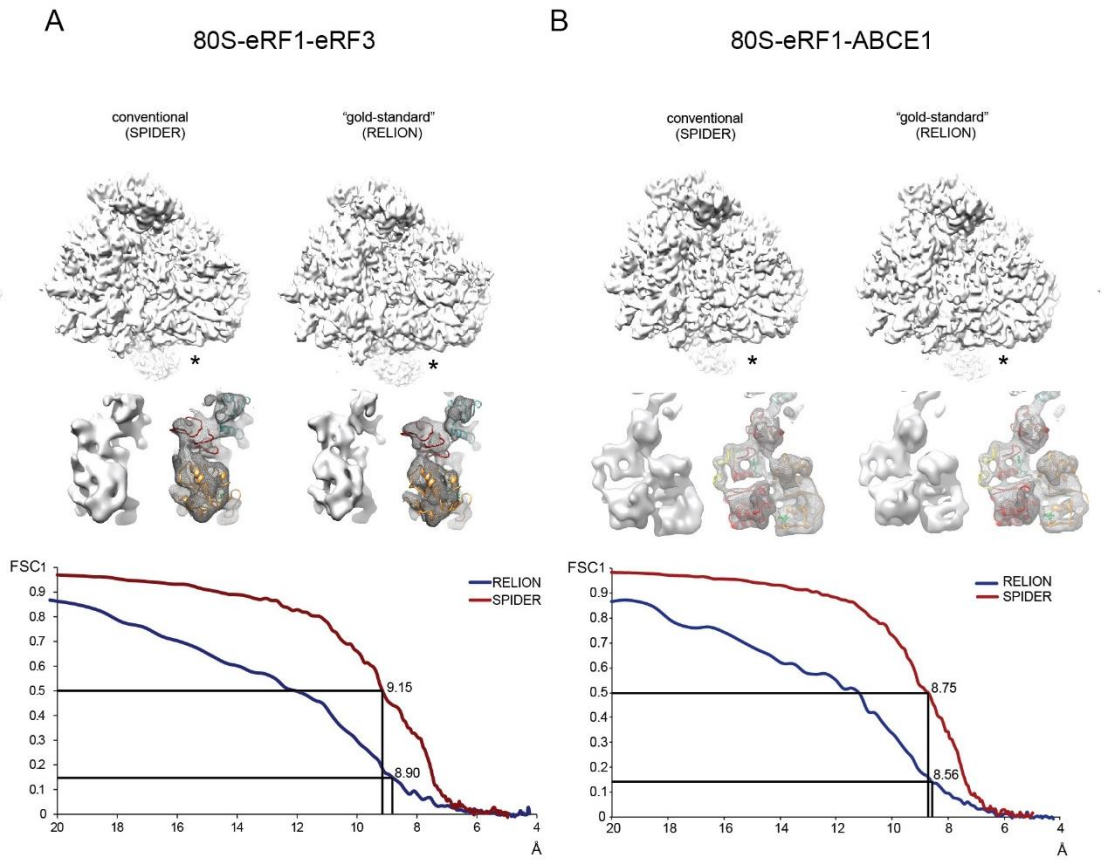


Figure 11. **Comparison between conventional refinement in SPIDER and "gold-standard" refinement in RELION**. Final refined volumes and resolution curves for the 80S-eRF1-eRF3 complex (**A**) and 80S-eRF1-ABCE1 complex (**B**) using both methods. Sec61 at the tunnel exit is marked with an asterisk. From Preis et al., 2014.

Most secondary structure was resolved in both complexes and allowed fitting the *T. aestivum* ribosome model containing a P-site tRNA (Armache et al., 2010a, 2010b) and homology models of termination or recycling factors into the assigned densities.

### 4.2.3 Validation of resolution determination

To validate the calculated resolution in SPIDER and how well the models fit the experimentally obtained maps, FSC analysis was performed between the expected densities generated from the models and the experimentally obtained densities (Figure 15). Typically, the ribosome is resolved better than its ligands. Hence, using soft masks,

factors were isolated and resolution was calculated separately from the ribosome. In the 80S-eRF1-eRF3 complex, the signal–to–noise ratio of 0.5 was reached at 8.2 Å filtering for the model of the *T. aestivum* ribosome and 10 and 10.2 Å for the models of eRF1 and eRF3, respectively. With a map at a resolution of 9.15 Å, this was evaluated to be sufficiently accurate. In the 80S-eRF1-ABCE1 complex, the signal–to–noise ratio of 0.5 was reached at 7.3 Å filtering for the model of the ribosome and 7.6 and 7.3 Å for the models of eRF1 and ABCE1, respectively. With a map at a resolution of 8.75 Å, this was evaluated as accurate.

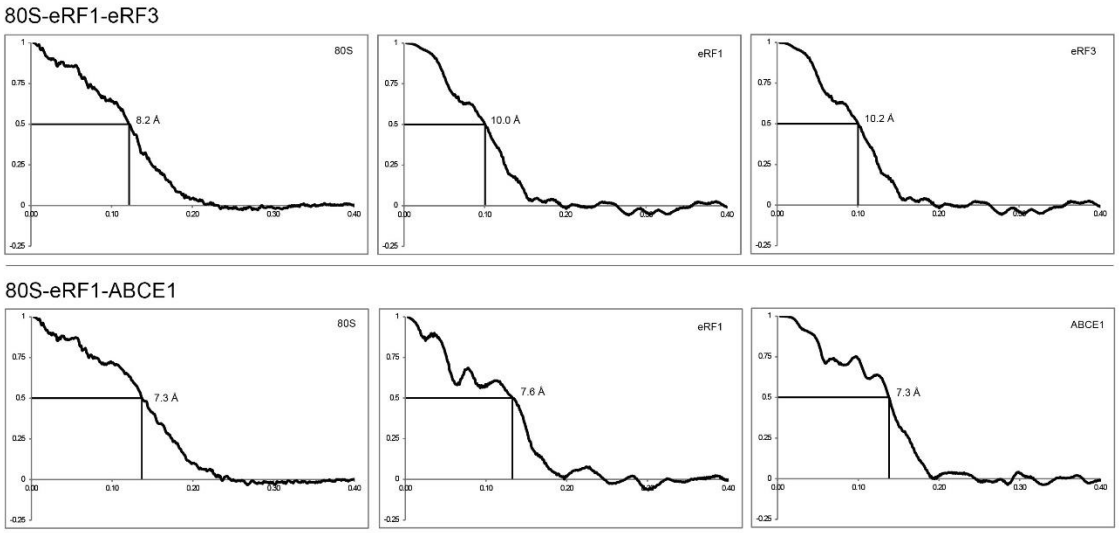


Figure 15. **FSC curves between models and maps for the 80S-eRF1-eRF3 dataset (top row) and the 80S-eRF1- ABCE1 dataset (bottom row).** Calculated for the entire 80S ribosome using the model for the T. aestivum ribosome (PDB codes 3J5Z, 3J60, 3J61 and 3J62) and for individual ligands. From Preis et al., 2014.

## 4.3 PRE-TERMINATION COMPLEX

The 80S-eRF1-eRF3 complex (further termed pre-termination complex) showed extra densities for the nascent chain, eRF1, eRF3 and P-site tRNA, overall in locations similar to previous reconstructions of the rabbit pre-termination complex and the *S. cerevisiae* complex containing Dom34 and Hbs1 described previously by Becker et al., 2012. Namely, eRF1 is in the A-site and its NTD containing the functionally important NIKS motif reaches into the decoding center of the small ribosomal subunit. The CTD and the

central domain of eRF1 are packed against eRF3. eRF3 binds to the ribosome like a classical EF-Tu-like translational GTPase. No density could be identified for the NTD of eRF3 (residues 97-255), likely due to flexibility in the complex (Figure 16).

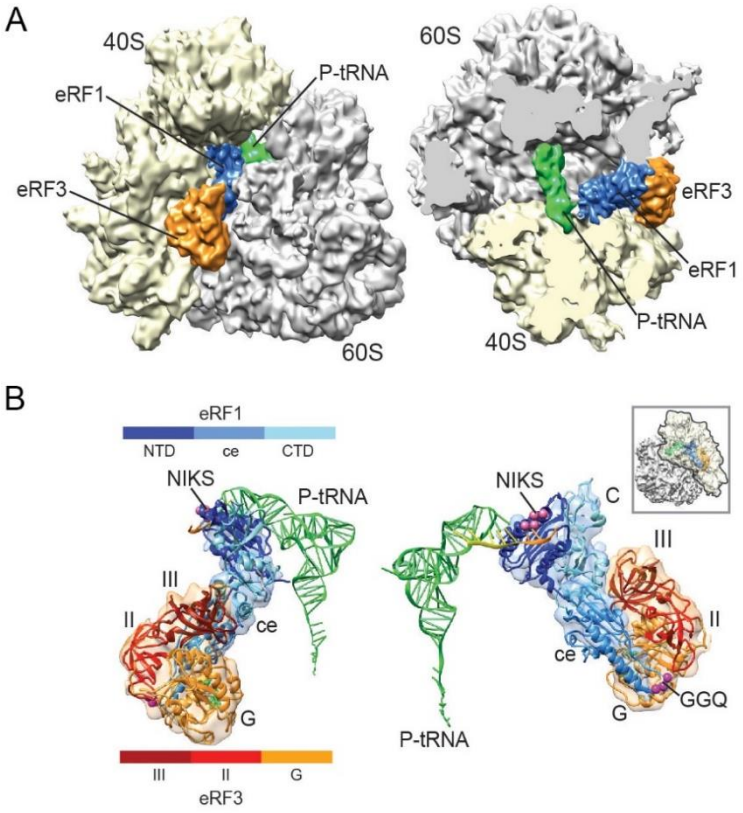


Figure 16. **Cryo-EM structure of the 80S-eRF1-eRF3 pre-termination complex**. Side and top views of the complex (**A**). Density attributed to eRF1 occupies the A-site. Molecular models for peptidyl-tRNA, eRF1, eRF3 on the ribosome fit into the assigned densities (**B**). Color bars represent protein domains. The NIKS motif is marked with pink spheres. Stop codon is marked in orange. The GGQ loop is marked with magenta spheres. From Preis et al., 2014.

The ribosome adopts a non-ratcheted conformation, and eRF1-eRF3 establishes practically identical contacts to the ribosome compared to Pelota-Hbs1, with an additional contact formed at the rRNA h8-h14 junction of the SSU (Figure 17, Table S1 and S2).

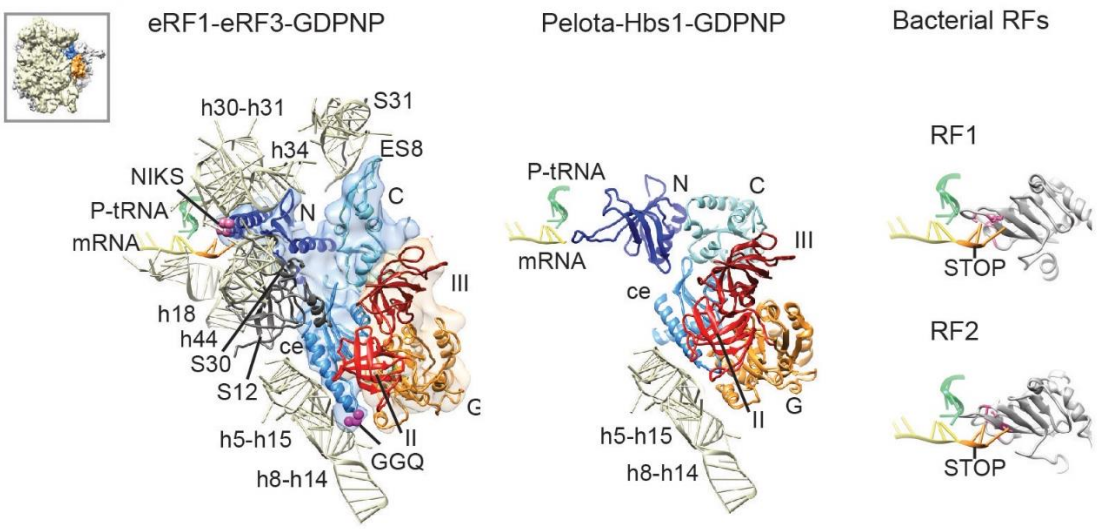


Figure 17. **Contacts to the ribosome made by the eRF1-eRF3 complex.** Comparison to Pelota-Hbs1 complex. Positioning of PVT/SPF motifs (marked in pink) implied in bacterial translation termination is similar. From Preis et al., 2014.

### 4.3.1 NTD of eRF1 reaches into ribosomal A-site

Consistent with contacts reported for the rabbit pre-termination complex (Des Georges et al., 2014), eRF1 forms multiple interactions with the ribosome, with main contacts established between eRF1 NTD and the SSU (Figure 18; Table S1), involving ribosomal RNA helices h18, h31, h34 and r-proteins S30 and S31 (now and further on according to the nomenclature introduced by Jenner et al., 2012).

The conserved (TAS)NIKS loop of the NTD is proximal to the stop codon positioned in the A-site (Figure 18). This is consistent with its critical role in stop codon recognition: the (TAS)NIKS loop takes a similar position relative to the stop codon when compared to the PVT or SPF motifs of bacterial RF1 or RF2, respectively (Figure 17). However, the density for the NTD of eRF1 was not defined clearly enough and did not allow unambiguous positioning of the mRNA or individual residues of the (TAS)NIKS motif. This behavior of the NTD could be explained by the proposed two-step model of stop codon recognition, postulated based on toeprinting and chemical crosslinking data. Here, the NTD of eRF1 first recognizes the first two nucleotides in the stop codon and changes its conformation to recognize the second and third nucleotides (Kryuchkova et al., 2013).

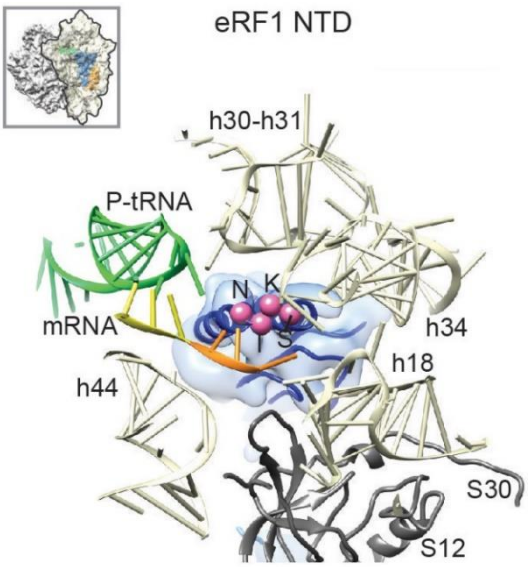


Figure 18. **Contacts within the A-site established by the NTD of eRF1.** The NIKS loop is marked with pink spheres and is near the stop codon (orange). From Preis et al., 2014.

### 4.3.2 eRF1-eRF3 interact tightly

The contacts between the CTD of eRF1 and domain III of eRF3 are formed by similar structural elements as previously reported in the crystal structure of human eRF1-eRF3 complex (Cheng et al., 2009). Namely, the connections are made between helices α8, α11, and strand β10 of eRF1 CTD and eRF3 domain III loop regions connecting β15–β16, β16–β17, β18–β19, and β21–β22 (Table S3) (numbering as in Kong et al., 2004). In comparison to the crystal structure, helices α8 and α11 of the CTD of eRF1 are in tighter contact to domain III of eRF3 (Figure 19). The mini domain on top of the CTD of eRF1,

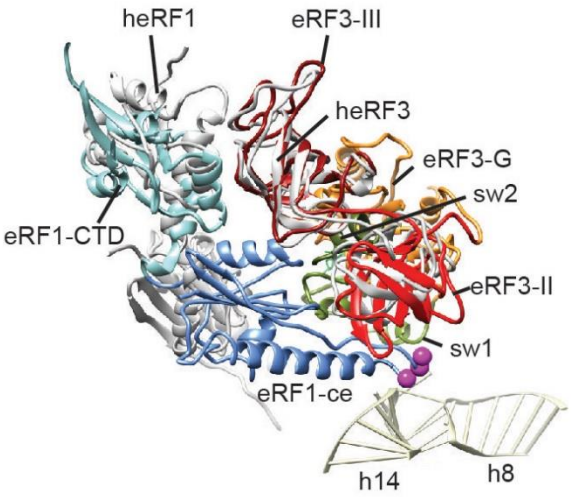


Figure 19. **Overlay of model for eRF1-eRF3 with the crystal structure of the human eRF1-eRF3 complex.** Crystal structure, PDB accession 3E1Y (Cheng et al., 2009), lacking the eRF3-G domain (grey). From Preis et al., 2014.

previously identified with NMR (Mantsyzov et al., 2010), adopts an extended conformation and connects to the beak of the SSU, contacting the rRNA expansion segment ES8 and r-protein S31 (Figure 17). The central domain of eRF1 is packed against all three domains of eRF3 and forms a large interaction surface of 1,088 Å$^2$. As a result, both the switch I and switch II regions of the G domain of eRF3 contact eRF1 (Figure 19, Table S3). The GGQ motiv important for peptide release is masked and 90 Å away from the CCA-end, explaning why in stalled pre-termination complexes no release of the peptide was observed.

### 4.3.3 eRF1-eRF3 are bound in a more outward position

When comparing the pre-termination complex structure to the RNC-Pelota-Hbs1 structure (Becker et al., 2011) or the rabbit pre-termination complex (Des Georges et al., 2014), notable differences can be observed for the movement of the stalk base (rRNA helices H43 and H44 and r-protein L11). Compared to the factor-free state, the inward movement is less pronounced in the pre-termination complex described here (Figure 20). As a result, the central domain and the CTD (including the mini domain) of eRF1 as well as eRF3 are bound in a more outward position. Thus, the central domain of eRF1 is positioned closer to the small subunit and contacts rRNA helix h14 of the SSU via helix α5.

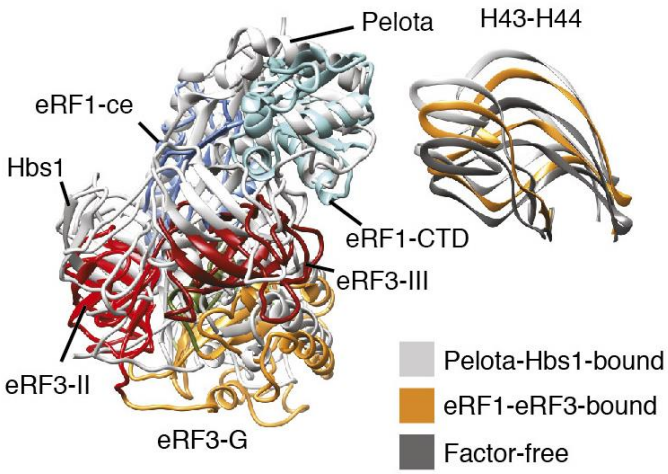


Figure 20. **Movement of the stalk base in the pre-termination complex.** eRF1-eRF3 are bound in a more outward position than Pelota-Hbs1. From Preis et al., 2014.

(Figure 20, Table S1). As a result, the GGQ loop at the tip of helix α5 is tightly locked between the G domain of eRF3 and the SSU. This conformation of eRF1 is incompatible with peptide release.

## 4.4 TERMINATION/PRE-RECYCLING COMPLEX

The 80S-eRF1-ABCE1 complex (further termed termination/pre-recycling complex), with the ribosome in a non-rotated state, showed extra densities for P-site tRNA, eRF1 in the A-site and ABCE1 at the translation factor binding site. eRF1 stretches between the P-site tRNA and ABCE1 (Figure 21, contacts listed in Table S4). The CTD of eRF1 contacts the FeS-domain of ABCE1, and the central domain is stretched out towards the PTC, contacting the P-site tRNA at the CCA-end (Tables S5 and S6). Density for the NTD of eRF1 appeared to be fragmented in the reconstruction and could only be visualized after low-pass filtering at around 20 Å, indicating a delocalization of the domain.

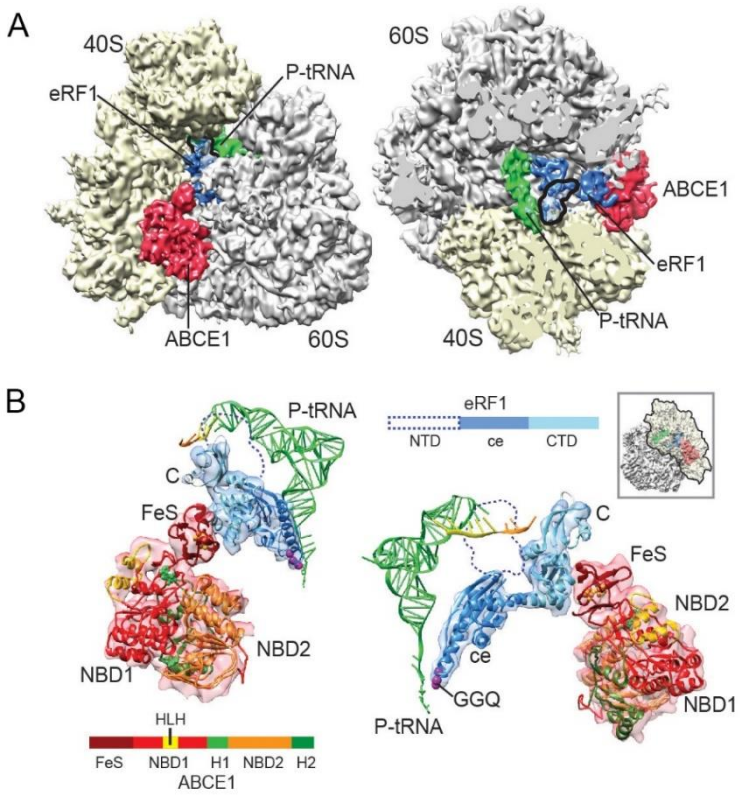


Figure 21. **Cryo-EM structure of the 80S-eRF1-ABCE1 termination/pre-recycling complex**. Side and top views of complex with delocalized NTD of eRF1 marked with a black line (**A**). Molecular model fits for peptidyl-tRNA, eRF1 and ABCE1 on the ribosome (**B**). Delocalized NTD of eRF1 is marked with a dotted blue line. Stop codon (orange) and GGQ loop (magenta spheres) are marked. Color bars represent protein domains. From Preis et al., 2014.

### 4.4.1 Conformation of ABCE1

The conformation of ABCE1 bound to the ribosome is identical to that in the Pelota-ABCE1-containing complex described previously by Becker et al., 2012. ABCE1 binds in the translation factor binding site at the inter-subunit space and adopts an intermediate conformation of its NBDs, between the open, ADP-bound structure, and the modelled closed ATP-bound form (Figure 22) (Becker et al., 2012; Karcher et al., 2008). Here, the final resolution did not allow to identify the bound nucleotides. ABCE1 contacts the small subunit (h5-h15, h8-h14) mainly via the HLH and hinge motifs (Table S5). Additional contacts are observed between NBD2 and r-protein L10. The stalk base is moved toward the SRL (H95), although the movement is less pronounced when compared to the Pelota-ABCE1 complex (Figure 22).

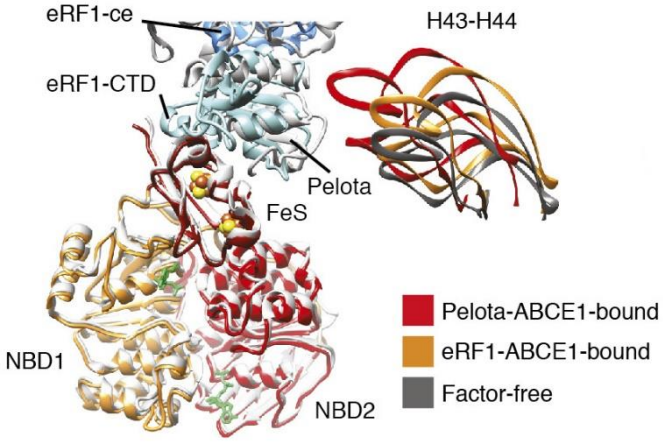


Figure 22. **Movement of the stalk base in the termination/pre-recycling complex.** The conformation of ABCE1 is identical to the one observed in complex with Pelota (in grey). From Preis et al., 2014.

### 4.4.2 eRF1 changes its conformation in complex with ABCE1

eRF1 changes its conformation dramatically in the termination/pre-recycling complex, in a similar way that ribosome-bound Pelota extends in the presence of ABCE1 (Figure 23). This elongated conformation is overall analogous to that of bacterial ribosome-bound RFs (Korostelev et al., 2008; Laurberg et al., 2008; Weixlbaumer et al., 2008). However, in contrast to the structures of bacterial termination complexes, the NTD of eRF1 appears to be delocalized, and thus probably disengaged from the A-site. The CTD of eRF1 contacts the FeS cluster domain of ABCE1 (Table S6), the stalk base (H43-H44 and L11), and the SRL (H95) in the LSU (Table S4). The central domain of eRF1 undergoes the most significant rearrangement and establishes multiple contacts to the rRNA (H71, H89, H91, H92, and H93), stretching out toward the P-site tRNA (Figure 24B, Table S4). The

nascent peptide is still intact in the ribosomal exit tunnel, indicating that practically no peptide release has occurred in this particle population (Figure 24A). The conserved loop containing the catalytical GGQ motif is located at the PTC of the LSU, close to the CCA end of the peptidyl tRNA (Table S4).

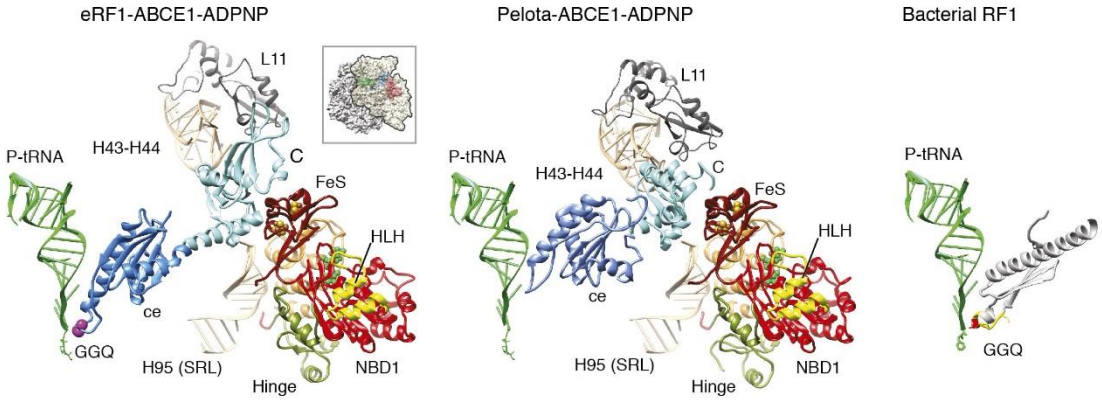


Figure 23. **eRF1 undergoes a drastic conformational change in complex with ABCE1 on the ribosome.** Analogously to Pelota, the central domain of eRF1 reaches toward the P-site tRNA. The corresponding domain 3 of bacterial RF1 containing the catalytic GGQ loop adopts a broadly similar extended conformation. Contacts of the CTD of eRF1 to the ribosome are shown. From Preis et al., 2014.

### 4.4.3 Positioning of the GGQ loop

eRF1 is unrelated to bacterial RF1 or RF2 in sequence and structure. However, when modeling the GGQ loop in the obtained termination/pre-recycling complex map on the example of bacterial crystal structures, the catalytic motif adopts the same conformation as in the corresponding domains of bacterial RFs (Figure 24C). This structural finding could indicate that the GGQ loops functions in an identical, highly conserved way, to coordinate peptidyl-tRNA hydrolysis.

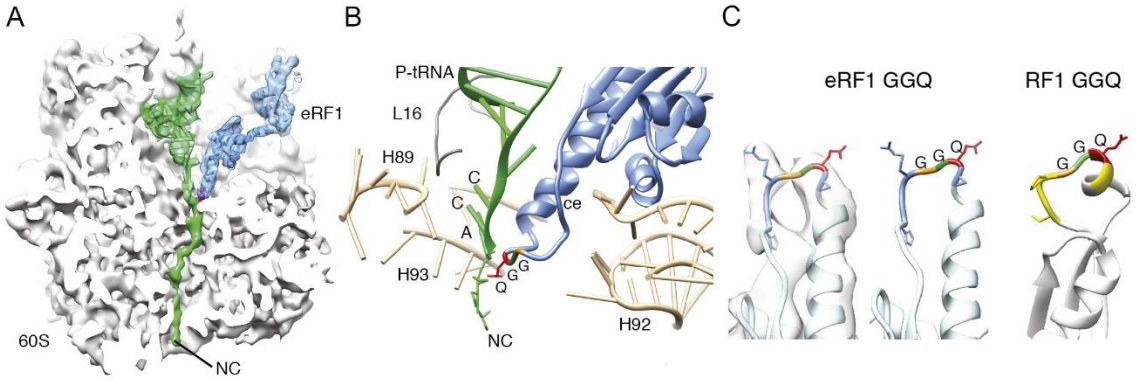


Figure 24. **The central domain of eRF1 extends toward the P-site tRNA.** The nascent chain (NC) is still intact in the ribosomal exit tunnel (**A**). Contacts formed between the central domain of eRF1 and the ribosome (**B**). Comparison of conformations of GGQ motifs in eRF1 and bacterial RF1 (**C**). From Preis et al., 2014.

ABCE1 contacts the CTD of eRF1 (Table S6), possibly stabilizing the active conformation of eRF1 and thus exerting the reported stimulatory effect on its peptide release activity (Shoemaker and Green, 2011). For an accurate claim, however, a ribosomal complex containing eRF1 alone would have to be analyzed. Interestingly, attempts to reconstitute such a complex in this hybrid system (or with *S. cerevisiae* RNCs) have not enabled visualizing eRF1 on the ribosome. Also, no population of 80S containing only eRF1 could be sorted out in either of the datasets described here.

To sum up, two complexes representing the pre-termination and termination/pre-recycling stages of translation could be reconstituted and visualized by cryo-EM at sub-nanometer resolution. eRF1, as predicted earlier by Becker et al., 2012, changes its conformation drastically from the locked, eRF3-bound state to the active, stretched conformation with ABCE1.

## 4.5 NATIVE 40S-ABCE1 COMPLEX

The second goal of this work was to obtain native ABCE1-containing post-splitting complexes. In a collaboration with the Tampé group at the University of Frankfurt, the structure of the *in vitro* reconstituted 40S-ABCE1 complex was solved at high resolution (Heuer et al., 2017) and shed light on the role and conformation of ABCE1 during ribosome splitting. It was of interest to find out if a native post-splitting complex would contain ABCE1 in a similar conformation and whether the complex would contain initiation factors.

*S. cerevisiae* cells expressing C-terminally TAP-tagged ABCE1 and cultivated in logarithmic growth phase were used to purify native 40S-ABCE1 complexes. The tandem affinity purification method utilizes a two-component tag consisting of Protein A and calmodulin binding protein (CBP) connected by a Tobacco Etch Virus (TEV) protease cleavage site. In this work, the purification only consisted of the first step, i.e. binding to IgG-Sepharose to minimize material loss, followed by extensive washing, and subsequent elution by incubation with TEV protease. ADPNP was added at the cell lysis stage. The entire TEV-eluate was then applied onto a 5%-30% sucrose gradient, specifically to enrich for 40S (Figure 25A). The gradient purification was performed overnight at low *g* to prevent factor dissociation. The separate peak fractions were then applied onto PD10 columns to remove sucrose and vitrified immediately after elution.

### 4.5.1 Native ABCE1 tandem affinity purifications contain translation initiation factors

Mass spectrometry (MS) analysis was performed on the exact sample that was analyzed by cryo-EM (analysis kindly performed by Thomas Fröhlich of Gene Center Munich). Here, following SDS-PAGE, the gel band was cut into several parts down to the 35 kDa mark, and the parts were analyzed separately. The highest scoring accessions could be identified in the protein band profile, although not all components detected with a high level of confidence were equally prominent in the stained SDS-PAGE gel, indicating that the observed complexes were not stoichiometric (Figure 25B). As expected, the

eluate contained ABCE1 and fatty acid synthetase (FAS), which commonly co-sediments with 40S preparations (Lomakin et al., 2007). Additionally, the abundant eukaryotic elongation factor 2 (eEF2) was present. Importantly, multiple components of translation initiation complexes were identified with a high level of confidence: namely, all subunits of eIF3 (eIF3a, eIF3b, eIF3c, eIF3g, eIF3i and the separate factor eIF3j), and all three subunits of initiator-tRNA-binding eIF2 (eIF2α, eIF2β and eIF2γ). Also, eIF5 was identified at a low confidence level.

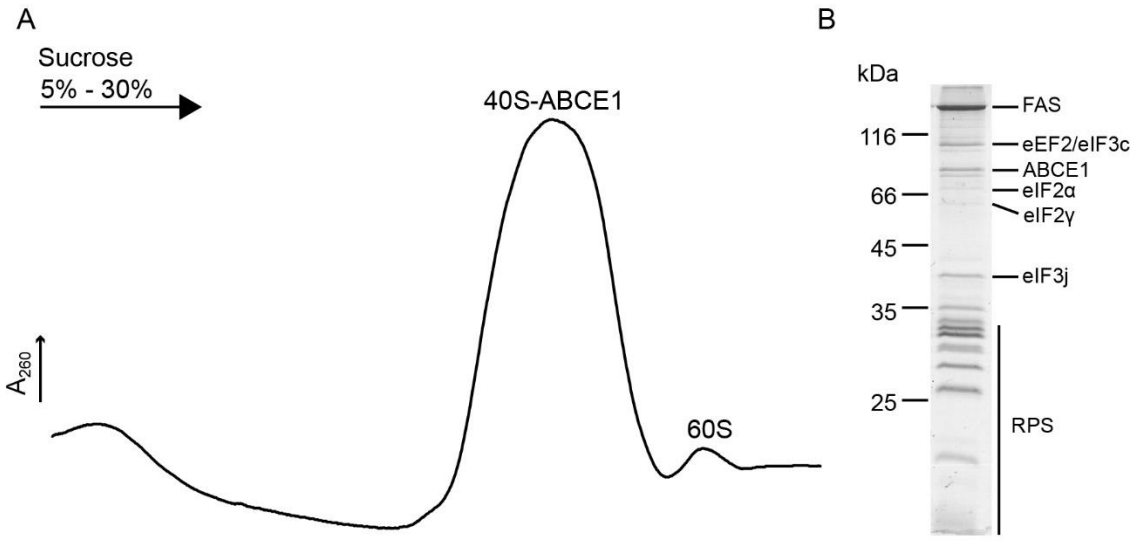


Figure 25. **Purification of 40S-ABCE1 complexes.** 5% - 30% sucrose gradient purification of ABCE1-TAP eluate (**A**). SDS-PAGE of peak 40S-ABCE1 fraction after sucrose removal (**B**). Distinct protein bands were identified by MS. From Heuer et al., 2017.

### 4.5.2 Cryo-EM analysis of native 40S-ABCE1 complexes

Cryo-EM analysis was performed on the buffer-exchanged 40S-ABCE1 eluate using RELION (Figure 26). 2D classification in RELION allowed removing the barrel shaped FAS from the dataset, and 3D classification produced 5 classes of 40S particles. Two classes, comprising 37% of all particles, represented poorly resolved 40S, and 63% of the particles contained extra density at the translation factor binding site, which was assigned to ABCE1. Two classes showed extra density in the P-site as well and were joined and

reclassified. The final class, with densities assigned to ABCE1, initiator $tRNA_i$ and eIF1A (positioning based on Passmore et al., 2007) was finally refined to 14 Å.

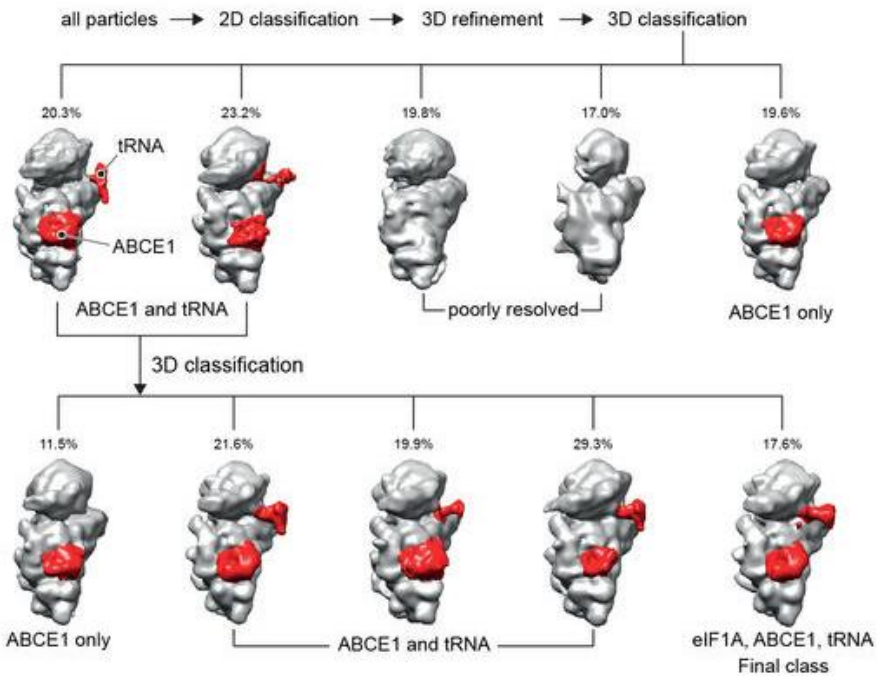


Figure 26. **3D classification scheme of native ABCE1-containing complexes.** Extra densities on 40S could be assigned to ABCE1, tRNAi and eIF1A (marked in red). From Heuer et al., 2017.

The resolution of the final map did not allow unambiguous positioning of ABCE1 secondary structure into the density. However, comparison with the 3,9 Å reconstruction of the *in vitro* post-splitting complex (Heuer et al., 2017) revealed a strong overall similarity in shape and in the binding site on the SSU to ABCE1 in a "closed" conformation. The conformation change of ABCE1 in the *in vitro* reconstituted post-splitting complex and a model of domain rearrangement of ABCE1 during ribosome splitting is described in detail in the corresponding publication by Heuer et al. Difference maps between the *in vitro* reconstituted and the native 40S–ABCE1 complexes confirmed the presence of eIF1A and $tRNA_i$ (Figure 27).

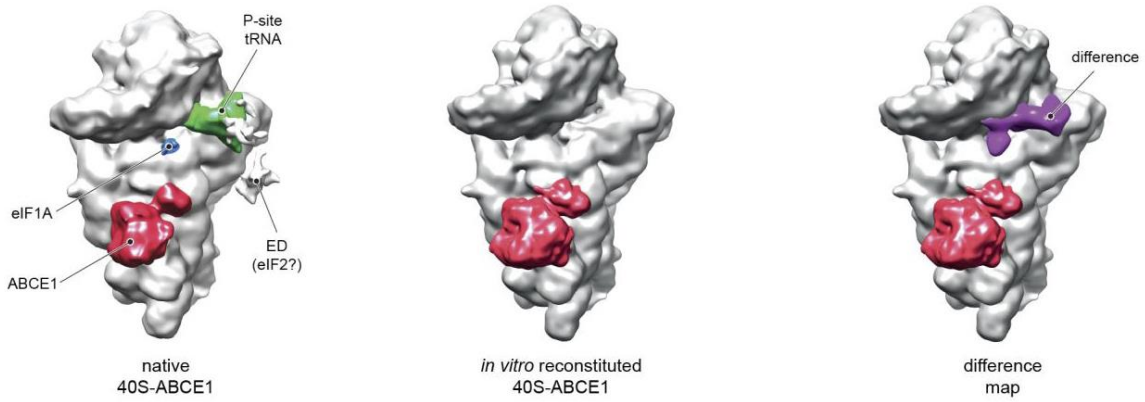


Figure 27. **Difference map calculated between the native and *in vitro* reconstituted 40S-ABCE1 complexes.** Calculated additional density (purple) confirms presence of P-site tRNA (green) and eRF1 (blue), while ABCE1 (red) conformation is identical in both maps. From Heuer et al., 2017.

Although detected by MS analysis, no pronounced extra densities were observed for eIF2 or any of the eIF3 subunits – likely due to factor dissociation in the given freezing conditions.

# 5 DISCUSSION

The main aim of this work was to study the structural rearrangements of eukaryotic translation termination and ribosome recycling factors eRF1, eRF3 and ABCE1 on the ribosome during translation termination and ribosome recycling using cryo-EM. Structural studies of translation termination complexes have proven to be challenging over the years, and our understanding of these processes was mostly based on the behavior of paralogous ribosome rescue factors Dom34 (Pelota in mammals) and Hbs1, where the A-site factor Dom34/Pelota split stalled ribosomes in concert with ABCE1 (Becker et al., 2012). Additionally, first structural insights into a mammalian pre-termination complex containing eRF1 and eRF3 showed that in the initial stage of termination factor attachment, the confirmation of eRF1 is incompatible with peptide release, with its catalytical central domain packed tightly against eRF3 (Des Georges et al., 2014; Taylor et al., 2012).

## 5.1 TERMINATION COMPLEXES COULD BE GENERATED USING A MULTI-SPECIES, "HYBRID" SYSTEM *IN VITRO*

In this work, trapping stable termination complexes required the utilization of a multi-species, "hybrid" system, in contrast to *in vitro* translation reaction in the (translation initiation- and elongation-factor-supplemented) rabbit reticulocyte lysate described by Taylor et al, 2012. Taylor et al. essentially isolated pre-termination complexes positioned on MVHL-STOP mRNA and incubated them with termination factors and GDPNP. In this work, using a truncated mRNA containing the hCMV stalling sequence at its 3' end (which was shown to accumulate eRF1 in human cells (Janzen et al., 2002) but inhibit peptide release due to perturbing the PTC (Bhushan et al., 2010), programmed ribosome-nascent chain complexes could be sourced from a wheat germ (*T. aestivum*) translation extract. *S. cerevisiae* termination and recycling factors eRF1, eRF3 and ABCE1 were purified separately and reconstituted with the CMV-RNCs for cryo-EM analysis. Incubation of wheat RNCs together with eRF1 and ABCE1 in the presence of ADPNP lead to peptide release, showing firstly the overall suitability of the substrate for

termination, and secondly the previously known stimulating effect of ABCE1 on peptide release by eRF1. Thus, this “hybrid” system was not only shown to be functional, but also allowed trapping the termination/recycling complexes at distinct stages of termination. Lastly, the system allowed to finally confirm the predicted rearrangements of eRF1 domains, from the closed conformation at the stage of factor attachment/stop codon recognition to the anticipated open conformation during peptide release (Becker et al., 2012). The sub-nanometer-resolved structures described here marked an important milestone on the way to fully understanding translation termination in eukaryotes.

## 5.2 General model of eukaryotic translation termination and ribosome splitting

Two eukaryotic ribosomal complexes were obtained as part of this study and visualized by cryo-EM at sub-nanometer resolution. The pre-termination complex containing eRF1 and eRF3, depicts eRF1 in an overall conformation previously described for the rabbit pre-termination complex (Des Georges et al., 2014; Taylor et al., 2012). The NTD of eRF1 reaches into the decoding center on the SSU, with the (TAS)NIKS loop positioned closely to the stop codon. There is a small degree of flexibility observed for the NTD in this complex, which will be discussed later on. The central domain of eRF1 is packed tightly against eRF3, contacting its switch regions which control its GTP-hydrolyzing activity. In comparison to Dom34/Pelota, the central domain of eRF1 forms an additional prominent contact with the SSU, further promoting this packed conformation. This stage of initial factor attachment would be followed by GTP hydrolysis by eRF3, eRF3 dissociation and full accommodation of eRF1 into the A-site (Figure 28).

The termination/pre-recycling complex obtained in this work showed for the first time the active conformation of eRF1 on a terminating ribosome. In complex with ribosome recycling factor ABCE1, eRF1 adopted an extended conformation, where its central domain is swung toward the P-site tRNA. ABCE1 further stabilized this active conformation by binding to the CTD of eRF1. The catalytic GGQ motif was positioned next to the CCA-end of the P-site tRNA, where it may coordinate a water molecule to cause peptide release (Figure 28).

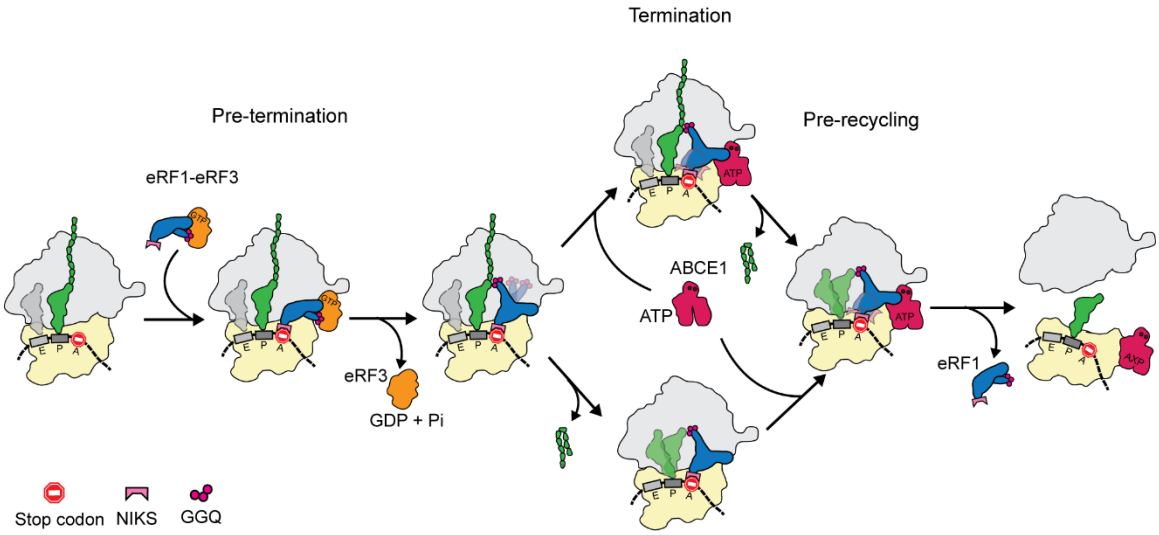


Figure 28. **General model of eukaryotic translation termination.** At pre-termination stage, eRF1 (blue) and eRF3 (orange) bind in tertiary complex with GTP to a ribosome (LSU in grey and SSU in light yellow) poised on a stop codon. NTD of eRF1 recognizes the stop codon and GTP hydrolysis by eRF3 leads to eRF1 accommodation and peptide hydrolysis (GGQ motif, pink spheres). Peptide release occurs with or without stimulation by ABCE1 (magenta). Ultimately, ABCE1 and eRF1 facilitate ribosome splitting. From Preis et al., 2014.

Overall, the finding confirms the model for structural changes of eRF1 on the ribosome during translation termination proposed by Becker et al., 2012.

The extended conformation of eRF1 is overall similar to that of bacterial RFs on the ribosome. The NIKS motif on the NTD is in close proximity to the stop codon, in a similar manner that bacterial RFs SPF and PVT motifs are positioned during termination. The GGQ loop of the central domain of eRF1 fits very well with the positioning of this loop in bacterial RFs, indicating that peptide hydrolysis is a highly conserved step across the different kingdoms of life.

eRF1 is still required for ribosome splitting after termination. Its CTD contacts the FeS cluster domain of ABCE1. The conformation of ABCE1 in the termination/pre-recycling complex shown in this work is identical to the one observed in the no-go rescue

complex with Dom34/Pelota (Becker et al., 2012), with its two NBDs positioned in a half-closed conformation. This suggests that the process of ribosome splitting by ABCE1 is a general one, regardless whether it occurs after canonical translation termination or ribosome rescue. ABCE1 would work in concert with a fully accommodated A-site binding factor and its FeS can be seen as a structural bolt, exerting the energy from bringing the two NBDs together and pushing eRF1/Pelota deeper into the inter-subunit space. The work performed by Heuer et al. on an *in vitro* - reconstituted post-splitting complex containing the SSU and ABCE1 (Figure 29A) clearly shows that ABCE1 generally adopts the predicted closed conformation, with the FeS cluster domain of ABCE1 rotated away by approximately 150 degrees from the cleft between its two NBDs (Figure 29B). Furthermore, the binding site of the FeS cluster domain on the SSU is incompatible with the CTD of eRF1/Pelota. Additionally, the FeS cluster domain exerts anti-association properties by binding on the SSU in a position that would be incompatible with (re-)joining of the LSU (Heuer et al., 2017).

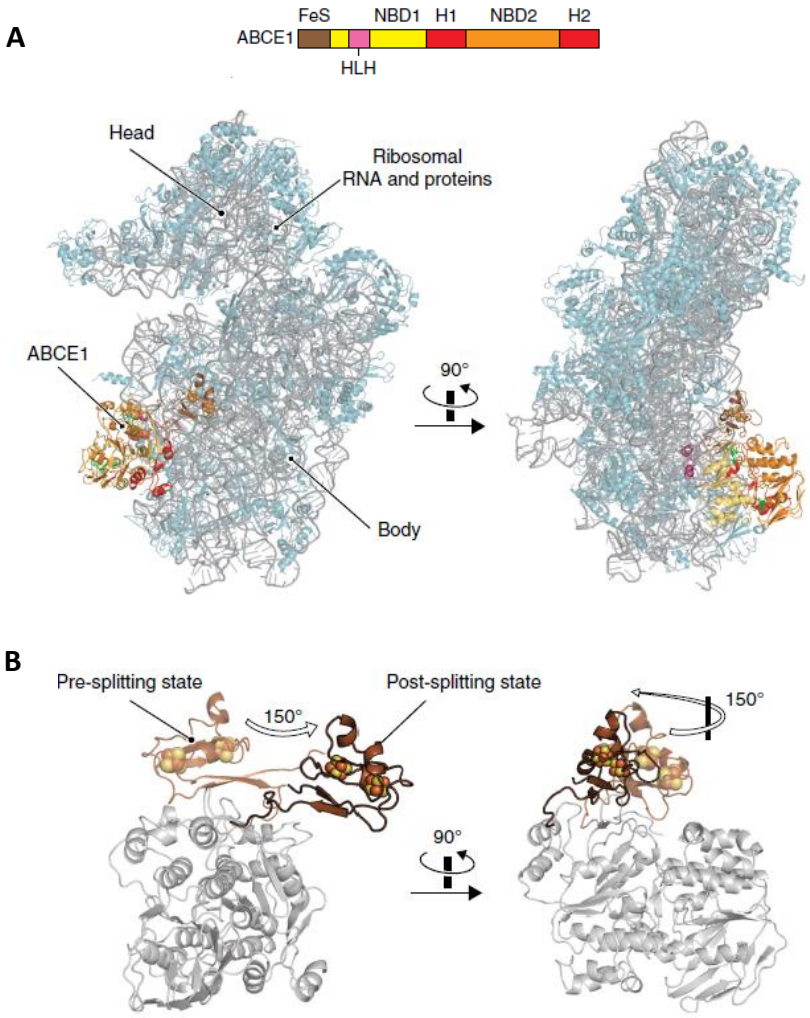


Figure 29. **Model of the 40S–ABCE1 post-splitting complex.** (**A**) Front and side views, r-proteins in teal, rRNA in grey, ABCE1 with domains colored as indicated above, and ADPNP in green. (**B**) 150°- rotation of the FeS cluster domain from the pre-splitting state (PDB 4CRM; ref. 12; transparent) to the post-splitting state (brown). From Heuer et al., 2017.

## 5.3 ABCE1 MIGHT BE FURTHER IMPLICATED IN TRANSLATION INITIATION

Supporting the data and conclusions drawn from the *in vitro* reconstituted post-splitting complex, a native ABCE1-containing 40S post-splitting complex could be obtained from TAP pull-downs in *S. cerevisiae*. Even though the final resolution of 14 Å was not enough to exactly assign secondary structure elements, the characteristic overall shape of ABCE1 superimposes well with the corresponding confirmation in the *in vitro* complex and fits into the extra density. Interestingly, in addition to ABCE1 bound to the SSU, extra densities were observed for initiator tRNA (30% of all particles) and initiator tRNA together with eIF1A (7,5% of all particles).

The identities of these "initiation" complexes are enigmatic. During formation of the 43S pre-initiation complex, initiator tRNA is bound to the P-site directly as part of a eIF2/GTP/Met-tRNA$_i$ ternary complex. The cryo-EM reconstruction did not contain a clear extra density that would correspond to the heterotrimeric eIF2, however all three subunits were identified in the pull-downs by MS with a high confidence level. Additionally, the native pull-downs contain all subunits of the multimeric initiation factor eIF3, which promotes ternary complex recruitment to the 40S and is required to subsequently recruit mRNA. Finally, eIF1A, which is bound to the A-site in the observed complex (positioning based on Passmore et al., 2007), is essential in *S. cerevisiae* and serves multiple functions in translation initiation. It has been shown to promote ternary complex binding to the 40S and stimulate 48S complex initiation on the start codon (reviewed by Jackson et al., 2010 and Hinnebusch and Lorsch, 2012). eIF1A also interacts with eIF5B which in turn is involved in 60S subunit joining. eIF5, which acts as a GAP for GTP-bound eIF2 upon pairing of initiator tRNA to the start codon, has also been identified at low levels in these native pull-downs. It is possible that the multimeric eIF3 and heterotrimeric eIF2 dissociate from the complexes under the freezing conditions, leading to only partial structural information and therefore speculative conclusions. Together with the fact that the FeS cluster domain of ABCE1 occupies A-site on the 40S which is incompatible with 60S joining, the available clues point to a role of ABCE1 in 43S pre-initiation complex formation. The absence of any factor implicated in mRNA cap

interaction such as eIF4 further support this hypothesis, however it remains to be seen at what point in the process of initiation ABCE1 would be required to dissociate and how this process would be regulated exactly.

## 5.4 THE NTD OF ERF1 RETAINS VARIOUS DEGREES OF FLEXIBILITY IN THE OBTAINED TERMINATION COMPLEXES

As mentioned briefly in the results section, the NTD of eRF1 was observed to retain a degree of flexibility in the pre-termination complex described here, which at the time was thought to have been representative of the two-step process of stop codon recognition in eukaryotes, as suggested by Kryuchkova et al., 2013. According to this model, after recognition of first and second nucleotide, eRF1 would change its conformation slightly to recognize the second and/or third nucleotides, causing therefore a certain heterogeneity of conformations and consequently a slightly lower resolution of the NTD in the pre-termination complex.

Next, in the termination/pre-recycling complex with ABCE1, the NTD of eRF1 seems to be delocalized entirely, suggesting that stop codon engagement may not be necessary at this stage, or possibly in this particular system.

## 5.5 STABILIZING THE NTD OF ERF1 – FURTHER STUDIES OF MAMMALIAN TERMINATION COMPLEXES

Since publication of the work on translation pre-termination and termination/recycling complexes, translation termination was studied further using the rabbit and human systems, and with the rapid developments in the field of cryo-EM, fascinating details were provided about the mechanism of stop codon engagement by eRF1. A high-resolution 3,8 Å structure of the human termination complex containing eRF1 was published by colleagues Matheisl et al., 2015. Analogously to the termination complexes described in this work, this human termination complex was generated by programming a (human) translation extract with an mRNA containing the hCMV stalling sequence, with a few notable differences. In addition to a viral internal ribosomal entry site (IRES) sequence for easing translation initiation in the sensitive extract, the construct also contained a poly-(A) tail following the hCMV staller (in contrast to the structures

described here, where the mRNA ended with the UAA stop codon). Additionally, the work employed Jumonji domain-containing 4 (Jmjd4), a 2-oxoglutarate- and Fe(II)-dependent oxygenase, which catalyzes carbon 4 (C4) lysyl hydroxylation of eRF1 at K63 of the NIKS motif in human cells (Feng et al., 2014). Hydroxylated K63 reduced stop codon read-through and promoted the release of polypeptides from pre-termination complexes. The obtained high-resolution structure from Matheisl et al. showed, as predicted, an accommodated eRF1 in its extended conformation, with a fully resolved NTD and the GGQ motif of the central domain positioned in close proximity to the CCA end of the P-site tRNA. At the same time, 3,5 – 3,8 Å structures of rabbit termination complexes containing eRF1 and ABCE1 were released by Brown et al., 2015, where the NTD of eRF1 was well resolved and engaged the stop codon. The mRNA used to general RNCs in the rabbit reticulocyte lysate coded for part of Sec61ß and importantly, also contained a 3'UTR following the stop codon.

## 5.6 THE STOP CODON ADOPTS A U-TURN-LIKE GEOMETRY

The high resolution of the termination complexes obtained by Matheisl et al. and Brown et al. allowed deciphering how eRF1 discriminates between stop and sense codons. The UAA stop codon appears to adopt a U-turn-like geometry (not unlike the UNR type), compacting into a pocket formed by eRF1 and 18S rRNA (Brown et al., 2015; Matheisl et al., 2015). U-turns of this type are a common RNA element and are observed, for example, in tRNA anticodon loops or 23S rRNA (Gutell et al., 2000). Binding of eRF1 results in flipping out of A1825 (A1493 in bacteria) of 18S rRNA, which then forms a stacking interaction on top of the second and third stop codon bases. Importantly, the fourth position base is pulled into the A-site and stabilized by a stacking interaction with G626 (bacterial G530) of 18S rRNA (Matheisl et al., 2015). Taken together, two rRNA nucleotides normally used during cognate tRNA selection are used to give the stop codon mRNA its compacted state (Brown et al., 2015). This is different for the bacterial system, where the stop codon causes the flipping out of A1492 (and not A1493), which positions A3 of the stop codon on the G530 but does not participate in any stacking interaction (Korostelev, 2011).

Overall, during mammalian stop codon decoding, stop codons are selected on the basis of their geometry. This resembles the readout of a cognate codon-anticodon interaction, where the geometry of the A-helix is monitored by several ribosomal elements in the A-site. The binding pocket formed between 18S rRNA and eRF1 involves all the previously described motifs in eRF1 which are crucial for translation termination: the TAS-NIKS (with a contribution from the K63 hydroxylation, which supports accommodation of the U in the first position), the YxCxxxF and the GST motifs (Matheisl et al., 2015).

## 5.7 THE NTD OF ERF1 COULD REQUIRE A FOUR-BASE STOP CODON FOR ACCOMMODATION

Considering the conclusions above, the stop codon can therefore be seen rather as a four-base element in mammals. The termination complexes described in this work were generated using a truncated mRNA, ending at a UAA stop codon, without a 3'UTR. Knowing what we know now, it is possible that the higher flexibility (in the pre-termination complex) or full delocalization (for the termination/pre-recycling complex) of the NTD of eRF1 is a direct consequence of the inability of the stop codon to fully adopt the U-turn conformation, causing an important interaction with the 18S rRNA to be ultimately missing and thus somewhat destabilizing the interaction network in the stop codon binding pocket. Perhaps this destabilizing effect is mild in the case of termination factor attachment and exacerbated at the termination/pre-recycling stage when ABCE1 associates. Interestingly, eRF1 together with ABCE1 still release the peptide from these "CMV-stalled" RNCs, suggesting that the destabilizing effect is not highly critical for peptide release. Additionally, it would be interesting to explore whether full stop codon engagement after peptide release improves ribosome splitting. It is likely, based on the observations in the post-splitting complex, that the CTD of eRF1 is the main structural driver of the process as it would directly clash with the FeS custer domain (Heuer et al., 2017), and ABCE1 binding to the eRF1-containing termination complex is enough to facilitate splitting.

## 5.8 BOOMING DEVELOPMENTS IN THE CRYO-EM FIELD CONTRIBUTE TO OUR UNDERSTANDING OF EUKARYOTIC TRANSLATION TERMINATION

Taken together, there are of course several technical differences as to how the "hybrid" termination complexes and the mammalian complexes which came afterwards were generated, however the other important difference is technological. The field of cryo-EM has been seeing significant development recently, with the use of direct electron detectors and new image processing approaches now allowing modelling protein complexes at an atomic level. The structure by Heuer et al. of the *in vitro* post-splitting complex and the mammalian termination complex by Matheisl et al. are both great examples of the information gain one can now expect as a result of these developments. Curiously, stop codon decoding was one of the first processes investigated by high-resolution cryo-EM in the Beckmann group. The scientific community has honored the technique by awarding its developers the Nobel Prize in Chemistry in 2017. With all eyes on cryo-EM, the method is serving more and more scientists in studying protein complexes of ever smaller molecular weight, however, there remains a requirement for a unified approach on how the models and maps are validated (Neumann et al., 2018). Nevertheless, cryo-EM remains beneficial for studying native complexes in solution or membrane proteins that resist crystallization and is raising curiosity in the pharmaceutical industry.

# 6 SUMMARY AND OUTLOOK

The sub-nanometer cryo-EM structures of pre-termination- and termination/pre-recycling complexes described here represent an order of events in translation termination that largely resemble stalled ribosome rescue by Pelota, Hbs1 and ABCE1.

The A-site factor eRF1 is delivered to the ribosome by its EF-Tu-like GTPase partner eRF3, which in turn dissociates after GTP hydrolysis. The eRF1-eRF3 complex is bound to the ribosome in a conformation incompatible with peptide release, while the NIKS motif is in close proximity to the stop codon. The conformation of eRF1 changes drastically upon binding to, and being stabilized by, ABCE1. At this stage, eRF1 has adopted its active, extended conformation, with the central domain swung through to the PTC, allowing the GGQ motif to coordinate a water molecule for peptide release. In this structure, the NTD of eRF1 appears to be delocalized, suggesting that the stop codon is not engaged in the given system. With subsequent mammalian studies having solved the interaction network required for stop codon decoding, this NTD delocalization is likely explained by the requirement of the stop codon to adopt a U-turn-like, compacted geometry, which also requires interactions with the next base after the stop codon triplet. In this conformation, the “four-base” stop codon interacts with the relevant eRF1 NTD sequence motifs and 18S rRNA.

In the termination/pre-recycling complex, ABCE1 adopts a half-closed conformation on the ribosome, previously observed by Becker et al., 2012, in the pre-recycling complex with Pelota. This indicates that the process of ribosome splitting follows a general principle, regardless of the nature of the ribosome to be split. As shown by Heuer et al., 2017, in a post-splitting complex with the SSU, ABCE1 adopts a closed conformation, with its FeS cluster domain rotated away from the cleft between the two NBDs. The domain’s ultimate binding site on the SSU after the splitting event would clash with the CTD of eRF1 in a pre-recycling complex, indicating a general function of the A-

site factor (eRF1 or Pelota) as a type of “molecular wedge” for disruption of inter-subunit bridges.

In a native 40S-ABCE1 complex obtained from TAP-tagged ABCE1 *S.cerevisiae* strain, ABCE1 is bound in an identical, closed conformation, with its FeS cluster domain remaining on the SSU in a position that would further prevent reassociation of the LSU. The presence of initiation factor eIF1A and initiator tRNA in the obtained structure suggest an additional role of ABCE1 in initiation of translation. The fact that all subunits of initiation factors eIF3 and eIF2 were detected in these native pull-downs further support this hypothesis, with further investigation required to explore the possible role of ABCE1 in coordination of events in translation initiation.

Overall, this work marked an important milestone in studying translation termination and ribosome recycling. Although stop codon decoding is now considered solved, it would be of great interest to continue the exploration of associated processes by high-resolution cryo-EM, such as mechanisms of stop codon read-through, influence of accessory factors on termination efficiency, premature termination and quality control pathways and furthermore, initiation of a new round of translation.

# 7 REFERENCES


Agirrezabala, X., and Frank, J. (2009). Elongation in translation as a dynamic interaction among the ribosome, tRNA, and elongation factors EF-G and EF-Tu. Q. Rev. Biophys. *42*, 159–200.

Agrawal, R.K., Spahn, C.M., Penczek, P., Grassucci, R.A., Nierhaus, K.H., and Frank, J. (2000). Visualization of tRNA movements on the Escherichia coli 70S ribosome during the elongation cycle. J. Cell. Biol. *150*, 447--60.

Alkalaeva, E.Z., Pisarev, A. V, Frolova, L.Y., Kisselev, L.L., and Pestova, T. V (2006). In vitro reconstitution of eukaryotic translation reveals cooperativity between release factors eRF1 and eRF3. Cell *125*, 1125–1136.

Andersen, D., and Leevers, S. (2007). The Essential Drosophila ATP-binding Cassette Domain Protein, Pixie, Binds the 40 S Ribosome in an ATP-dependent Manner and Is Required for Translation Initiation. J. Biol. Chem. *282*, 14752–14760.

Andersen, C.B., Becker, T., Blau, M., Anand, M., Halic, M., Balar, B., Mielke, T., Boesen, T., Pedersen, J.S., Spahn, C.M., Kinzy, T.G., Andersen, G.R., and Beckmann, R. (2006). Structure of eEF3 and the mechanism of transfer RNA release from the E-site. Nature *443*, 663–668.

Anger, A.M., Armache, J.P., Berninghausen, O., Habeck, M., Subklewe, M., Wilson, D.N., and Beckmann, R. (2013). Structures of the human and Drosophila 80S ribosome. Nature *497*, 80–85.

Anraku, Y., Mizutani, R., and Satow, Y. (2005). Protein Splicing: Its Discovery and Structural Insight into Novel Chemical Mechanisms. IUBMB Life (International Union Biochem. Mol. Biol. Life) *57*, 563–574.

Armache, J.P., Jarasch, A., Anger, A.M., Villa, E., Becker, T., Bhushan, S., Jossinet, F., Habeck, M., Dindar, G., Franckenberg, S., Marquez, V., Mielke, T., Thomm, M., Berninghausen, O., Beatrix, B., Söding, J., Westhof, E., Wilson, D.N., and Beckmann, R. (2010a). Cryo-EM structure and rRNA model of a translating eukaryotic 80S ribosome at 5.5-Å resolution. Proc. Natl. Acad. Sci. USA. *107*, 19748–19753.

Armache J.P., Jarasch, A., Anger, A.M., Villa, E., Becker, T., Bhushan, S., Jossinet, F., Habeck, M., Dindar, G., Franckenberg, S., Marquez, V., Mielke, T., Thomm, M., Berninghausen, O., Beatrix, B., Söding, J., Westhof, E., Wilson, D.N., and Beckmann, R. (2010b). Localization of eukaryote-specific ribosomal proteins in a 5.5-Å cryo-EM map of the 80S eukaryotic ribosome. Proc. Natl. Acad. Sci. USA. *107*, 19754–19759.

Atkinson, G.C., Baldauf, S.L., and Hauryliuk, V. (2008). Evolution of nonstop, no-go and nonsense-mediated mRNA decay and their termination factor-derived components. BMC Evol. Biol. *8*, 290.

Aylett, C.H.S., Boehringer, D., Erzberger, J.P., Schaefer, T., and Ban, N. (2015). Structure of a yeast 40S-eIF1-eIF1A-eIF3-eIF3j initiation complex. Nat. Struct. Mol. Biol. *22*, 269–271.

Bai, X., McMullan, G., and Scheres, S.H.W. (2015). How cryo-EM is revolutionizing structural biology. Trends Biochem. Sci. *40*, 49–57.

Ban, N., Nissen, P., Hansen, J., Moore, P.B., and Steitz, T.A. (2000). The complete atomic structure of the large ribosomal subunit at 2.4 Å resolution. Science *289*, 905--20.

Barthelme, D., Scheele, U., Dinkelaker, S., Janoschka, A., Macmillan, F., Albers, S. V, Driessen, A.J., Stagni, M.S., Bill, E., Meyer-Klaucke, W., Schünemann, V., and Tampé, R. (2007). Structural organization of essential iron-sulfur clusters in the evolutionarily highly conserved ATP-binding cassette protein ABCE1. J. Biol. Chem. *282*, 14598–14607.

Barthelme, D., Dinkelaker, S., Albers, S.-V., Londei, P., Ermler, U., and Tampé, R. (2011). Ribosome recycling depends on a mechanistic link between the FeS cluster domain and a conformational switch of the twin-ATPase ABCE1. Proc. Natl. Acad. Sci. U. S. A. *108*, 3228–3233.

Becker, T., Armache, J.-P., Jarasch, A., Anger, A.M., Villa, E., Sieber, H., Motaal, B.A., Mielke, T., Berninghausen, O., and Beckmann, R. (2011). Structure of the no-go mRNA decay complex Dom34-Hbs1 bound to a stalled 80S ribosome. Nat. Struct. Mol. Biol. *18*, 715–720.

Becker, T., Franckenberg, S., Wickles, S., Shoemaker, C.J., Anger, A.M., Armache, J.-P., Sieber, H., Ungewickell, C., Berninghausen, O., Daberkow, I., Karcher, A., Thomm, M., Hopfner, K.P., Green, R., and Beckmann, R. (2012). Structural basis of highly conserved ribosome recycling in eukaryotes and archaea. Nature *482*, 501–506.

Ben-Shem, A., Jenner, L., Yusupova, G., and Yusupov, M. (2010). Crystal structure of the eukaryotic ribosome. Science *330*, 1203–1209.

Ben-Shem, A., Garreau de Loubresse, N., Melnikov, S., Jenner, L., Yusupova, G., and Yusupov, M. (2011). The structure of the eukaryotic ribosome at 3.0 Å resolution. Science *334*, 1524–1529.

Berg, P., and Offengand, E.J. (1958). An Enzymatic Mechanism for Linking Amino Acids to RNA. Proc. Natl. Acad. Sci. U. S. A. *44*, 78–86.

Bertram, G., Bell, H.A., Ritchie, D.W., Fullerton, G., and Stansfield, I. (2000). Terminating eukaryote translation: domain 1 of release factor eRF1 functions in stop codon recognition. RNA *6*, 1236–1247.

Bhushan, S., Meyer, H., Starosta, A.L., Becker, T., Mielke, T., Berninghausen, O., Sattler, M., Wilson, D.N., and Beckmann, R. (2010). Structural basis for translational stalling by human cytomegalovirus and fungal arginine attenuator peptide. Mol. Cell *40*, 138–146.

Bisbal, C., Martinand, C., Silhol, M., Lebleu, B., and Salehzada, T. (1995). Cloning and characterization of a RNase L inhibitor. A new component of the interferon-regulated 2-5A pathway. J. Biol. Chem. *270*, 13308–13317.

Brown, A., Shao, S., Murray, J., Hegde, R.S., and Ramakrishnan, V. (2015). Structural basis for stop codon recognition in eukaryotes. Nature *524*, 493–496.

Bulygin, K.N., Khairulina, Y.S., Kolosov, P.M., Ven'yaminova, A.G., Graifer, D.M., Vorobjev, Y.N., Frolova, L.Y., Kisselev, L.L., and Karpova, G.G. (2010). Three distinct peptides from the N domain of translation termination factor eRF1 surround stop codon in the ribosome. RNA *16*, 1902–1914.

Carr-Schmid, A., Pfund, C., Craig, E.A., and Kinzy, T.G. (2002). Novel G-protein complex whose requirement is linked to the translational status of the cell. Mol. Cell. Biol. *22*, 2564–2574.

Cech, T.R. (2000). Structural biology. The ribosome is a ribozyme. Science *289*, 878–879.

Chavatte, L., Seit-Nebi, A., Dubovaya, V., and Favre, A. (2002). The invariant uridine of stop codons contacts the conserved NIKSR loop of human eRF1 in the ribosome. EMBO J. *21*, 5302–5311.

Chen, L., Muhlrad, D., Hauryliuk, V., Cheng, Z., Lim, M.K., Shyp, V., Parker, R., and Song, H. (2010). Structure of the Dom34-Hbs1 complex and implications for no-go decay. Nat. Struct. Mol. Biol. *17*, 1233–1240.

Cheng, Z., Saito, K., Pisarev, A. V, Wada, M., Pisareva, V.P., Pestova, T. V, Gajda, M., Round, A., Kong, C., Lim, M., Nakamura, Y., Svergun, D.I., Ito, K., and Song, H. (2009). Structural insights into eRF3 and stop codon recognition by eRF1. Genes Dev. *23*, 1106–1118.

Dever, T.E., and Green, R. (2012). The elongation, termination, and recycling phases of translation in eukaryotes. Cold Spring Harb. Perspect. Biol. *4*, 1–16.

Dong, J., Lai, R., Nielsen, K., Fekete, C.A., Qiu, H., and Hinnebusch, A.G. (2004). The essential ATP-binding cassette protein RLI1 functions in translation by promoting preinitiation complex assembly. J. Biol. Chem. *279*, 42157–42168.

ElAntak, L., Tzakos, A.G., Locker, N., and Lukavsky, P.J. (2007). Structure of eIF3b RNA Recognition Motif and Its Interaction with eIF3j. J. Biol. Chem. *282*, 8165–8174.

Emsley, P., and Cowtan, K. (2004). Coot: Model-building tools for molecular graphics. Acta Crystallogr. Sect. D Biol. Crystallogr. *60*, 2126–2132.

Erickson, A.H., and Blobel, G. (1983). [3] Cell-free translation of messenger RNA in a wheat germ system. Methods Enzymol. *96*, 38–50.

Feng, T., Yamamoto, A., Wilkins, S.E., Sokolova, E., Yates, L.A., Münzel, M., Singh, P., Hopkinson, R.J., Fischer, R., Cockman, M.E., et al. (2014). Optimal Translational Termination Requires C4 Lysyl Hydroxylation of eRF1. Mol. Cell *53*, 645–654.

Frank, J., Zhu, J., Penczek, P., Li, Y., Srivastava, S., Verschoor, a, Radermacher, M., Grassucci, R., Lata, R.K., and Agrawal, R.K. (1995). A model of protein synthesis based on cryo-electron microscopy of the E. coli ribosome. Nature *376*, 441–444.

Frank, J., Radermacher, M., Penczek, P., Zhu, J., Li, Y., Ladjadj, M., and Leith, A. (1996). SPIDER and WEB: processing and visualization of images in 3D electron microscopy and related fields. J. Struct. Biol. *116*, 190–199.

Frolova, L., Seit-Nebi, A., and Kisselev, L. (2002). Highly conserved NIKS tetrapeptide is functionally essential in eukaryotic translation termination factor eRF1. RNA *8*, 129–136.

Frolova, L.Y., Tsivkovskii, R.Y., Sivolobova, G.F., Oparina, N.Y., Serpinsky, O.I., Blinov, V.M., Tatkov, S.I., and Kisselev, L.L. (1999). Mutations in the highly conserved GGQ motif of class 1 polypeptide release factors abolish ability of human eRF1 to trigger peptidyl-tRNA hydrolysis. RNA *5*, 1014–1020.

Gao, H., Zhou, Z., Rawat, U., Huang, C., Bouakaz, L., Wang, C., Cheng, Z., Liu, Y., Zavialov, A., Gursky, R., Sanyal, S., Ehrenberg, M., Frank, J., and Song, H. (2007). RF3 Induces Ribosomal Conformational Changes Responsible for Dissociation of Class I Release Factors. Cell *129*, 929–941.

Garreau de Loubresse, N., Prokhorova, I., Holtkamp, W., Rodnina, M. V, Yusupova, G., and Yusupov, M. (2014). Structural basis for the inhibition of the eukaryotic ribosome. Nature *513*, 517–522.

Des Georges, A., Hashem, Y., Unbehaun, A., Grassucci, R. a., Taylor, D., Hellen, C.U.T., Pestova, T. V, and Frank, J. (2014). Structure of the mammalian ribosomal pre-termination complex associated with eRF1•eRF3•GDPNP. Nucleic Acids Res. *42*, 3409–3418.

Gogala, M., Becker, T., Beatrix, B., Armache, J.-P.P., Barrio-Garcia, C., Berninghausen, O., and Beckmann, R. (2014). Structures of the Sec61 complex engaged in nascent peptide translocation or membrane insertion. Nature *506*, 107–110.

Graille, M., Chaillet, M., and Van Tilbeurgh, H. (2008). Structure of Yeast Dom34: A protein related to translation termination factor Erf1 and involved in No-Go decay. J. Biol. Chem. *283*, 7145–7154.

Gutell, R.R., Cannone, J.J., Konings, D., and Gautheret, D. (2000). Predicting U-turns in Ribosomal RNA with Comparative Sequence Analysis. J. Mol. Biol. *300*, 791–803.

Gutierrez, E., Shin, B.-S., Woolstenhulme, C.J., Kim, J.-R., Saini, P., Buskirk, A.R., and Dever, T.E. (2013). eIF5A promotes translation of polyproline motifs. Mol. Cell *51*, 35–45.

Halic, M., Becker, T., Pool, M.R., Spahn, C.M., Grassucci, R.A., Frank, J., and Beckmann, R. (2004). Structure of the signal recognition particle interacting with the elongation-arrested ribosome. Nature *427*, 808–814.

Halic, M., Blau, M., Becker, T., Mielke, T., Pool, M.R., Wild, K., Sinning, I., and Beckmann, R. (2006). Following the signal sequence from ribosomal tunnel exit to signal recognition particle. Nature *444*, 507–511.

Hashem, Y., des Georges, A., Dhote, V., Langlois, R., Liao, H.Y., Grassucci, R.A., Hellen, C.U.T., Pestova, T.V., and Frank, J. (2013). Structure of the Mammalian Ribosomal 43S Preinitiation Complex Bound to the Scanning Factor DHX29. Cell *153*, 1108–1119.

Hatchikian, E.C., Fardeau, M.L., Bruschi, M., Belaich, J.P., Chapman, A., and Cammack, R. (1989). Isolation, characterization, and biological activity of the Methanococcus thermolithotrophicus ferredoxin. J. Bacteriol. *171*, 2384–2390.

Hatin, I., Fabret, c., Rousset, J.P., and Namz, O. (2009). Molecular dissection of translation termination mechanism identifies two new critical regions in eRF1. Nucleic Acids Res. *37*, 1789-1798.

Heuer, A., Gerovac, M., Schmidt, C., Trowitzsch, S., Preis, A., Kötter, P., Berninghausen, O., Becker, T., Beckmann, R., and Tampé, R. (2017). Structure of the 40S–ABCE1 post-splitting complex in ribosome recycling and translation initiation. Nat. Struct. Mol. Biol. *24*, 453–460.

Hinnebusch, A.G., and Lorsch, J.R. (2012). The mechanism of eukaryotic translation initiation: New insights and challenges. Cold Spring Harb. Perspect. Biol. *4*.

Hirokawa, G., Demeshkina, N., Iwakura, N., Kaji, H., and Kaji, A. (2006). The ribosome-recycling step: consensus or controversy? Trends Biochem. Sci. *31*, 143–149.

Hirokawa, G., Iwakura, N., Kaji, A., and Kaji, H. (2008). The role of GTP in transient splitting of 70S ribosomes by RRF (ribosome recycling factor) and EF-G (elongation factor G). Nucleic Acids Res. *36*, 6676–6687.

Inagaki, Y., Blouin, C., Susko, E., and Roger, A.J. (2003). Assessing functional divergence in EF-1  and its paralogs in eukaryotes and archaebacteria. Nucleic Acids Res. *31*, 4227–4237.

Jackson, R.J., Hellen, C.U.T., and Pestova, T. V (2010). The mechanism of eukaryotic translation initiation and principles of its regulation. Nat. Rev. Mol. Cell Biol. *11*, 113–127.

Janzen, D.M., Frolova, L., and Geballe, A.P. (2002). Inhibition of Translation Termination Mediated by an Interaction of Eukaryotic Release Factor 1 with a Nascent Inhibition of Translation Termination Mediated by an Interaction of Eukaryotic Release Factor 1 with a Nascent Peptidyl-tRNA. Mol. and Cell. Biol. *22 (24)*, 8562-8570

Jenner, L., Melnikov, S., de Loubresse, N.G., Ben-Shem, A., Iskakova, M., Urzhumtsev, A., Meskauskas, A., Dinman, J., Yusupova, G., and Yusupov, M. (2012). Crystal structure of the 80S yeast ribosome. Curr. Opin. Struct. Biol. *22*, 759–767.

Jin, H., Kelley, A.C., Loakes, D., and Ramakrishnan, V. (2010). Structure of the 70S ribosome bound to release factor 2 and a substrate analog provides insights into catalysis of peptide release. Proc. Natl. Acad. Sci. *107*, 8593–8598.

Kaminishi, T., Wilson, D.N., Takemoto, C., Harms, J.M., Kawazoe, M., Schluenzen, F., Hanawa-Suetsugu, K., Shirouzu, M., Fucini, P., and Yokoyama, S. (2007). A Snapshot of the 30S Ribosomal Subunit Capturing mRNA via the Shine-Dalgarno Interaction. Structure *15*, 289–297.

Karcher, A., Büttner, K., Märtens, B., Jansen, R.P., and Hopfner, K.P. (2005). X-ray structure of RLI, an essential twin cassette ABC ATPase involved in ribosome biogenesis and HIV capsid assembly. Structure *13*, 649–659.

Karcher, A., Schele, A., and Hopfner, K.-P. (2008). X-ray structure of the complete ABC enzyme ABCE1 from Pyrococcus abyssi. J. Biol. Chem. *283*, 7962–7971.

Khatter, H., Myasnikov, A.G., Natchiar, S.K., and Klaholz, B.P. (2015). Structure of the human 80S ribosome. Nature *520*, 640–645.

Khoshnevis, S., Neumann, P., and Ficner, R. (2010). Crystal Structure of the RNA Recognition Motif of Yeast

Translation Initiation Factor eIF3b Reveals Differences to Human eIF3b. PLoS One *5*, e12784.

Kispal, G., Sipos, K., Lange, H., Fekete, Z., Bedekovics, T., Janáky, T., Bassler, J., Aguilar Netz, D.J., Balk, J., Rotte, C., et al. (2005). Biogenesis of cytosolic ribosomes requires the essential iron-sulphur protein Rli1p and mitochondria. EMBO J. *24*, 589–598.

Kisselev, L.L., and Buckingham, R.H. (2000). Translational termination comes of age. Trends Biochem. Sci. *25*, 561–566.

Kisselev, L., Ehrenberg, M., and Frolova, L. (2003). NEW EMBO MEMBER'S REVIEW: Termination of translation: interplay of mRNA, rRNAs and release factors? EMBO J. *22*, 175–182.

Klinge, S., Voigts-Hoffmann, F., Leibundgut, M., and Ban, N. (2012). Atomic structures of the eukaryotic ribosome. Trends Biochem. Sci. *37*, 189–198.

Knorr, A.G., Schmidt, C., Tesina, P., Berninghausen, O., Becker, T., Beatrix, B., and Beckmann, R. (2019). Ribosome–NatA architecture reveals that rRNA expansion segments coordinate N-terminal acetylation. Nat. Struct. Mol. Biol. *26*, 35–39.

Kobayashi, K., Kikuno, I., Kuroha, K., Saito, K., Ito, K., Ishitani, R., Inada, T., and Nureki, O. (2010). Structural basis for mRNA surveillance by archaeal Pelota and GTP-bound EF1α complex. Proc. Natl. Acad. Sci. U. S. A. *107 (41),* 17575-17579.

Kong, C., Ito, K., Walsh, M.A., Wada, M., Liu, Y., Kumar, S., Barford, D., Nakamura, Y., and Song, H. (2004). Crystal structure and functional analysis of the eukaryotic class II release factor eRF3 from *S. pombe*. Mol. Cell *14*, 233–245.

Kononenko, A. V., Mitkevich, V.A., Dubovaya, V.I., Kolosov, P.M., Makarov, A.A., and Kisselev, L.L. (2007). Role of the individual domains of translation termination factor eRF1 in GTP binding to eRF3. Proteins Struct. Funct. Bioinforma. *70*, 388–393.

Kononenko, A. V, Dembo, K.A., Kiselev, L.L., and Volkov, V. V (2004). Molecular morphology of eukaryotic class I translation termination factor eRF1 in solution. Mol. Biol. (Mosk). *38*, 303–311.

Korkhov, V.M., Mireku, S.A., Veprintsev, D.B., and Locher, K.P. (2014). Structure of AMP-PNP–bound BtuCD and mechanism of ATP-powered vitamin B12 transport by BtuCD–F. Nat. Struct. Mol. Biol. *21*, 1097–1099.

Korostelev, A.A. (2011). Structural aspects of translation termination on the ribosome. RNA *17*, 1409–1421.

Korostelev, A., Trakhanov, S., Asahara, H., Laurberg, M., Lancaster, L., and Noller, H.F. (2007). Interactions and dynamics of the Shine Dalgarno helix in the 70S ribosome. Proc. Natl. Acad. Sci. U. S. A. *104*, 16840–16843.

Korostelev, A., Asahara, H., Lancaster, L., Laurberg, M., Hirschi, A., Zhu, J., Trakhanov, S., Scott, W.G., and Noller, H.F. (2008). Crystal structure of a translation termination complex formed with release factor RF2. Proc. Natl. Acad. Sci. *105*, 19684–19689.

Korostelev, A., Zhu, J., Asahara, H., and Noller, H.F. (2010). Recognition of the amber UAG stop codon by release factor RF1. EMBO J. *29*, 2577–2585.

Kryuchkova, P., Grishin, A., Eliseev, B., Karyagina, A., Frolova, L., and Alkalaeva, E. (2013). Two-step model of stop codon recognition by eukaryotic release factor eRF1. Nucleic Acids Res. *41*, 4573–4586.

Kuroha, K., Akamatsu, M., Dimitrova, L., Ito, T., Kato, Y., Shirahige, K., and Inada, T. (2010). Receptor for activated C kinase 1 stimulates nascent polypeptide-dependent translation arrest. EMBO Rep. *11*, 956–961.

Laemmli, U.K. (1970). Cleavage of structural proteins during the assembly of the head of bacteriophage T4. Nature *227*, 680–685.

Laurberg, M., Asahara, H., Korostelev, A., Zhu, J., Trakhanov, S., and Noller, H.F. (2008). Structural basis for translation termination on the 70S ribosome. Nature *454*, 852–857.

Laursen, B.S., Sorensen, H.P., Mortensen, K.K., and Sperling-Petersen, H.U. (2005). Initiation of Protein Synthesis in Bacteria. Microbiol. Mol. Biol. Rev. *69*, 101–123.

Lee, H.H., Kim, Y.S., Kim, K.H., Heo, I., Kim, S.K., Kim, O., Kim, H.K., Yoon, J.Y., Kim, H.S., Kim, D.J., Lee, S.J., Yoon, H.J., Kim, S.J., Lee, B.G., Song, H.K., Kim, V.N., Park, C.M., and Suh, S.W. (2007). Structural and functional insights into Dom34, a key component of no-go mRNA decay. Mol Cell *27*, 938–950.

Leidig, C., Bange, G., Kopp, J., Amlacher, S., Aravind, A., Wickles, S., Witte, G., Hurt, E., Beckmann, R., and Sinning, I. (2013). Structural characterization of a eukaryotic chaperone - the ribosome-associated complex. Nat. Struct. Mol. Biol. *20*, 23–28.

Llácer, J.L., Hussain, T., Marler, L., Aitken, C.E., Thakur, A., Lorsch, J.R., Hinnebusch, A.G., and Ramakrishnan, V. (2015). Conformational Differences between Open and Closed States of the Eukaryotic Translation Initiation Complex. Mol. Cell *59*, 399–412.

Loh, P.G., and Song, H. (2010). Structural and mechanistic insights into translation termination. Curr. Opin. Struct. Biol. *20*, 98–103.

Lomakin, I.B., Xiong, Y., and Steitz, T.A. (2007). The crystal structure of yeast fatty acid synthase, a cellular machine with eight active sites working together. Cell *129*, 319–332.

Mantsyzov, A.B., Ivanova, E. V, Birdsall, B., Alkalaeva, E.Z., Kryuchkova, P.N., Kelly, G., Frolova, L.Y., and Polshakov, V.I. (2010). NMR solution structure and function of the C-terminal domain of eukaryotic class 1 polypeptide chain release factor. FEBS J. *277*, 2611–2627.

Matheisl, S., Berninghausen, O., Becker, T., and Beckmann, R. (2015). Structure of a human translation termination complex. Nucleic Acids Res. *43*, 8615–8626.

Melnikov, S., Ben-Shem, A., Garreau de Loubresse, N., Jenner, L., Yusupova, G., and Yusupov, M. (2012). One core, two shells: bacterial and eukaryotic ribosomes. Nat. Struct. Mol. Biol. *19*, 560–567.

Merkulova, T.I., Frolova, L.Y., Lazar, M., Camonis, J., and Kisselev, L.L. (1999). C-terminal domains of human translation termination factors eRF1 and eRF3 mediate their in vivo interaction. FEBS Lett. *443*, 41–47.

Mitroshin, I. V., Garber, M.B., and Gabdulkhakov, A.G. (2016). Investigation of structure of the ribosomal L12/P stalk. Biochem. *81*, 1589–1601.

Morgan, D.G., Ménétret, J.-F., Radermacher, M., Neuhof, A., Akey, I. V, Rapoport, T.A., and Akey, C.W. (2000). A comparison of the yeast and rabbit 80S ribosome reveals the topology of the nascent chain exit tunnel, inter-subunit bridges and mammalian rRNA expansion segments. J. Mol. Biol. *301*, 301–321.

Mozdzanowski, J., and Speicher, D.W. (1992). Microsequence analysis of electroblotted proteins. I. Comparison of electroblotting recoveries using different types of PVDF membranes. Anal. Biochem. *207*, 11–18.

Nakano, H., Yoshida, T., Uchiyama, S., Kawachi, M., Matsuo, H., Kato, T., Ohshima, A., Yamaichi, Y., Honda, T., Kato, H., Yamagata, Y., Ohkubo, T., and Kobayashi, Y. (2003). Structure and binding mode of a ribosome recycling factor (RRF) from mesophilic bacterium. J. Biol. Chem. *278*, 3427–3436.

Neumann, P., Dickmanns, A., and Ficner, R. (2018). Validating Resolution Revolution. Structure *26*, 785-795.e4.

Nissen, P., Hansen, J., Ban, N., Moore, P.B., and Steitz, T.A. (2000). The structural basis of ribosome activity in peptide bond synthesis. Science *289*, 920–930.

Ogle, J.M., and Ramakrishnan, V. (2005). Structural insights into translational. Annu. Rev. Biochem. *74*, 129–177.

Ogle, J.M., Brodersen, D.E., Clemons, W.M., Tarry, M.J., Carter, A.P., and Ramakrishnan, V. (2001). Recognition of cognate transfer RNA by the 30S ribosomal subunit. Science *292*, 897–902.

Oldham, M.L., and Chen, J. (2011). Snapshots of the maltose transporter during ATP hydrolysis. Proc. Natl. Acad. Sci. U. S. A. *108*, 15152–15156.

Pallesen, J., Hashem, Y., Korkmaz, G., Koripella, R.K., Huang, C., Ehrenberg, M., Sanyal, S., and Frank, J. (2013). Cryo-EM visualization of the ribosome in termination complex with apo-RF3 and RF1. Elife *2*, e00411.

Passmore, L.A., Schmeing, T.M., Maag, D., Applefield, D.J., Acker, M.G., Algire, M.A., Lorsch, J.R., and Ramakrishnan, V. (2007). The Eukaryotic Translation Initiation Factors eIF1 and eIF1A Induce an Open Conformation of the 40S Ribosome. Mol. Cell *26*, 41–50.

Passos, D.O., Doma, M.K., Shoemaker, C.J., Muhlrad, D., Green, R., Weissman, J., Hollien, J., and Parker, R. (2009). Analysis of Dom34 and its function in no-go decay. Mol. Biol. Cell *20*, 3025–3032.

Peske, F., Rodnina, M. V, and Wintermeyer, W. (2005). Sequence of Steps in Ribosome Recycling as Defined by Kinetic Analysis. Mol. Cell *18*, 403–412.

Pettersen, E.F., Goddard, T.D., Huang, C.C., Couch, G.S., Greenblatt, D.M., Meng, E.C., and Ferrin, T.E. (2004). UCSF Chimera-a visualization system for exploratory research and analysis. J Comput Chem *25*, 1605-1612.

Phillips, J.C., Braun, R., Wang, W., Gumbart, J., Tajkhorshid, E., Villa, E., Chipot, C., Skeel, R.D., Kalé, L., and Schulten, K. (2005). Scalable molecular dynamics with NAMD. J. Comput. Chem. *26*, 1781–1802.

Pisarev, A. V., Skabkin, M.A., Pisareva, V.P., Skabkina, O. V., Rakotondrafara, A.M., Hentze, M.W., Hellen, C.U.T., and Pestova, T. V. (2010). The Role of ABCE1 in Eukaryotic Posttermination Ribosomal Recycling. Mol. Cell *37*, 196–210.

Pisareva, V.P., Skabkin, M.A., Hellen, C.U., Pestova, T. V, and Pisarev, A. V (2011). Dissociation by Pelota, Hbs1 and ABCE1 of mammalian vacant 80S ribosomes and stalled elongation complexes. EMBO J. *30(9)*, 1804-1817.

Preis, A., Heuer, A., Barrio-Garcia, C., Hauser, A., Eyler, D.E., Berninghausen, O., Green, R., Becker, T., and Beckmann, R. (2014). Cryoelectron microscopic structures of eukaryotic translation termination complexes containing eRF1-eRF3 or eRF1-ABCE1. Cell Rep. *8*, 59–65.

Ramesh, M., and Woolford, J.L. (2016). Eukaryote-specific rRNA expansion segments function in ribosome biogenesis. RNA *22*, 1153–1162.

Salas-Marco, J., and Bedwell, D.M. (2004). GTP hydrolysis by eRF3 facilitates stop codon decoding during eukaryotic translation termination. Mol. Cell. Biol. *24*, 7769–7778.

Scheres, S.H. (2012). RELION: implementation of a Bayesian approach to cryo-EM structure determination. J Struct Biol *180*, 519–530.

Scheres, S.H.W. (2016). Processing of Structurally Heterogeneous Cryo-EM Data in RELION Methods Enzymol. *579*, 125-157.

Scheres, S.H.W., and Chen, S. (2012). Prevention of overfitting in cryo-EM structure determination. Nat. Methods *9*, 853–854.

Schluenzen, F., Tocilj, A., Zarivach, R., Harms, J., Gluehmann, M., Janell, D., Bashan, A., Bartels, H., Agmon,

I., Franceschi, F., and Yonath, A. (2000). Structure of functionally activated small ribosomal subunit at 3.3 angstroms resolution. Cell *102*, 615–623.

Selmer, M., Dunham, C.M., Murphy, F. V, Weixlbaumer, A., Petry, S., Kelley, A.C., Weir, J.R., and Ramakrishnan, V. (2006). Structure of the 70S ribosome complexed with mRNA and tRNA. Science *313*, 1935–1942.

Sergiev, P. V., Bogdanov, A.A., and Dontsova, O.A. (2005). How can elongation factors EF-G and EF-Tu discriminate the functional state of the ribosome using the same binding site? FEBS Lett. *579*, 5439–5442.

Shine, J., and Dalgarno, L. (1974). The 3'-terminal sequence of Escherichia coli 16S ribosomal RNA: complementarity to nonsense triplets and ribosome binding sites. Proc. Natl. Acad. Sci. U. S. A. *71*, 1342–1346.

Shoemaker, C.J, and Green, R. (2011). Kinetic analysis reveals the ordered coupling of translation termination and ribosome recycling in yeast. Proc. Natl. Acad. Sci. U. S. A. *108*, E1392-1398.

Shoemaker, C.J., and Green, R. (2012). Translation drives mRNA quality control. Nat. Struct. Mol. Biol. *19*, 594–601.

Shoemaker, C.J., Eyler, D.E., and Green, R. (2010). Dom34:Hbs1 promotes subunit dissociation and peptidyl-tRNA drop-off to initiate no-go decay. Science *330*, 369–372.

Siridechadilok, B., Fraser, C.S., Hall, R.J., Doudna, J.A., and Nogales, E. (2005). Structural Roles for Human Translation Factor eIF3 in Initiation of Protein Synthesis. Science *310*, 1513–1515.

Skabkin, M.A., Skabkina, O.V., Hellen, C.U.T., and Pestova, T.V. (2013). Reinitiation and Other Unconventional Posttermination Events during Eukaryotic Translation. Mol. Cell *51*, 249–264.

Smith, P.C., Karpowich, N., Millen, L., Moody, J.E., Rosen, J., Thomas, P.J., and Hunt, J.F. (2002). ATP binding to the motor domain from an ABC transporter drives formation of a nucleotide sandwich dimer. Mol. Cell *10*, 139–149.

Soding, J., Biegert, A., and Lupas, A.N. (2005). The HHpred interactive server for protein homology detection and structure prediction. Nucleic Acids Res. *33*, W244--8.

Song, H., Mugnier, P., Das, A.K., Webb, H.M., Evans, D.R., Tuite, M.F., Hemmings, B.A., and Barford, D. (2000). The crystal structure of human eukaryotic release factor eRF1--mechanism of stop codon recognition and peptidyl-tRNA hydrolysis. Cell *100*, 311–321.

Taylor, D., Unbehaun, A., Li, W., Das, S., Lei, J., Liao, H.Y., Grassucci, R. a, Pestova, T. V, and Frank, J. (2012). Cryo-EM structure of the mammalian eukaryotic release factor eRF1-eRF3-associated termination complex. Proc. Natl. Acad. Sci. U. S. A. *109*, 18413–18418.

Ter-Avanesyan, M.D., Dagkesamanskaya, A.R., Kushnirov, V. V, and Smirnov, V.N. (1994). The SUP35 omnipotent suppressor gene is involved in the maintenance of the non-Mendelian determinant [psi+] in the yeast Saccharomyces cerevisiae. Genetics *137*, 671–676.

Towbin, H., Staehelin, T., and Gordon, J. (1979). Electrophoretic transfer of proteins from polyacrylamide gels to nitrocellulose sheets: procedure and some applications. Proc. Natl. Acad. Sci. *76*, 4350–4354.

Trabuco, L.G., Villa, E., Mitra, K., Frank, J., and Schulten, K. (2008). Flexible Fitting of Atomic Structures into Electron Microscopy Maps Using Molecular Dynamics. Structure *16*, 673–683.

Trabuco, L.G., Schreiner, E., Eargle, J., Cornish, P., Ha, T., Luthey-Schulten, Z., and Schulten, K. (2010). The Role of L1 Stalk–tRNA Interaction in the Ribosome Elongation Cycle. J. Mol. Biol. *402*, 741–760.

Trappl, K., and Joseph, S. (2016). Ribosome Induces a Closed to Open Conformational Change in Release

Factor 1. J. Mol. Biol. *428*, 1333–1344.

Wei, Z., Zhang, P., Zhou, Z., Cheng, Z., Wan, M., and Gong, W. (2004). Crystal structure of human eIF3k, the first structure of eIF3 subunits. J. Biol. Chem. *279*, 34983–34990.

Weixlbaumer, A., Jin, H., Neubauer, C., Voorhees, R.M., Petry, S., Kelley, A.C., and Ramakrishnan, V. (2008). Insights into Translational Termination from the Structure of RF2 Bound to the Ribosome. Science *322*, 953–956.

Wimberly, B.T., Brodersen, D.E., Clemons Jr., W.M., Morgan-Warren, R.J., Carter, A.P., Vonrhein, C., Hartsch, T., and Ramakrishnan, V. (2000). Structure of the 30S ribosomal subunit. Nature *407*, 327–339.

Zavialov, A. V, Buckingham, R.H., and Ehrenberg, M. (2001). A posttermination ribosomal complex is the guanine nucleotide exchange factor for peptide release factor RF3. Cell *107*, 115–124.

Zavialov, A. V, Mora, L., Buckingham, R.H., and Ehrenberg, M. (2002). Release of peptide promoted by the GGQ motif of class 1 release factors regulates the GTPase activity of RF3. Mol. Cell *10*, 789–798.

Zavialov, A. V, Hauryliuk, V. V, and Ehrenberg, M. (2005). Splitting of the Posttermination Ribosome into Subunits by the Concerted Action of RRF and EF-G. Mol. Cell *18*, 675–686.

Zhou, J., Korostelev, A., Lancaster, L., and Noller, H.F. (2012). Crystal structures of 70S ribosomes bound to release factors RF1, RF2 and RF3. Curr. Opin. Struct. Biol. *22*, 733–742.

# 8 SUPPLEMENTARY TABLES

| Ribosomal subunit | rRNA/protein | *S.cerevisiae* numbering | *T. aestivum* numbering | eRF1 domain | eRF1 residue | mutation/ defect |
|---|---|---|---|---|---|---|
| SSU | h18 | 565-566 | 569-570 | **NTD** (YxCxxxF-loop) | 124-127 | |
| | | 577-579 | 581-58 | **NTD** (GTx-loop) | 27-29 | N27H/Readthrough (Hatin et al., 2009) |
| | h31 | 1158-1161 | 1163-1166 | **NTD** | 64-70 | R65A/ribosome binding (Frolova et al., 2002) |
| | | 1186-1188 | 1190-1192 | **NTD** | 74-78 | Q76R/Q76K/Readthrough (Hatin et al., 2009) |
| | h34 | 1271-1274 | 1275-1278 | **NTD** (TASNIKS-loop) | 59-66 | I59A, S61D/ GTPase-activation (Kryuchkova et al., 2013) R62A, R65A ribosome binding (Frolova et al., 2002) |
| | | 1441-1442 | 1447-1448 | **NTD** | 99-103 | E104K/Readthrough (Hatin et al., 2009) |
| | h14 | 413-415 | 417-419 | **ce** (GGQ-loop) | 182-184,186; 189 | R189A/growth, read-through, GTPase-activation (Cheng et al., 2009) |
| | ES8 | 1255-1257 | 1259-1261 | **CTD** (mini-domain) | 355-358 | G363A;E365A (*H.s.*)/ termination efficiency, ribosome binding (Mantsyzov et al., 2010) |
| | S12 | 94-96 | - | **ce** | 166-168 | |
| | | 141-142 | - | **ce** | 208-209 | |

Table S1 (continues on next page). **80S-eRF1 interactions in the pre-termination complex**. From Preis et al., 2014.

| Ribosomal subunit | rRNA/protein | *S.cerevisiae* numbering | *T. aestivum* numbering | eRF1 domain | eRF1 residue | mutation/ defect |
|---|---|---|---|---|---|---|
| SSU | S30E | 1-6 | - | NTD (YxCxxxF-loop) | 125-129 | |
| | S31E | 1-13 | - | NTD | 100-106 | E104K, D101G, D101V/ Readthrough (Hatin et al., 2009) |
| | | 15-18 | - | CTD (mini-domain) | 360-362 | E360V, E360G Readthrough (Hatin et al., 2009) |
| LSU | H43 | 1242 | 1246 | CTD | 309-312 | |
| | H69 | 2254-2258 | 2249-2253 | NTD | 38-46; 117-121 | Q46K/ Readthrough (Hatin et al., 2009) |
| | H95 | 3029-3030 | 3030-3031 | ce | 249-251 269-271 | |
| LSU | L11 | 24-29 | 24-29 | CTD | 413-418 | |
| | L14 | 68-70 | 71-73 | ce | 236-238 | |

Table S1 (continued from previous page). **80S-eRF1 interactions in the pre-termination complex.** From Preis et al., 2014.

| Ribosomal subunit | Ribosomal protein/RNA | *S.cerevisiae* numbering | *T. aestivum* numbering | eRF3 domain | eRF3 residue | mutation/ defect |
|---|---|---|---|---|---|---|
| SSU | **h14** | 416-417 | 420-421 | **G/sw1** | 289-297 | |
| | **h15** | 428-430 | 432-434 | **II** | 498-501 | |
| LSU | **S12** | 144-145 | 141-142 | **III** | 559-561 | |
| | **H95** | 3020-3027 | 3021-3028 | **G** | 300-306<br>373-380 | |

Table S2. **80S-eRF3 interactions in the pre-termination complex**. From Preis et al., 2014.

| eRF1 domain | eRF1 residue | eRF3 domain | eRF3 domain | mutation/defect |
|---|---|---|---|---|
| ce | 169-173 | II | 496-498 | |
| | 174-177 | II | 502-506 | |
| | 183-186 | G/sw1 | 290-296 | |
| | 226-228 | G/sw1 | 318-323 | |
| | 252-257 | G/sw1<br>G/sw2<br>III | 318-323<br>345-353<br>607-610 | |
| | 257-265 | III | 607-610 | |
| CTD | 284-292 | III | 591-595 | F288A,I291A;<br>S593A,I594A/<br>complex formation<br>(Cheng et al., 2009) |
| | 395-401 | III<br>III | 595-599<br>611-615 | Q396A,F401A;<br>F599A/<br>complex formation<br>(Cheng et al., 2009) |

Table S3. **eRF1-eRF3 interactions in the pre-termination complex**. From Preis et al., 2014.

| Ribosomal subunit | rRNA/protein | *S.cerevisiae* numbering | *T. aestivum* numbering | eRF1 domain | eRF1 residue | mutation/ defect |
|---|---|---|---|---|---|---|
| LSU | **H43** | 1242 | 1246 | **CTD** | 311-314<br>379-381<br>409-411 | |
| | **H44** | 1270 | 1274 | **CTD** | 409-411 | |
| | **H69** | 2257-2258<br>2254-2255 | 2252-2253<br>2249-2250 | **ce** | 161;163<br>262 | N161I/<br>Readthrough<br>(Hatin et al., 2009) |
| | **H71** | 2285-2287<br>2287-2290<br>2306 | 2280-2282<br>2282-2285<br>2301 | **ce** | 149-151<br>173-175<br>226-228<br>252-254<br>255 | |
| | **H89** | 2820-2822<br>2838-2839<br>2861-2864 | 2822-2824<br>2840-2841<br>2863-2865 | **ce** | 182-184;186<br>212-214<br>184-189 | I R189A/growth,<br>readthrough,<br>GTPase-activation<br>(Cheng et al., 2009)<br>211V, D214G<br>Readthrough<br>(Hatin et al., 2009) |

Table S4 (continues on next page). **80S1-eRF1 interactions in the termination/pre-recycling complex**. From Preis et al., 2014.

| Ribosomal subunit | rRNA/protein | *S.cerevisiae* numbering | *T. aestivum* numbering | eRF1 domain | eRF1 residue | mutation/ defect |
|---|---|---|---|---|---|---|
| LSU | H92 | 2922-2923<br>2927-2928 | 2924-2925<br>2929-2930 | ce | 177<br>227-231 | |
| | H93 | 2954<br>2971 | 2956<br>2973 | ce | 179<br>187179 | |
| | H95 | 3027 | 3028 | ce | 291-294 | |
| | L11 | 24-26 | 24-26 | CTD | 310-312 | |
| tRNA | P-site | 1<br>68 | | ce | 194<br>168 | |

Table S4 (continued from previous page). **80S-eRF1 interactions in the termination/pre-recycling complex**. From Preis et al., 2014.

| Ribosomal subunit | Ribosomal protein/RNA | *S.cerevisiae* numbering | *T. aestivum* numbering | ABCE1 domain | ABCE1 residue | mutation/ defect or effect |
|---|---|---|---|---|---|---|
| SSU | **h8** | 155-156 | 153-154 | **H2** | 584-586 | |
| | **h14** | 415<br>416-417 | 419<br>420-421 | **H1**<br>**H2** | 311<br>587-589 | R311E<br>S588E/<br>Lethality<br>(Karcher et al., 2007) |
| | **h15** | 429-430<br>438-440 | 433-434<br>442-44 | **HLH** | 150-152 | L152E/<br>Lethality<br>(Karcher et al., 2007) |
| | **S24E** | 115-116 | - | **NBD1** | 270-271 | |
| LSU | **H95** | 3024-3025 | 3025-3026 | **NBD2** | 445-446 | |
| | **L6** | 96<br>98-100 | 97<br>99-101 | **NBD2** | 445-446<br>516-517 | |
| | **L10** | 133-134<br>144-145 | 138-139<br>149-150 | **NBD2** | 439<br>431-432 | |
| | **L14** | 128-131 | 131-134 | **H2** | 576-577 | |

Table S5. **80S-ABCE1 interactions in the termination/pre-recycling complex**. From Preis et al., 2014.

| eRF1 domain | eRF1 residue | ABCE1 domain | ABCE1 residue | mutation/ defect |
|---|---|---|---|---|
| **CTD** | 299-300;<br>303-304<br>399-401 | **FeS** | 28-33 | ∆FeS/ ribosome splitting (Barthelme et al., 2011) |

Table S6. **eRF1-ABCE1 interactions in the termination/pre-recycling complex**. From Preis et al., 2014.

# 9 ABBREVIATIONS

| | |
|---|---|
| µg | Microgram |
| µL | Microliter |
| µM | Micromolar |
| Å | Ångstroem |
| aa | Amino acid |
| aa-tRNA | Aminoacyl-transfer ribonucleic acid |
| ABC | ATP-binding cassette |
| ADP | Adenosine diphosphate |
| AMP (antibiotic) | Ampicillin |
| AMP | Adenosine monophosphate |
| A-site | Aminoacyl-site |
| ATP | Adenosine triphosphate |
| ATPase | Adenosine triphosphatase |
| CAM | Chloramphenicol |
| CBD | Chitin-binding domain |
| ce | Central domain |
| CMV | Cytomegalovirus |
| Cryo-EM | Cryo-electron microscopy |
| CTD | Carboxyterminal domain |
| C-terminal | Carboxyterminal |
| CTF | Contrast transfer function |
| CV | Column volume |
| DC | Decoding center |
| DNA | Deoxyribonucleic acid |
| DTT | Dithiothreitol |
| *E. coli* | *Escherichia coli* |
| ECL | Enhanced chemiluminescence |
| eEF | Eukaryotic elongation factor |
| EF | Elongation factor |
| eIF | Eukaryotic initiation factor |

| | |
|---|---|
| eRF1 | Eukaryotic release factor 1 |
| eRF3 | Eukaryotic release factor 3 |
| E-site | Exit-site |
| FeS cluster | Iron-Sulphur cluster |
| FSC | Fourier shell correlation |
| g | g-force |
| GAC | GTPase-associated center |
| GDP | Guanosine diphosphate |
| GEF | Guanine nucleotide exchange factor |
| GMP | Guanosine monophosphate |
| GTP | Guanosine triphosphate |
| GTPase | Guanosine triphosphatase |
| h (unit) | Hour |
| HA | Hemagglutinin |
| H-bonds | Hydrogen bonds |
| $His_6$ | Hexahistidine |
| HLH | Helix-loop-helix |
| HRP | Horseradish peroxidase |
| IF | Initiation factor |
| kDa | Kilodalton |
| LSU | Large ribosomal subunit |
| M | Molar |
| mg | Milligram |
| min (unit) | Minute |
| mM | Millimolar |
| mRNA | Messenger RNA |
| MS (or Mass Spec) | Mass spectrometry |
| MW | Molecular weight |
| NBD | Nucleotide binding domain |
| NC | Nascent chain |
| N-terminal | Aminoterminal |

| | |
|---|---|
| ng | Nanogram |
| NGD | No-go decay |
| nm | Nanometer |
| NMR | Nuclear magnetic resonance |
| nt | Nucleotide |
| NTD | N-terminal domain |
| OD | Optical density |
| ORF | Open reading frame |
| PABP | Poly(A)-binding protein |
| PAGE | Polyacrylamide gel electrophoresis |
| PCR | Polymerase chain reaction |
| PDB | Protein Data Bank |
| PIC | Pre-initiation complex |
| P-site | Peptidyl-site |
| PTC | Peptidyl transferase center |
| RF | Release factor |
| RNA | Ribonucleic acid |
| RNAse | Ribonuclease |
| RNC | Ribosome-nascent chain complex |
| rpm | Revolutions per minute |
| RRF | Ribosome recycling factor |
| rRNA | Ribosomal ribonucleic acid |
| s | Second |
| S | Svedberg unit |
| *S. cerevisiae* | *Saccharomyces cerevisiae* |
| *S. pombe* | *Schizosaccharomyces pombe* |
| SA | Signal anchor |
| SAXS | X-ray scattering |
| SD | Shine-Dalgarno |
| SDS | Sodium dodecyl sulfate |
| SRL | Sarcin/ricin loop |

| | |
|---|---|
| SSU | Small ribosomal subunit |
| *T. aestivum* | *Triticum aestivum* |
| TAP | Tandem affinity purification |
| TCA | Trichloroacetic acid |
| tRNA | Transfer ribonucleic acid |
| UTR | Untranslated region |
| V (unit) | Volt |
| v/v (concentration) | Volume/Volume |
| W (unit) | Watt |
| YPD | Yeast extract peptone dextrose |

# 10 ACKNOWLEDGEMENTS

Es ist so weit!

First of all I would like to thank Prof. Beckmann for taking me in as a master student back in the day to tackle eukaryotic termination with (now considered “low-res”) Cryo, and for letting me continue working on this, and several other topics in my PhD. I appreciate the freedom I had to explore different approaches and methods and try out different things. These were exciting times and I have learned a lot. I am grateful for having had the opportunity to work with some great people on some great projects in the Beckmann lab.

Thank you to Prof. Alexej Kedrov for agreeing to be my second advisor and members of my thesis committee: PD Dietmar Martin, Prof. Klaus Förstemann, Prof. Karl-Peter Hopfner and Prof. Karl-Klaus Conzelmann. Thank you for your support during these last steps to the finish line.

I would also like to thank all the collaborators I had the pleasure to work with in my main project: Prof. Rachel Green, Dan Eyler and Anthony Schueller, and Prof. Robert Tampe, Milan Gerovac and Elena Nuernberg in the ABCE1 project. Additionally, I would like to say it was great to be a part of the Forschergruppe meetings and discussions. Regardless of some obstacles, the scientific world remains a collaborative one which is something to admire.

Thank you to Andre Heuer for being the driving force behind the ABCE1 project, and generally for a very fruitful collaboration! I wish you the best of success in all future endeavors.

I am very grateful to the technical team: Heidi Sieber, Joanna Musial and Andrea Gilmozzi, for keeping the lab running and for all your help and stoic patience.

Thank you to the microscopy team: Otto Berninghausen, Charlotte Ungewickell and Susi Rieder for maintaining the facility, teaching me my way around it, prepping grids and collecting all that (sweet and sometimes not-so-sweet) data.

A very special thank you goes out to Thomas Becker. The list of everything you taught me is so long, from the first relevant practical skills in the lab to writing structure to being honest with oneself to maintaining integrity as a scientist and human being. Thank you for all your help, for having my back and most of all - for believing in me. Your support has meant the world to me and I will always remember it. You lead by example and anyone that gets to work with you should consider themselves lucky! I hope we stay in touch for years to come.

Thank you to all my lab mates who I am lucky to call friends today: Clara Barrio-Garcia, Marko Gogala, Katharina Braunger, Ting Su and Maximiliane Wieland. You guys have been a real support system, in lab times and off-lab-times, especially in the couple of years leading up to this day. The road can get rocky and I appreciate having you by my side.

A big thank you to Jennifer Wells, lab mate for one day, and friend for life. I am rooting for you to complete your PhD and get that next gig! See you Anne day!

Thank you to my friends Karina, Katja, Natalja, Arto and Julia for always rooting for me!

Christian, thank you for your love and for believing in me.

Lastly, I would like to thank my loving family. Dad, thank you for your unshakeable faith in me and all kinds of support during tough times. Mom, thank you for always finding the right words. Helen, you are a real inspiration and motivation. I am happy that we get to see each other so often regardless of which corner of the world we live in and I look forward to many more family reunions. Thank you for being there for me no matter what.